NASA
TP
1608
c.1

NASA
Technical Paper 1608

AVRADCOM
Technical Report 80-B1

LOAN COPY: RETURN TO
AFWL TECHNICAL LIBRARY
KIRTLAND AFB, N. M.

TECH LIBRARY KAFB, NM
0134861

Evaluation of Helicopter Noise Due to Blade-Vortex Interaction for Five Tip Configurations

Danny R. Hoad

DECEMBER 1979

NASA

U.S. ARMY AVRADCOM

TECH LIBRARY KAFB, NM

0134861

NASA
Technical Paper 1608

AVRADCOM
Technical Report 80-B1

Evaluation of Helicopter Noise Due to Blade-Vortex Interaction for Five Tip Configurations

Danny R. Hoad
Structures Laboratory, AVRADCOM Research and Technology Laboratories
Langley Research Center
Hampton, Virginia

NASA
National Aeronautics
and Space Administration

Scientific and Technical
Information Branch

1979

SUMMARY

An experimental investigation has been conducted of the effect of tip-shape modification on helicopter blade-slap noise induced by blade-vortex interaction. The general rotor model system (GRMS) with a 3.148-m (10.33-ft) diameter, four-bladed, fully articulated rotor was installed in the Langley V/STOL tunnel. Tests were conducted over a range of simulated flight and descent velocities which have been shown to produce blade slap. Aerodynamic performance parameters of the rotor system were monitored to ensure properly matched flight conditions among the tip shapes. The tunnel was operated in the open-throat configuration, with treatment to improve the acoustic characteristics of the test chamber.

Four promising tips (based on previous investigations) were used (ogee, subwing, 60° swept tapered, and end plate), along with a standard square tip as a baseline configuration. This investigation provided a detailed acoustic evaluation of the relative applicability of the various tip configurations on the same rotor system for blade-slap noise reduction.

Acoustic evaluations indicated that the ogee-, subwing-, and swept-tapered-tip configurations were effective in reducing the measured blade slap as compared with the square tip. This evaluation was based on peak-impulse amplitude and flight-scaled, A-weighted overall sound-pressure-level analyses. These analyses indicated that the end-plate tip actually increased blade-slap noise throughout the test envelope.

INTRODUCTION

Blade slap, when present, is typically rated as the most objectionable source of helicopter noise (refs. 1 and 2). This impulsive characteristic noise source can be generated on a helicopter by two mechanisms: (1) high-speed thickness noise or shock-wave formation on the advancing blade tip; and (2) blade-vortex interaction in low-power descending flight or maneuvers. The blade-vortex interaction (BVI) source of blade slap is the only form of helicopter noise mechanism which will be discussed herein.

The BVI noise generation occurs when a blade intersects or passes near the shed tip vortex of a previous blade passage. Single-rotor vehicles experience this form of blade slap during conditions of low rotor-disk inflow such as partial-power descents and certain transient maneuvers. The vortex core can interact with the blade at various inclinations relative to the blade span, as described in reference 3. These various interactions can cause unique local flow phenomena which can, in turn, cause different characteristic noise generation (all impulsive in nature). The precise local flow phenomenon generated is very difficult to determine and is not the intent of this report; however, the prime cause of low-speed blade slap is BVI. The strong velocity profile within the vortex core seems to be the prime influence on the rotor blade. Regardless

of the local flow phenomenon, a reduction of the peak velocity, or vortex strength, would reduce this very annoying impulsive noise during low-speed flight.

Attempts to reduce the peak velocities in wing-tip vortices have concentrated on inhibiting the formation of the vortex or causing early instability in the vortex after formation by wing-tip alterations. Four of the most promising tip configurations were chosen for this investigation to be compared (both in acoustic and aerodynamic performance) with the conventional square tip on the same rotor system. These tips are the ogee (refs. 4 to 9), the subwing (refs. 10 and 11), the swept tapered (refs. 12 to 14), and the end plate (ref. 15). This investigation was conducted on a realistically scaled model rotor system with interchangeable tips in a semianechoic wind-tunnel facility. Tests were conducted for a range of simulated flight velocities (40 to 90 knots) and for a range of simulated descent velocities at each flight velocity sufficient to bracket the BVI phenomenon. Rotor revolutions per minute (rpm) and lift were held constant, at 1200 rpm and 1.78 kN (400 lb), respectively, throughout the test. Due to variations in rotor-radius advance ratio, thrust coefficient and lift coefficient varied slightly among the tips. The rotor system was carefully trimmed at each simulated flight condition for zero moments with respect to rotor-balance moment center. Careful attention was applied to rotor-system operating parameters to ensure that the tip configuration tested was performing aerodynamically similar to the baseline (square) tip. An evaluation of the aerodynamic performance comparison can be obtained in reference 3.

SYMBOLS

The units for the physical quantities defined in this paper are presented in both the International System of Units (SI) and, where appropriate, parenthetically in U.S. Customary Units. Conversion factors used for these units are given in reference 16.

c	blade chord, 10.77 cm (4.24 in.)
D	rotor drag, N (lb)
L	rotor lift, N (lb)
p_{peak}	peak impulse pressure, dynes/cm^2
R	rotor radius with square tip, 1.574 m (5.165 ft)
V_D	descent velocity, m/sec (ft/min), $V_\infty \sin \gamma$
V_T	rotor tip speed, m/sec (ft/sec)
V_∞	free-stream velocity, m/sec (ft/sec)
x_c, r	coordinates for ogee tip, cm (in.)

x,y,z	coordinates for microphone location in tunnel, m (ft)
α	rotor-shaft angle of attack, deg
γ	descent angle, $\tan^{-1}$ (D/L), deg
μ	advance ratio, V_∞/V_T
Ω	rotor rotational speed, 1200 rpm

Abbreviations:

BVI	blade-vortex interaction
OASPL	overall sound pressure level, flight-scaled, A-weighted, dBA
rpm	revolutions per minute
SPL	sound pressure level, dB, (re 0.0002 dynes/cm^2)
TPP	rotor tip-path-plane attitude, referenced to tunnel geometric centerline, deg

HELICOPTER MODEL AND TEST FACILITY

Helicopter Model

The general rotor model system (GRMS) in the Langley V/STOL tunnel was used for this investigation (ref. 17). The fuselage, 1 rotor diameter in length, was designed to enclose the basic model, transmission, and controls for the rotor system. A sketch of the helicopter model is provided in figure 1.

The main rotor used in this investigation had four blades mounted on a fully articulated hub. Rotor-blade construction was a graphite composite spar with balsa-ribbed, trailing-edge surfaces wrapped by fiberglass skins. The five blade-tip configurations are illustrated in figure 2. All rotor radii were identical except for the subwing-tip extension and the ogee tip. The latter had an increased radius to keep the same planform area as the square-tip blade. The chord distribution for this tip is presented in table I. The NACA 0012 airfoil section was maintained to the tip for the ogee-tip configuration, which resulted in a nonuniform taper. The swept-tapered tip used linear taper between each airfoil section. The dimensional characteristics of the rotor system may be found in table II.

The rotor hub was fully articulated, with cyclic and collective pitch on the blades controlled by a swash plate driven by remotely controlled actuators. Blade flapping and lead-lag angles were measured at the flapping-hinge offset which was 7.71-cm (3.04-in.) radius from the rotor axis. The rotor was driven by twin 67-kW (90-hp) electric motors through a common transmission. The entire system - rotor, transmission, and motor - was mounted on a six-component strain-gage balance within the model to measure rotor forces and moments. The fuselage

was on a separate balance, and the complete model was balance mounted. The limited aerodynamic data presented in this report are based on measurements obtained from the rotor balance alone.

Wind-Tunnel Facility

The model investigation was conducted in the Langley V/STOL tunnel. The facility includes an open-throat test chamber with a variable-wall configuration that is accomplished by raising the side walls and the ceiling. The dimensions of the rectangular jet entrance to the test chamber are 4.42 m (14.50 ft) high by 6.63 m (21.75 ft) wide. The ceiling height in the configuration is approximately 7.50 m (24.60 ft) above the test chamber floor.

Instrumentation

The acoustic transducers used for this investigation were 1.27-cm (0.50-in.) diameter condenser microphones fitted with standard nose cones. Seven microphones were positioned in the flow around the model, as shown in figure 3. A photograph of the model installed in the tunnel with floor treatment and microphones is presented in figure 4. The locations of these microphones relative to the rotor hub with the model at $\alpha = 0^{\circ}$ are presented in table III. Microphones 1, 2, and 3, considered to be in the near field, were mounted close to the fuselage in locations shown to be relatively sensitive to BVI blade slap (refs. 18 and 19). Microphones 5, 6, and 7, considered to be in the far field, were mounted ahead of the model as far as possible from the rotor, yet in the free-field environment of the facility, at about 30° below rotor tip-path plane. Microphone 6 was located on the helicopter centerline, and microphones 5 and 7 were located right and left of the centerline, respectively. The directivity of the BVI blade slap has been shown experimentally (refs. 1 and 20) and theoretically (ref. 21) to be a maximum at about 30° below rotor tip-path plane. Microphone 4 was positioned in the tip-path plane to measure thickness noise at high tip speeds. Signals from each microphone were fed through an amplifier attenuator and into a 14-channel, frequency-modulated (FM) tape recorder operating at 76.2 cm/sec (30.0 in/sec) tape speed. Blade azimuth and time code were also recorded.

An evaluation was conducted of the feasibility of obtaining realistic free-field noise measurements in this facility in the open-throat configuration (ref. 22). The results of a subsequent modeling study are available in reference 23. The recommended treatment to the floor, 12.7-cm (5.0-in.) thick aluminum panels filled with fiberglass, was installed. Open-cell polyurethane (10.2-cm (4.00-in.) thick) pads were installed on the ceiling. A follow-on evaluation of the effectiveness of this treatment was conducted and reported in reference 24. Results indicated that the hall radius was increased substantially and that accurate free-field measurements would be obtained up to about 0.3 m (1.0 ft) from any surface.

OPERATING PROCEDURES AND DATA REDUCTION

Operating Procedures

The occurrence of BVI impulsive noise has been shown to be at partial-power descending flight. It was, therefore, necessary to determine the flight conditions (tunnel velocity and simulated descent angle) critical to BVI generation for this particular rotor system. The square-tip rotor was used as the baseline to establish this flight envelope. At each tunnel velocity simulated, descent angle was varied, beginning at a climb condition with no observable BVI, through maximum BVI, to a high descent angle where BVI was not observed. This procedure provided a matrix of flight conditions (fig. 5) at which the rotor system with other tips installed was operated. Acoustic data acquisition at each flight condition for other tips was taken selectively based on on-line interpretation of the acoustic wave forms.

The procedure used to establish each flight condition was to set a constant tunnel velocity equal to the desired flight speed, thus setting the advance ratio ($\mu = V_\infty/V_T$). This was followed by adjusting collective, cyclics, and model angle of attack to obtain desired rotor lift (in this case, 1.78 kN (400 lb)), as well as balanced rotor pitching moment, rolling moment, and the desired descent angle ($\gamma \equiv \tan^{-1}$ (D/L)). With the rotor system at the desired condition, 30 sec of information from the microphones were recorded on the FM tape recorder. Corresponding model and tunnel information was recorded simultaneously on the tunnel computer data-acquisition system.

Critical to comparison of the noise resulting from tip shape are model position and attitude consistency at each matched test condition. Special consideration was given to carefully matching each test condition of the various tips to those with the square tip. Cyclic control and collective settings may have been different due to performance differences, but certain parameters were carefully matched as much as possible between tip tests. These parameters and estimated variations are: angle of attack, $\pm 0.5^\circ$; lift, ±44 N (±10 lb); pitching and rolling moment, ±560 cm-N (±50 in-lb); rotor rotational speed, ±5 rpm; and most importantly, TPP, $\pm 1^\circ$. The TPP must remain consistent between tip configurations at identical model operating conditions to minimize ambiguity related to directivity characteristics of the noise source. At each tunnel velocity tested, background noise measurements were made with blades off and rotor hub turning at the test condition (1200 rpm).

Data Reduction

Corrections for jet-boundary and blockage effects have been made to the aerodynamic parameters presented herein, except the tip-path-plane angle. These corrections in an open-throat tunnel primarily affect free-stream dynamic pressure (ref. 25).

Before and after the tests, "pink" and "white" noise signals were recorded to verify that the complete system (excluding the microphones) had a flat frequency response over the range of interest (50 to 10 000 Hz). All microphones were calibrated with a 125-dB piston phone at 250 Hz before and after each series of tests.

The acoustic data were analyzed for one-third-octave-band SPL, narrow-band SPL, and flight-scaled, overall A-weighted sound pressure level (OASPL). The analysis used is described in reference 26. Absolute values of peak-to-peak amplitude of the BVI impulses were determined. The one-third-octave-band and narrow-band analyses were obtained from a 2-sec (40-rotor revolution) digital record of each test condition. Each acoustic record was band-pass filtered at 50 to 10 000 Hz and digitized at the rate of 20 480 samples/sec. Each record was divided into a number of blocks, corresponding to 1 rotor revolution (0.05 sec), and triggered at the instant in time when the instrumented blade passed over the tail of the fuselage. This, with the digitizing rate of 20 480 samples/sec, resulted in a constant bandwidth of 19.5 Hz. The number of degrees of freedom obtained for this analysis is 80.

PRESENTATION OF RESULTS

The complete data set obtained during this investigation to bracket the complete envelope of BVI blade slap (see fig. 5) for each tip is available in reference 27. Samples and analyses of these data are presented as follows:

	Figure
Effect of descent angle variation on selected one-third-octave-band spectra, noise pressure time histories, and narrow-band spectra. $V_\infty \approx 51$ knots; square-tip shape	6 to 9
Sketch of typical wave forms at each microphone position	10
Direct comparison of noise generated by different tip shapes on helicopter model at similar operating conditions; $V_\infty \approx 51$ knots:	
One-third-octave-band analyses; microphone 3; $\gamma = 2.1^\circ$	11(a)
Pressure time histories; microphone 3; $\gamma = 2.1^\circ$	11(b)
One-third-octave-band analyses; microphone 5; $\gamma = 2.1^\circ$	11(c)
Pressure time histories; microphone 5; $\gamma = 2.1^\circ$	11(d)
One-third-octave-band analyses; microphone 3; $\gamma = 4.2^\circ$	11(e)
Pressure time histories; microphone 3; $\gamma = 4.2^\circ$	11(f)
One-third-octave-band analyses; microphone 5; $\gamma = 4.2^\circ$	11(g)
Pressure time histories; microphone 5; $\gamma = 4.2^\circ$	11(h)
Variation of peak-to-peak amplitude and flight-scaled, A-weighted OASPL with descent angle for different tips tested on helicopter model at similar operating conditions:	
$V_\infty \approx 51$ knots; microphones 3, 5, 6, and 7	12
$V_\infty \approx 56$ knots; microphones 3, 5, 6, and 7	13
$V_\infty \approx 61$ knots; microphones 3, 5, 6, and 7	14
$V_\infty \approx 66$ knots; microphones 3, 5, 6, and 7	15

Figure

$V_\infty \approx$ 71 knots; microphones 3, 5, 6, and 7 16
$V_\infty \approx$ 76 knots; microphones 3, 5, 6, and 7 17
$V_\infty \approx$ 82 knots; microphone 3 18
$V_\infty \approx$ 91 knots; microphone 3 19

Flight envelope of constant flight-scaled, A-weighted OASPL with various tips 20

Lateral-directivity characteristics of blade-slap intensity for square tip 21

DISCUSSION OF RESULTS

The BVI blade-slap phenomenon has been shown to be highly dependent on flight condition, particularly partial-power descents. The following analysis is structured to provide the reader with an understanding of the prime importance of the evaluation technique, as well as the comparison itself. Interpretation of the basic acoustic data can be very critical in evaluating even the existence of BVI blade slap. Though direct tip-to-tip comparison of the noise characteristics at identical flight conditions is important, it is shown that to effectively evaluate the relative effect of tip modification, the comparison must be presented over the complete flight envelope of importance. (See fig. 5.)

Interpretation of Basic Data

Samples of the basic noise data at $V_\infty \approx 51$ knots are presented in figures 6, 7, 8, and 9 for microphones 1, 3, 4, and 5, respectively. These data are presented for the square-tip configuration only. The complete set of data acquired for all tips at all flight velocities tested is available in reference 27. Each one-third-octave-band SPL spectrum plot contains both the data for all descent angles simulated at that velocity and background noise with blades removed but with hub turning at 1200 rpm. Selected pressure time histories and narrow-band spectra are presented for each microphone: one for no or light blade slap detected, and one for maximum blade slap detected (typified by an impulsive character (fig. 7(b)). These sample data are presented to illustrate the point discussed in reference 3 that one must be careful in identifying characteristic noise data as typically BVI.

Based on the analyses in references 19 and 27 of BVI induced blade-slap data in the frequency domain, it would appear that the one-third-octave-band spectra data measured at microphone 1 (fig. 6(a)) indicate the presence of blade slap. This is suggested by the broad-band increase in SPL above about the third harmonic of blade-passage frequency. This effect can be seen to be a direct function of descent angle. Pressure time-history information (fig. 6(b)), however, does not indicate a distinct impulsive character for the high descent angle even though the phenomenon causing the higher broad-band noise levels is periodic in nature, as evidenced by the harmonic content in the

narrow-band analysis of figure 6(d). This result would seem to indicate that it was difficult to conclude that BVI blade slap was experienced. The same result is evident in the data acquired at microphone 4 (fig. 8). However, as mentioned before, the prime directivity for BVI blade slap has been shown to be in the lower front quadrant relative to the tip-path plane (microphone 5), and the interaction primarily occurs on the advancing side of the rotor (microphone 3).

One-third-octave-band spectra data measured at microphone 3 (fig. 7(a)) also show the increase in broad-band SPL above the third harmonic of the blade-passage frequency. Pressure time-history information (fig. 7(b)) conclusively indicates the presence of BVI blade slap, with three distinct interactions evident at the descent angle for which this broad-band SPL was the greatest ($\gamma = 2.15^{\circ}$). In fact, if a microphone is properly located in the critical directivity pattern of BVI, the recorded pressure time history will always indicate blade slap if present. Narrow-band analysis of these data (fig. 7(d)), however, does not indicate harmonic content. This is probably the result of variability in the impulse characteristics from blade to blade and revolution to revolution, or simply the fact that more than one impulse occurred at each blade passage. Data measured at microphone 5 also indicate the presence of BVI blade slap.

These data analyses indicate the importance of microphone position in determining the effects of BVI blade slap. A sketch of the kind of wave form experienced at each location with blade slap is presented in figure 10. That measured at microphone 4 (fig. 8), near tip-path plane, was obviously not in the most sensitive directivity field of the phenomenon, and that measured at microphone position 1 (fig. 6), under the retreating side of the rotor, probably was a general periodic turbulent wake interaction with no distinct vortex interaction. At any rate, BVI blade slap was generated and most effectively measured at microphones 3 and 5. Microphones 5, 6, and 7 were all located in the lower front quadrant but were laterally spaced to provide some information about the lateral-directivity characteristics of BVI blade slap. These data (available in ref. 3) are very similar except in directivity characteristics, which will be addressed later.

Similar conclusions can be drawn from the basic BVI blade-slap characteristics generated at other simulated flight velocities and with different tips installed. However, the most important objective of this investigation was the determination of the effect of tip modification on the intensity of the measured BVI blade slap. The following discussion will be limited to data acquired at microphones 3 and 5 for reasons previously cited.

Tip-Shape Comparison at Similar Model Operating Conditions

Some effect of tip-shape configuration on acoustic characteristics can be evaluated with tips installed, with the rotor system operating at similar flight conditions. However, as discussed in references 9 and 10, the tip change can shift the position of maximum BVI blade-slap intensity to a different portion of the flight envelope. The effect of tip shape at similar operating conditions is considered first.

A direct comparison of noise associated with the five tip configurations as measured by microphones 3 and 5 at descent angles of about 2.1° and 4.2° is presented in figure 11. At a descent angle of 2.1°, the effect of tip shape on one-third-octave-band analyses (as measured by microphone 3, fig. 11(a)) indicates that the ogee and subwing tips are slightly quieter than the square tip in the frequency range important for blade slap, and the end-plate tip is noisier. These general conclusions also can be drawn from the data obtained from microphone 5 (fig. 11(c)). Generally, the ogee, subwing, and swept-tapered tips generate no more noise than the square tip across the spectrum. In general, at the higher descent angle (figs. 11(e) and 11(g)), one can draw different conclusions.

It is possible to continue this direct comparison for each flight speed and each descent angle tested. Obviously, this would lead to confusion and a lack of general understanding of the tip effects. Results presented in reference 3 show that the maximum value of blade slap for each tip does not occur at the same descent angle. That is, the descent angle for maximum blade slap for the square tip occurs between 2.15° and 4.23°, for the ogee tip between 2.07° and 4.24°, for the subwing tip between 1.15° and 2.15°, for the swept-tapered tip between 1.03° and 2.24°, and for the end-plate tip between 1.01° and 2.14°. Thus, even though the model operating conditions are nearly identical among the tip configurations, the conditions (descent angle) for maximum blade slap are not consistent.

The examination of acoustic wave-form details at a single test operating condition does allow the determination of some causes of acoustic differences for different tip-configuration changes. At a descent angle of 2.1° (measured by microphone 3 (fig. 11(b)), the ogee tip caused a reduction in magnitude and a broadening of the second impulse at each blade passage. All three impulses have shifted position relative to time zero compared with the square-tip data, which indicates a slight change in location of the blade-vortex interactions away from this microphone. Therefore, some of the amplitude reduction can be applied to decay versus distance of this noise. The data from the subwing tip show a slight reduction in impulse amplitudes and a shift in the position of the impulses, relative to time zero, towards the microphone. Thus, since these interactions are slightly closer to the microphone, the true impulse intensity at the source is probably even lower than what figure 11(b) indicates. The data for the swept-tapered and end-plate tips indicate that the first impulse at each blade passage has been narrowed, and the position of the interactions has probably been shifted closer to the microphone. This is especially true for the end-plate tip. In addition, data for the end-plate tip show that the third impulse at each blade passage has been greatly reduced in width and increased in magnitude, which explains the higher SPL at high frequencies in figure 11(a).

Tip-Shape Noise Variation With Descent Angle

Data for tunnel velocities of 51 to 91 knots are summarized in a manner which describes the impulse peak amplitude, impulse width, and number of

impulses and what might be heard subjectively by an observer. The impulse peak amplitude, of course, can be handled as done previously (ref. 9), by presenting the variation of peak amplitude of impulse with descent condition. (In this case, the largest at each blade passage averaged over 2 rotor revolutions.) The width of the impulse and the number of impulses can best be described for the mass of information enclosed herein by relating OASPL to descent angle. Since human response to this noise phenomenon is the primary concern, this OASPL should be weighted to the ear response capability. One method has been shown to be the A-weighted frequency scale (refs. 27 to 30). In this case, model-scale frequencies must be converted to realistic flight-scaled frequencies before the A-weighting can be applied to the data. This was accomplished by assuming that the model was 1/4 scale of a flight vehicle. This Strouhal scaling assumes that noise sources depend on rotor-tip Mach number and linear dimensions. These A-weighted OASPL variations with descent angle for each tip should provide a measure of the pulse-width characteristics and analysis of subjective response by an observer.

The variations of peak amplitude and flight-scaled, A-weighted OASPL with descent angle are presented in figures 12 to 19. These data are presented for microphones 3, 5, 6, and 7 for velocities of 51, 56, 61, 66, 71, and 76 knots; only data from microphone 3 are presented at 82 and 91 knots. Data from all tip configurations are presented on each figure except for velocities above 71 knots, at which the end-plate tip was not tested. Unfortunately, data for the ogee tip at velocity of 91 knots was not obtained. Lateral-directivity characteristics of blade slap as measured by microphones 5, 6, and 7 will be discussed later; therefore, the comparison of tip-shape effects discussed in this section will be limited to microphones 3 and 5. The data for the square tip will be considered the baseline for comparison purposes with other tip configurations.

Ogee tip.- In general, the ogee tip was effective in reducing the maximum peak amplitude of the blade-slap impulse for all the free-stream velocities tested (as much as 35 percent at V_∞ = 56 knots, fig. 13(a)), as measured in the near field by microphone 3. It was also effective in reducing the range of descent angles over which the impulse was measurable. However, at a free-stream velocity of 66 knots, the ogee tip was able to reduce only slightly the impulse peak amplitude. The flight-scaled, A-weighted OASPL shows a general reduction in SPL across the velocity range except at a free-stream velocity of 82 knots and at low descent angles at V_∞ = 51 knots where slight increases were measured. The maximum level of this OASPL variation with descent-angle decrease was as much as 3 dBA for free-stream velocities of 51, 56, 61, and 76 knots. A shift in the descent-angle value for maximum impulse as was found in reference 9 for the ogee tip was only observed in this investigation for peak-amplitude values at a free-stream velocity of 51 knots. It is important to remind the reader that this was a four-bladed rotor as compared with the two-bladed rotor used in references 6 and 9.

The impulse peak-amplitude data obtained in the acoustic far field, as measured by microphone 5 (figs. 12(b), 13(b), 14(b), 15(b), 16(b), 17(b), and 18), generally are consistent with that data measured under the rotor

disk, with a few exceptions. That is, the maximum value of peak amplitude was decreased by the ogee tip by as much as 25 percent at $V_\infty = 66$ knots (fig. 15(b)). An exception to this was found at $V_\infty = 71$ knots (fig. 16(b)), where the maximum peak amplitude was increased by 21 percent. The flight-scaled OASPL indicates different trends in the far field than in the near field; that is, the ogee tip did not effectively alter the variation of OASPL with descent angle from that measured by the square tip except at free-stream velocities of 56 and 61 knots (figs. 13(b) and 14(b)), where these values were decreased by as much as 3 dBA. In fact, at certain velocities (66 and 82 knots), the values of OASPL were slightly higher than that measured for the square tip.

Subwing tip.- The subwing tip, in general, was effective in reducing the peak amplitudes of blade slap as much as the ogee tip (as measured by microphone 3). At most free-stream velocities, it reduced the maximum of the peak amplitude a slight degree more than did the ogee tip. One exception can be seen at $V_\infty = 82$ knots (fig. 18) where the maximum value of peak amplitude was even higher than that obtained with the square tip. In general, the values obtained of flight-scaled, A-weighted OASPL were even lower than those for the ogee tip (even at $V_\infty = 82$ knots). This tip reduced the maximum OASPL measured by as much as 4 dBA (fig. 13(a)), as compared with the square tip. In the far field (as measured by microphone 5), the decrease in peak amplitude and OASPL was also noted to be even more than that obtained by the ogee tip. Two exceptions to this case are evident, however. At $V_\infty = 51$ knots (fig. 12(b)) and low descent angles, the data indicate higher peak amplitudes and OASPL than the square and ogee tips, and at $V_\infty = 76$ knots (fig. 17(b)) and very high descent angles, a slight increase in peak amplitude and OASPL is evident.

Swept-tapered tip.- The swept-tapered tip was effective in reducing the maximum peak amplitude as measured in the near field (microphone 3) at all free-stream velocities except 76 knots (fig. 17(a)) and 82 knots (fig. 18). The flight-scaled, A-weighted OASPL at 82 and 91 knots of free-stream velocity indicates a small region of higher OASPL than the square tip. In the far field (microphone 5), the swept-tapered tip was observed to cause even a greater reduction in maximum peak amplitude than did the ogee and subwing tips. This is even true for the general reduction in peak-amplitude variation with descent angle except at low descent angles at all velocities tested. At free-stream velocities of 51 knots (fig. 12(b)), 76 knots (fig. 17(b)), 82 knots (fig. 18), and 91 knots (fig. 19) and at low descent angles, the swept-tapered tip generated higher values of peak amplitude than did the square tip. In general, the measured values of the flight-scaled, A-weighted OASPL were observed to be lower by as much as 4.5 dBA compared with the square tip (fig. 13(b)), even more than that of the ogee and subwing tips except at low descent angles for free-stream velocities of 71 knots (fig. 16(b)), 76 knots (fig. 17(b)).

End-plate tip.- The effect of the end-plate tip as measured by microphone 3 can be seen to be relatively poor in reducing the maximum peak amplitude and flight-scaled, A-weighted OASPL. In fact, this maximum peak amplitude was greatly increased by as much as 50 percent at 71 knots (fig. 16(a)). This was also observed in the flight-scaled, A-weighted OASPL values. The general

effect on peak amplitude and OASPL was to shift the descent angle range of large impulse effect to lower descent angles (climb conditions as related to the rotor shaft axis) and to increase the effect of the impulse. In the far field (microphone 5), the end-plate tip caused a large increase in peak amplitude and OASPL at low descent angles that was consistent with that measured in the near field, except at $V_\infty = 51$ knots (fig. 12(b)), where no large increase in maximum peak amplitude or OASPL was observed. The greatest effect can be seen at a free-stream velocity of 66 knots (fig. 15(b)). An increase in maximum peak amplitude of 26 percent and an increase in maximum OASPL of 4 dBA were observed.

Noise Flight Envelope Comparison

A more general indication of the effect of tip shape on noise generation can be seen in figure 20. The data in figures 12 to 19 have been used to obtain the region of flight envelope at which the OASPL was greater than (or the same as) 103 dBA (microphone 3) or 92 dBA (microphone 5). At each free-stream velocity, the descent angles which bound the higher noise values were found. These boundaries are presented in terms of descent velocity in figure 20(a) for microphone 3 and figure 20(b) for microphone 5, as lines of constant OASPL as a function of free-stream velocity. For a particular tip shape, the OASPL values between these lines are greater than (or the same as) the reference value of OASPL on each figure. For clarity, each figure has four sections, each with data for the baseline tip (square) and one of the other tips. Maximum OASPL is indicated on each section. For the near-field microphone (no. 3), figure 20(a) shows a reduction in the flight envelope for constant OASPL of 103 dBA for the ogee and subwing tip, with an attendant reduction in peak OASPL as compared with the square tip. In fact, the subwing tip indicates a region of little to no blade slap (i.e., $V_\infty = 75$ knots). The swept-tapered tip data show very little reduction, and the end-plate tip data show an increase in flight envelope and peak OASPL. The data (fig. 20(b)) for the far-field microphone (no. 5), however, indicate that a considerable reduction in the flight envelope of constant OASPL and peak OASPL was achieved with the swept-tapered tip. Little or no reduction is evident with the ogee and subwing tips, and again, an increase in these values can be seen for the end-plate tip.

Lateral-Directivity Characteristics

Microphones 5, 6, and 7 were installed laterally in the far field (see fig. 3(b)), primarily to provide some information about the lateral-directivity characteristics of the measured blade slap. These data were not intended to provide a complete picture of the directivity of blade slap and should be regarded only as an indication of the trends in lateral-directivity characteristics 1.3 rotor diameters ahead of, and about 30° down from, the center of the rotor tip-path plane.

Figure 21 presents these data for the square-tip configuration at free-stream velocities of 51.4, 56.2, 61.3, 65.7, 71.1, and 75.9 knots. Peak ampli-

tude of the impulse and flight-scaled, A-weighted OASPL is presented for microphones 5, 6, and 7 as a function of descent angle. These figures show that impulsiveness, rated by peak amplitude and OASPL, is greatest (as much as 4 dBA (fig. 21(b)) on the advancing side of the rotor for descent angles greater than 2° (1° for V_{∞} = 65.7 knots) and is greatly reduced on the retreating side. At descent angles less than those previously quoted and greater than 0°, the impulsiveness is greater on the retreating side and on the centerline of the rotor, but at a much lower increment of about 2.5 dBA (fig. 20(d)). These lateral-directivity characteristics are typical of all tip configurations tested.

CONCLUDING REMARKS

An experimental investigation has been conducted in the Langley V/STOL tunnel to determine the overall character of blade-slap noise induced by blade-vortex interaction as affected by tip configuration. Four configurations tested, which have been shown to reduce vortex peak velocities, were an ogee tip, a subwing tip, a 60° swept-tapered tip, and an end-plate tip. A square tip was tested to establish a baseline for comparison. Evaluations of the acoustic performance are presented for each rotor configuration operating at identical conditions.

Blade slap induced by blade-vortex interaction is highly sensitive to descent angle and is evidenced in one-third-octave-band and narrow-band analyses by an increase in the sound pressure level above the third harmonic of blade-passage frequency. Care must be exercised in attributing this increase to blade slap without evidence of such in the pressure time histories. In this investigation, the three distinct multiple impulses generated by blade-vortex interaction and observed at each blade passage did not result in the typical distinct high harmonic content in the narrow-band analyses.

The ogee tip, as measured in the near field by microphone 3 on the right side of the fuselage, generally was effective in reducing the maximum level of the impulse peak by as much as 35 percent at a free-stream velocity V_{∞} of 56 knots. Flight-scaled, A-weighted OASPL analyses indicated a general reduction throughout the free-stream velocity spectrum, with maximum level reduction of as much as 3 dBA. Generally, far-field, A-weighted OASPL analyses indicated very little change in noise generation as compared with the square tip.

The subwing tip, as measured in the near field and the far field, generally was more effective than the ogee tip in reducing peak amplitudes and OASPL measurements (as much as 4 dBA (V_{∞} = 56 knots)).

The swept-tapered tip was generally the most effective in reducing the far-field maximum peak amplitude of the impulses and the flight-scaled, A-weighted OASPL measurements (as much as 4.5 dBA (V_{∞} = 56 knots)). However, in the near field, results indicate that the reductions were not as effective as the reductions caused by the ogee and subwing tips.

The end-plate tip, as measured in the near field and the far field, actually increased the maximum impulse peak amplitude by as much as 50 percent (V_∞ = 71 knots) and the OASPL measurements by as much as 4 dBA (V_∞ = 66 knots).

The lateral-directivity characteristics of blade slap as measured in the far field for these tests indicated that, at rotor-shaft-axes descent angles of 2° and greater, the measured blade slap was greater on the advancing blade side of the helicopter path. For descent angles between 0° and 2°, blade slap on the retreating blade side was greater but to a lesser degree.

Langley Research Center
National Aeronautics and Space Administration
Hampton, VA 23665
December 10, 1979

REFERENCES

1. Lowson, M. V.; and Ollerhead, J. B.: Studies of Helicopter Rotor Noise. USAAVLABS Tech. Rep. 68-60, U.S. Army, Jan. 1969.

2. Langenbucher, V.: Noise Phenomena With Helicopter Rotors and Possibilities of Noise Reduction. ESA TT-244, Feb. 1976.

3. Hoad, Danny Robert: Helicopter Blade-Slap Noise Variation With Tip Vortex Modification. M.S. Thesis, The George Washington Univ., 1979.

4. Ward, John F.; and Young, Warren H., Jr.: A Summary of Current Research in Rotor Unsteady Aerodynamics With Emphasis on Work at Langley Research Center. Aerodynamics of Rotary Wings, AGARD-CP-111, Feb. 1973, pp. 10-1 - 10-20.

5. Balcerak, John C.; and Feller, Raymond F.: Vortex Modification by Mass Injection and by Tip Geometry Variation. USAAMRDL Tech. Rep. 73-45, U.S. Army, June 1973. (Available from DDC as AD 771 966.)

6. Landgrebe, Anton J.; and Bellinger, E. Dean: Experimental Investigation of Model Variable-Geometry and Ogee Tip Rotors. NASA CR-2275, 1974.

7. Balcerak, John C.; and Feller, Raymond F.: Effect of Sweep Angle on the Pressure Distributions and Effectiveness of the Ogee Tip in Diffusing a Line Vortex. NASA CR-132355, 1973.

8. Rorke, James B.; and Moffitt, Robert C.: Wind Tunnel Simulation of Full Scale Vortices. NASA CR-2180, 1973.

9. Mantay, Wayne R.; Campbell, Richard L.; and Shidler, Phillip A.: Full-Scale Testing of an Ogee Tip Rotor. Helicopter Acoustics, NASA CP-2052, Pt. I, 1978, pp. 277-308.

10. Tangler, James L.: The Design and Testing of a Tip To Reduce Blade Slap. Preprint No. 963, 31st Annual National Forum, American Helicopter Soc., May 1975.

11. Tangler, James L.: Experimental Investigation of the Subwing Tip and Its Vortex Structure. NASA CR-3058, 1978.

12. Spencer, R. H.; Sternfeld, H., Jr.; and McCormick, B. W.: Tip Vortex Core Thickening for Application to Helicopter Rotor Noise Reduction. USA AVLABS Tech. Rep. 66-1, U.S. Army, Sept. 1966. (Available from DDC as AD 644 317.)

13. Spencer, R. H.: Noise Evaluation of CH-47A Helicopter With Rotor Blade Tip Covers Having 60° Leading Edge Sweepback. Doc. No. D8-0349. (AF 33(657)13157), Boeing Co., Apr. 1966.

14. Tangler, James L.; Wohlfeld, Robert M.; and Miley, Stan J.: An Experimental Investigation of Vortex Stability, Tip Shapes, Compressibility, and Noise for Hovering Model Rotors. NASA CR-2305, 1973.

15. White, Richard P., Jr.: Vortex Dissipator. U.S. Patent 3,845,918, Nov. 1974.

16. Mechtly, E. A.: The International System of Units - Physical Constants and Conversion Factors (Second Revision). NASA SP-7012, 1973.

17. Wilson, John C.: A General Rotor Model System for Wind-Tunnel Investigations. J. Aircr., vol. 14, no. 7, July 1977, pp. 639-643.

18. Cox, C. R.: Helicopter Rotor Aerodynamic and Aeroacoustic Environments. AIAA Preprint 77-1338, Oct. 1977.

19. Hoad, Danny R.; and Greene, George C.: Helicopter Noise Research at the Langley V/STOL Tunnel. Helicopter Acoustics, NASA CP-2052, Pt. I, 1978, pp. 181-204.

20. Schmitz, F. H.; and Boxwell, D. A.: In-Flight Far-Field Measurement of Helicopter Impulsive Noise. Preprint No. 1062, Proceedings of the 32nd Annual National V/STOL Forum, American Helicopter Soc., Inc., May 1976.

21. Widnall, S.: Helicopter Noise Due to Blade-Vortex Interaction. J. Acoust. Soc. America, vol. 50, Pt. 2, July 1971, pp. 354-365.

22. Vér, István L.: Acoustical Evaluation of the NASA Langley V/STOL Wind Tunnel. NASA CR-145087, [1976].

23. Vér, István L.; Andersen, Douglas W.; and Bliss, Donald B.: Acoustical Modeling Study of the Open Test Section of the NASA Langley V/STOL Wind Tunnel. NASA CR-145005, 1975.

24. Theobald, M. A.: Evaluation of the Acoustic Measurement Capability of the NASA Langley V/STOL Wind Tunnel Open Test Section With Acoustically Absorbent Ceiling and Floor Treatments. Rep. No. 3820, (Contract NAS1-14611-18), Bolt Beranek and Newman, Inc., May 1978.

25. Heyson, Harry H.: Use of Superposition in Digital Computers To Obtain Wind-Tunnel Interference Factors for Arbitrary Configurations, With Particular Reference to V/STOL Models. NASA TR R-302, 1969.

26. Brown, Thomas J.; Brown, Christine G.; and Hardin, Jay C.: Program for the Analysis of Time Series. NASA TM X-2988, 1974.

27. Hoad, Danny R.: An Experimental Investigation of the Effect of Rotor Tip Shape on Helicopter Blade-Slap Noise. NASA TM-80066, 1979.

28. Sternfeld, Harry, Jr.; and Doyle, Linda Bukowski: Evaluation of the Annoyance Due to Helicopter Rotor Noise. NASA CR-3001, 1978.

29. Leverton, John W.; Southwood, B. J.; and Pike, A. C.: Rating Helicopter Noise. Helicopter Acoustics, NASA CP-2052, Pt. II, 1978, pp. 419-437.

30. Powell, Clemans, A.: Annoyance Due to Simulated Blade-Slap Noise. Helicopter Acoustics, NASA CP-2052, Pt. II, 1978, pp. 463-477.

TABLE I.- OGEE PLANFORM AND TRAILING-EDGE COORDINATES

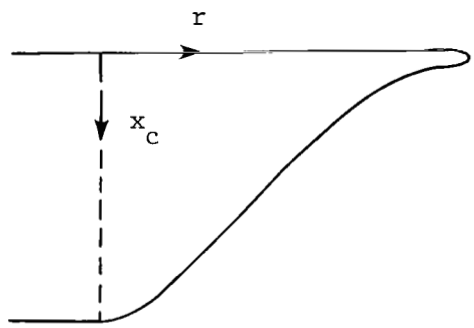

x_c/c	r/c
1.000	0
.990	.090
.970	.140
.950	.180
.920	.215
.900	.235
.850	.285
.800	.335
.750	.385
.700	.435
.650	.485
.600	.535
.550	.585
.500	.635
.450	.685
.400	.735
.350	.785

x_c/c	r/c
0.300	0.835
.250	.885
.225	.915
.200	.950
.175	.985
.150	1.025
.125	1.070
.115	1.100
.100	1.130
.090	1.160
.080	1.180
.070	1.210
.060	1.250
.050	1.290
.040	1.350
.020	1.370
0	1.350

TABLE II.- ROTOR CHARACTERISTICS

Number of blades	4
Airfoil section	NACA 0012
Radius, m (ft) (square tip)	1.574 (5.165)
Blade chord, m (ft)	0.1077 (0.3533)
Twist, deg	-8
Solidity (square tip)	0.0871
Root cutout, m (ft)	0.3148 (1.033)

TABLE III.- MICROPHONE LOCATIONS RELATIVE TO ROTOR HUB

WITH MODEL AT AN ANGLE OF ATTACK OF 0°

Microphone system	x		y		z	
	m	ft	m	ft	m	ft
1	0.015	0.05	-0.491	-1.61	-0.485	-1.59
2	-1.289	-4.23	.052	.17	-.485	-1.59
3	.018	.06	.515	1.69	-.482	-1.58
4	-3.536	-11.60	2.603	8.54	.079	.26
5	-3.536	-11.60	1.238	4.06	-2.124	-6.97
6	-3.530	-11.58	-.043	-.14	-2.121	-6.96
7	-3.514	-11.53	-1.280	-4.20	-2.131	-6.99

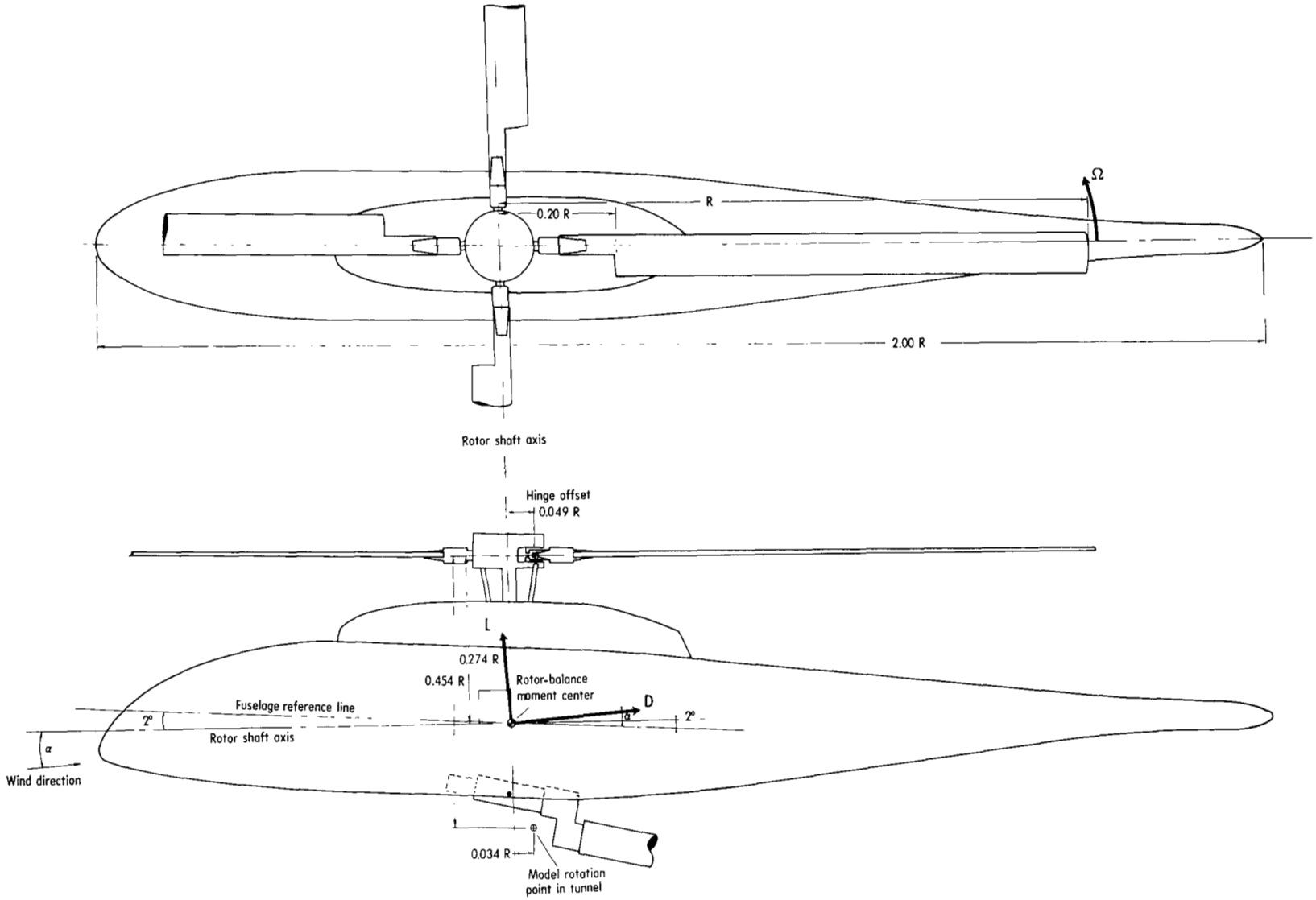

Figure 1.- Sketch of helicopter model with square tips installed.

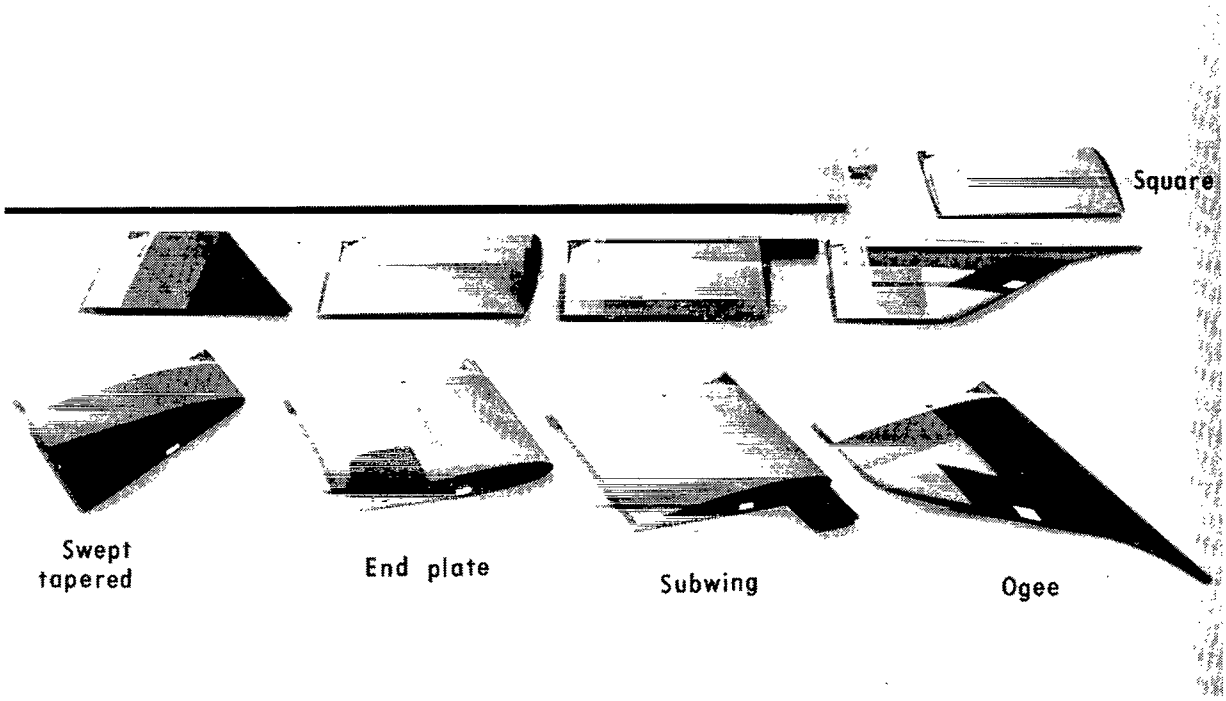

(a) Photograph.

Figure 2.- Tip configurations tested.

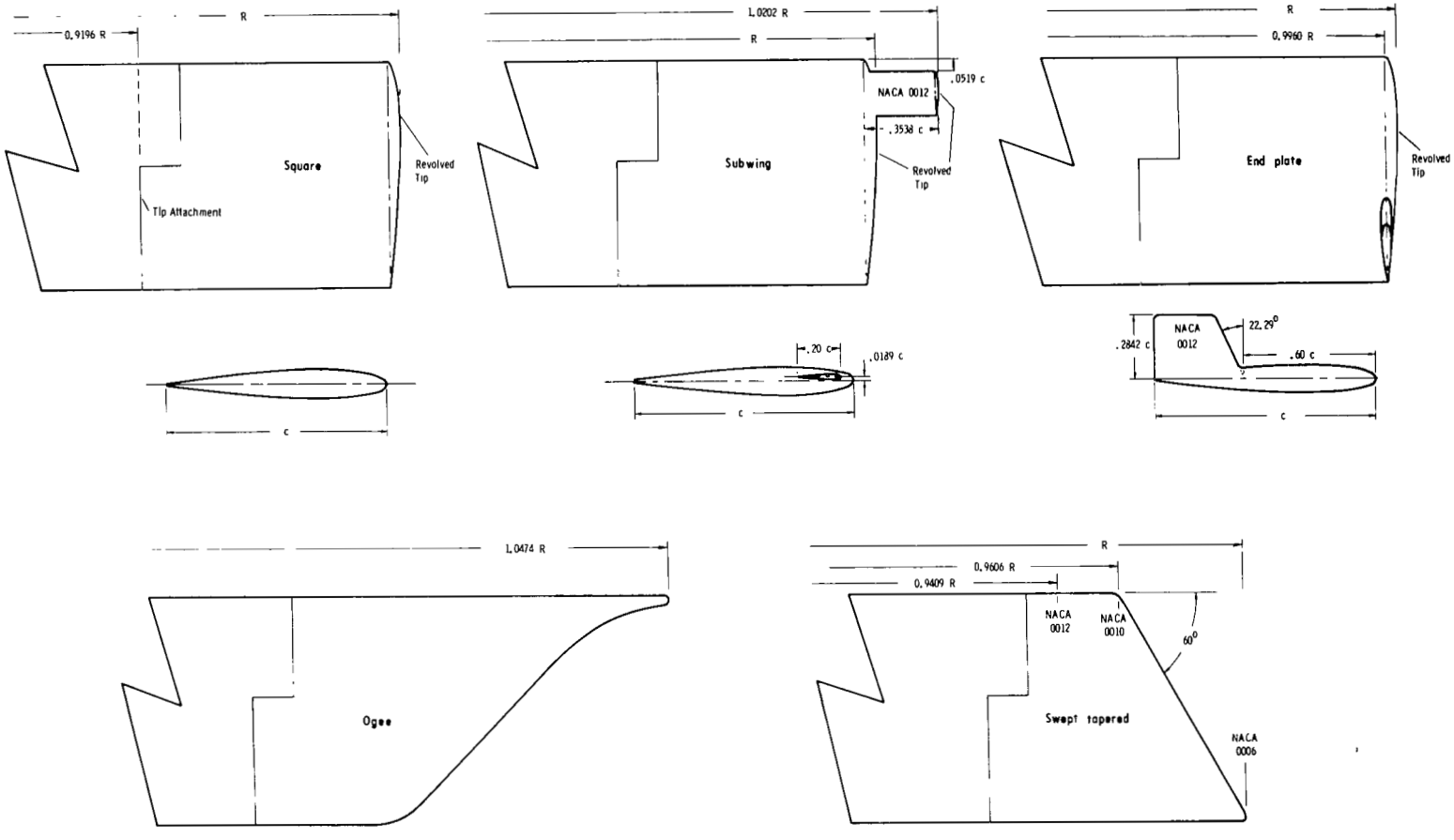

(b) Sketch and dimensional characteristics.

Figure 2.- Concluded.

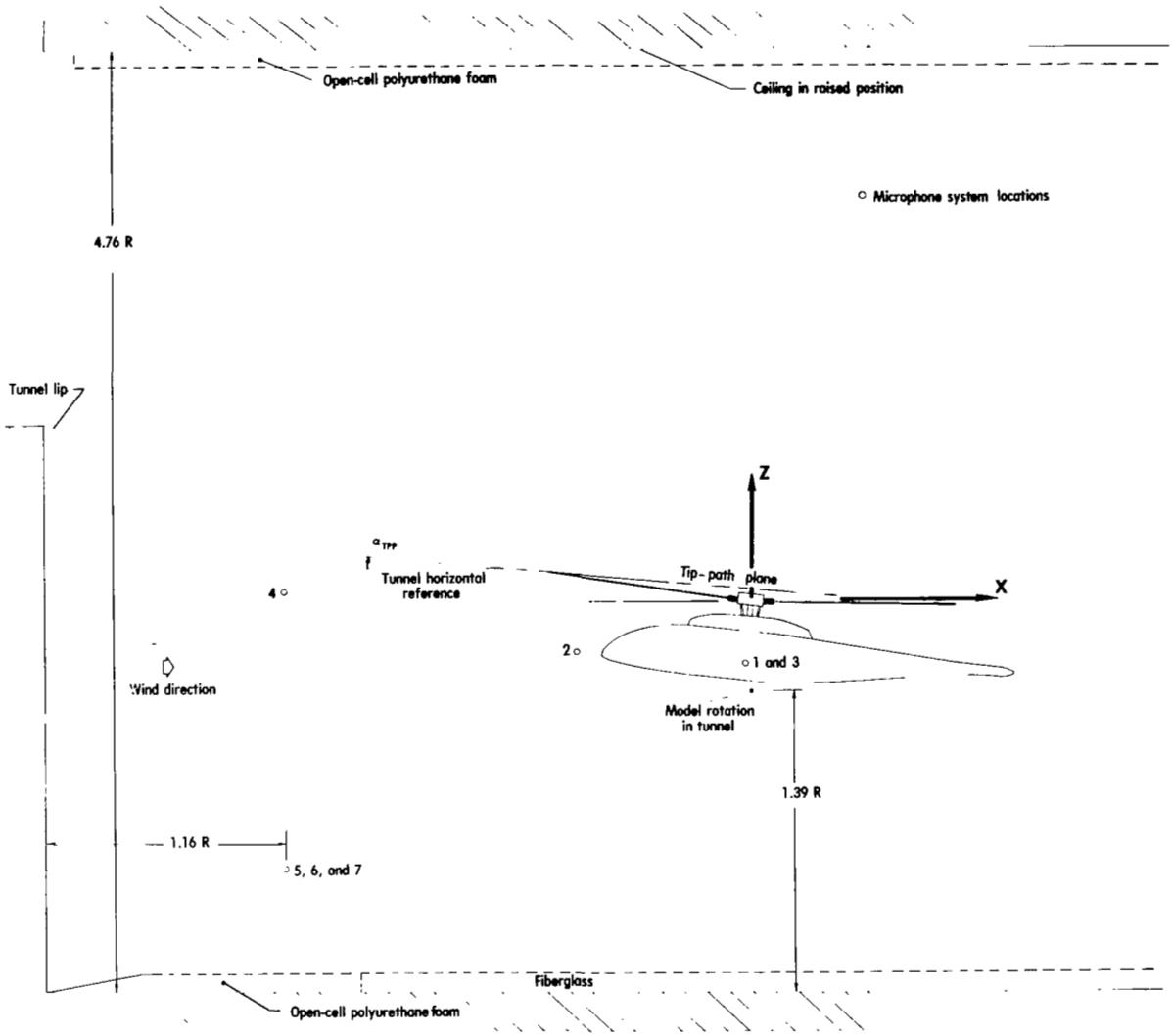

(a) Side view.

Figure 3.- Sketch of relative positions of model and microphone installed in tunnel.

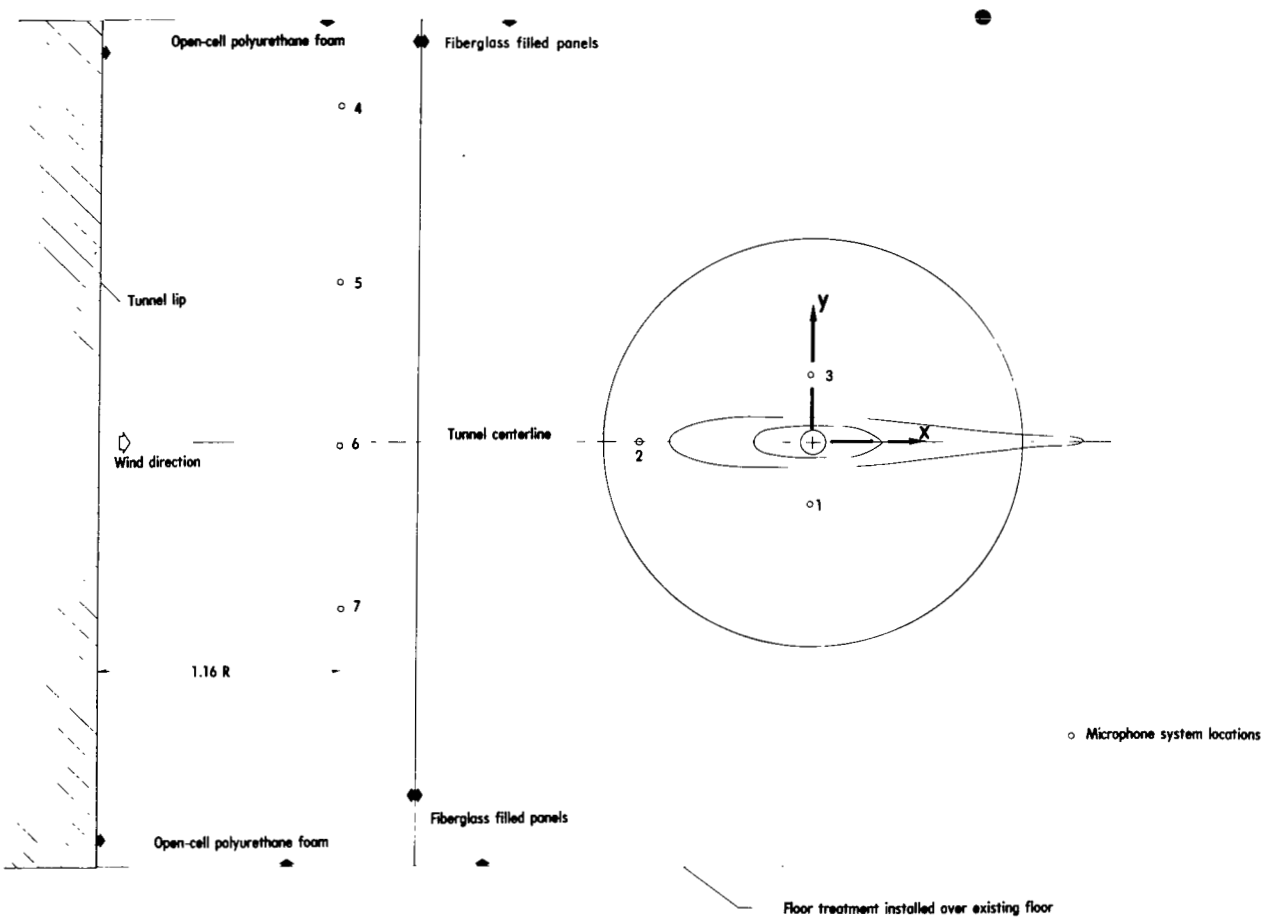

(b) Top view.

Figure 3.- Concluded.

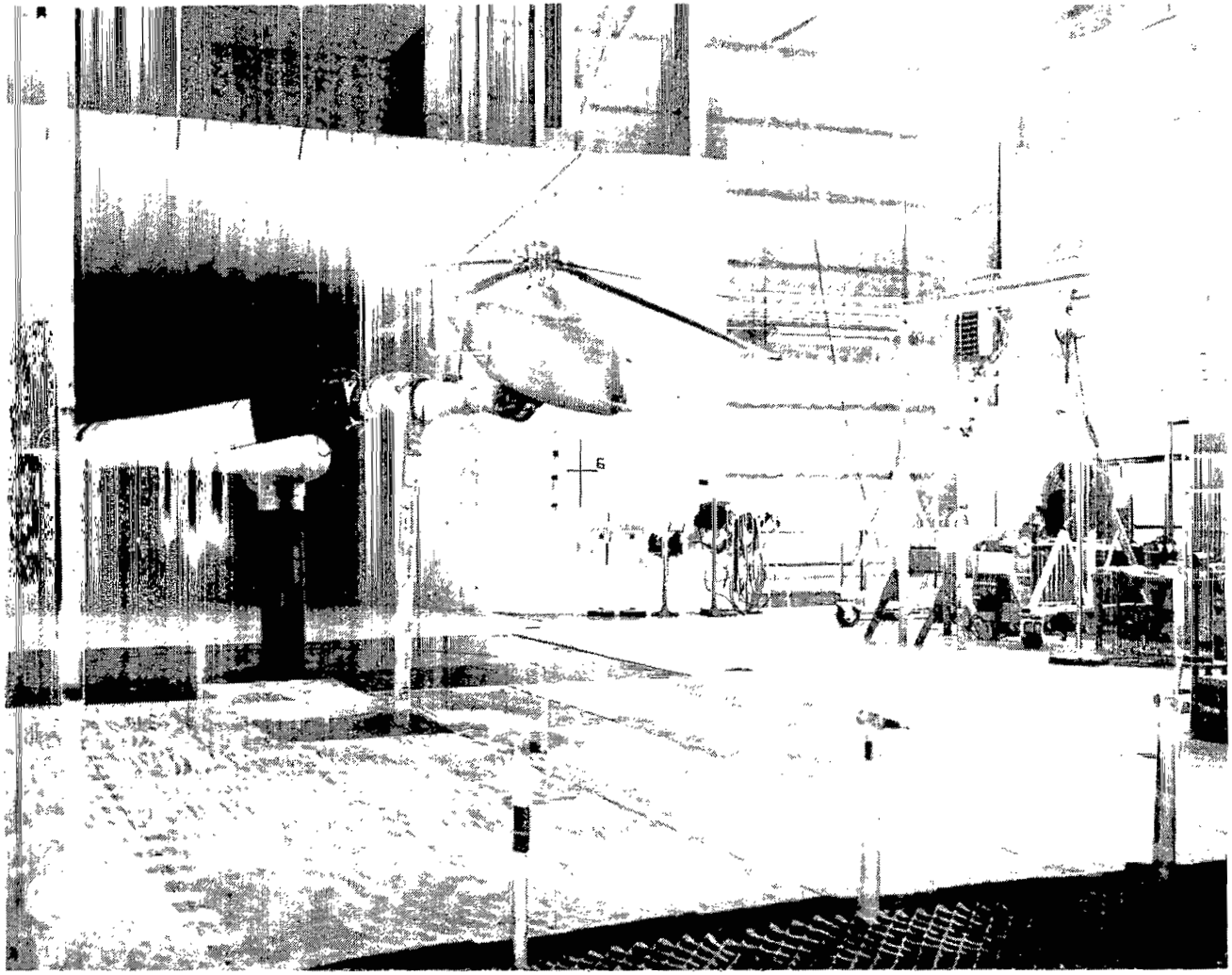

L-78-4820

Figure 4.- Model in tunnel with treatment and microphones installed.

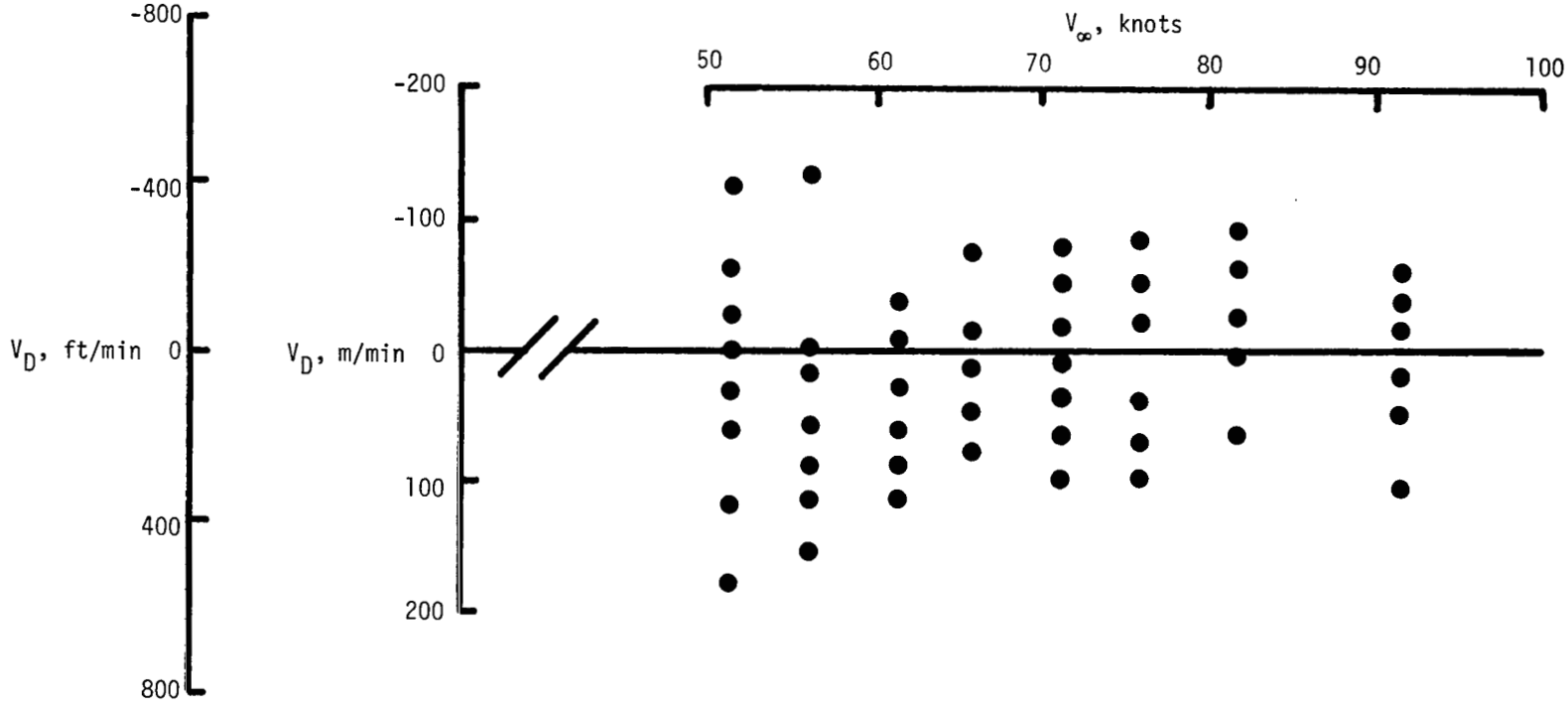

Figure 5.- Test conditions at which square-tip noise data were acquired. Descent velocity based on rotor balance data.

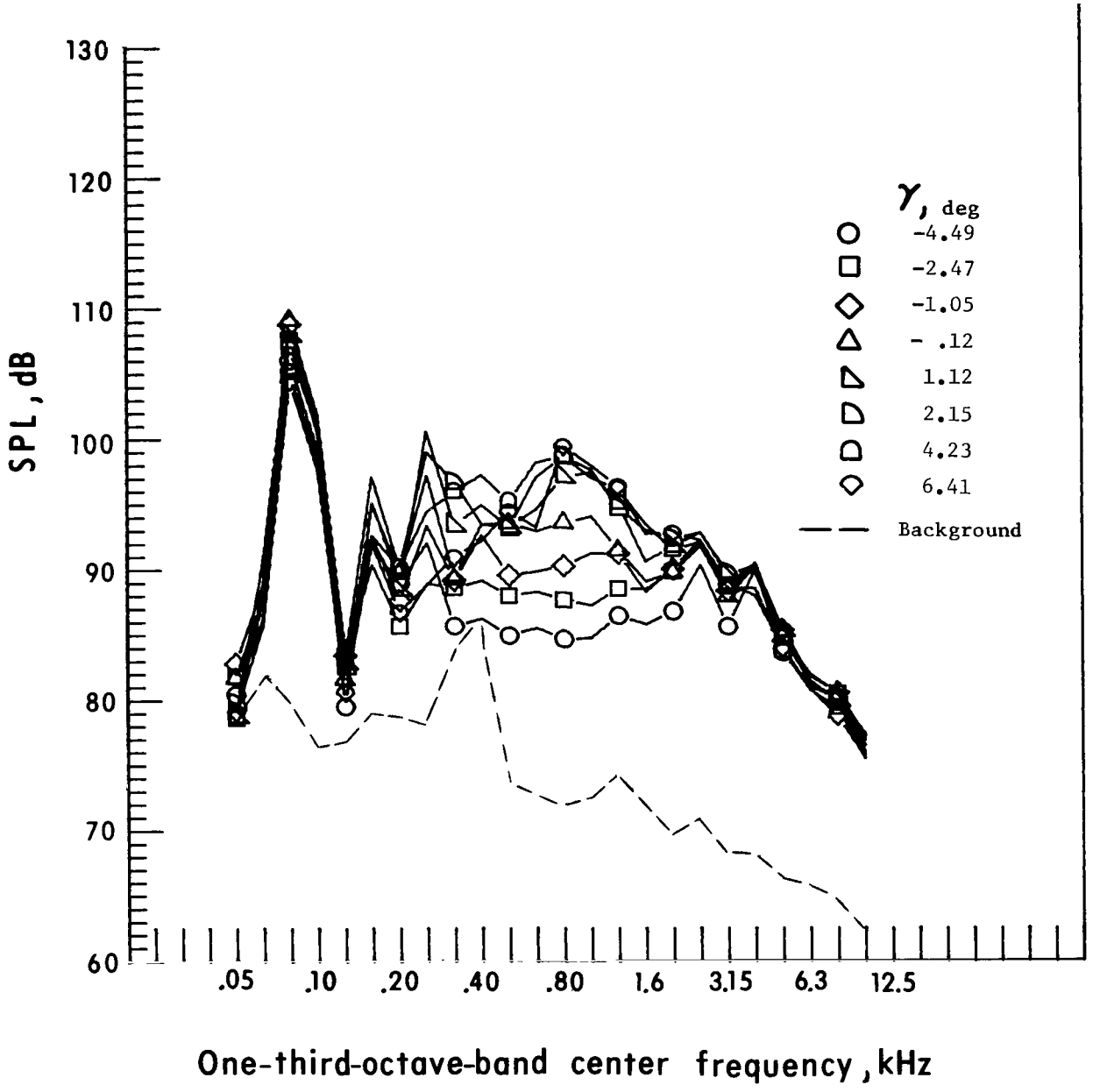

(a) One-third-octave-band spectra.

Figure 6.- Effect of descent-angle variation on noise generated by helicopter model as measured by microphone 1. V_∞ = 51.4 knots; square tips.

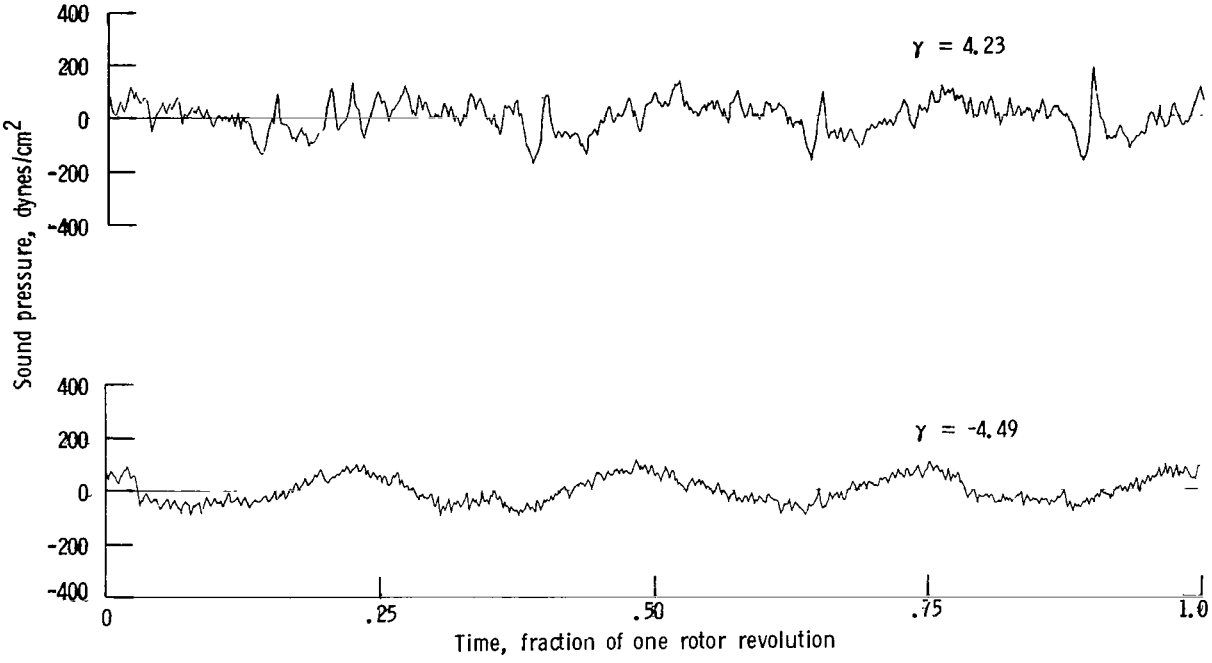

(b) Pressure time histories.

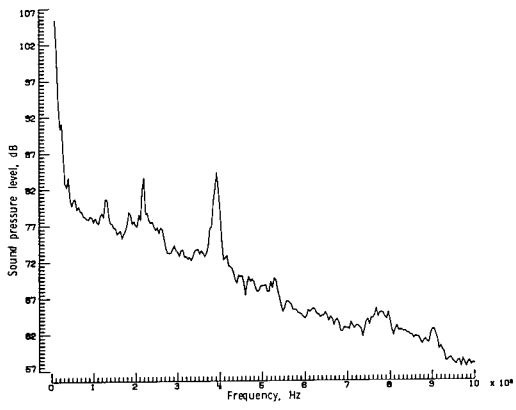

(c) Narrow-band analysis for $\gamma = -4.49^{\circ}$.

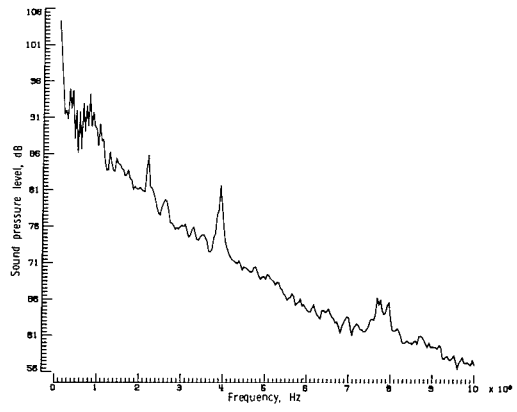

(d) Narrow-band analysis for $\gamma = 4.23^{\circ}$.

Figure 6.- Concluded.

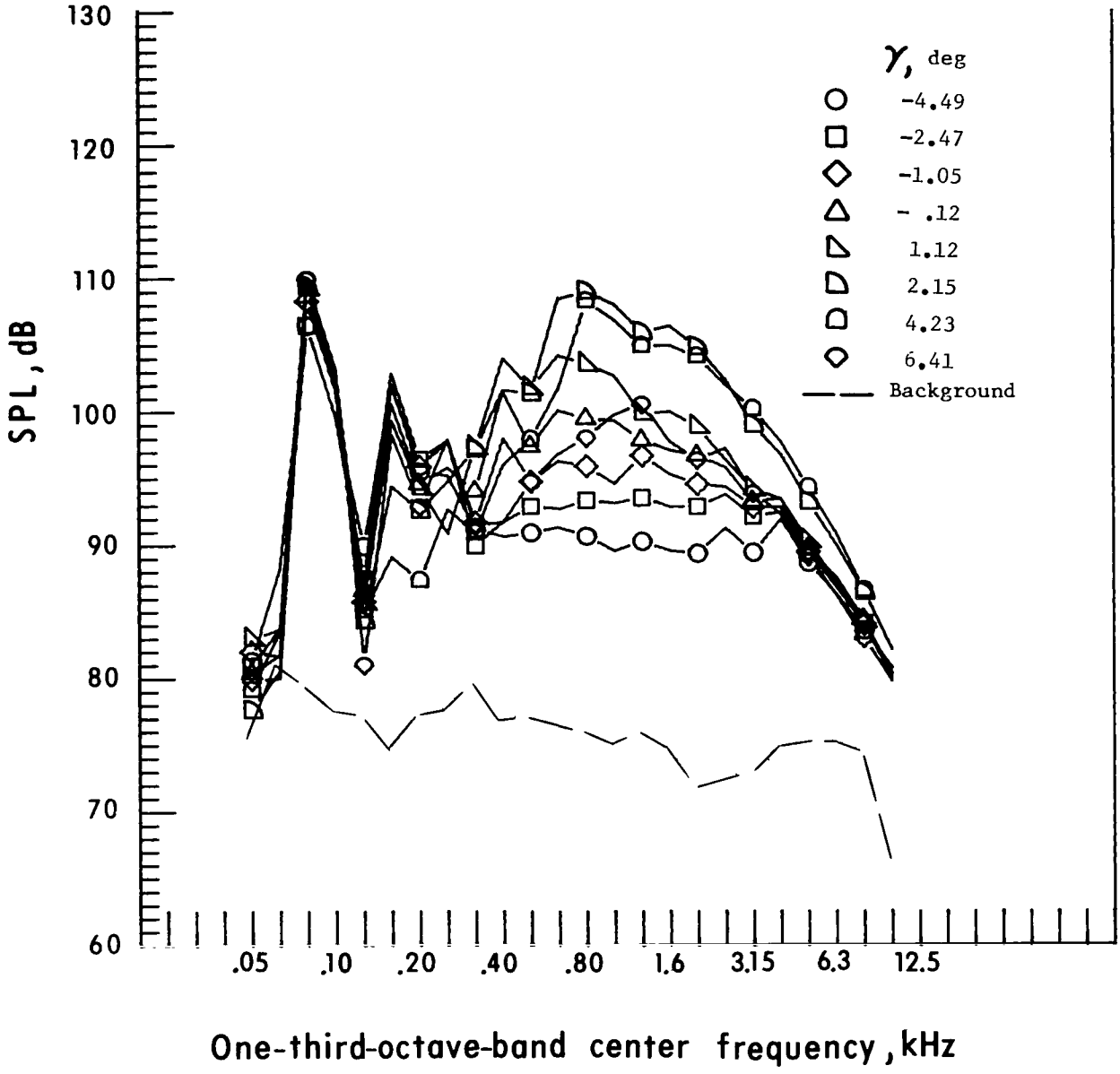

(a) One-third-octave-band spectra.

Figure 7.- Effect of descent-angle variation on noise generated by helicopter model as measured by microphone 3. V_∞ = 51.4 knots; square tips.

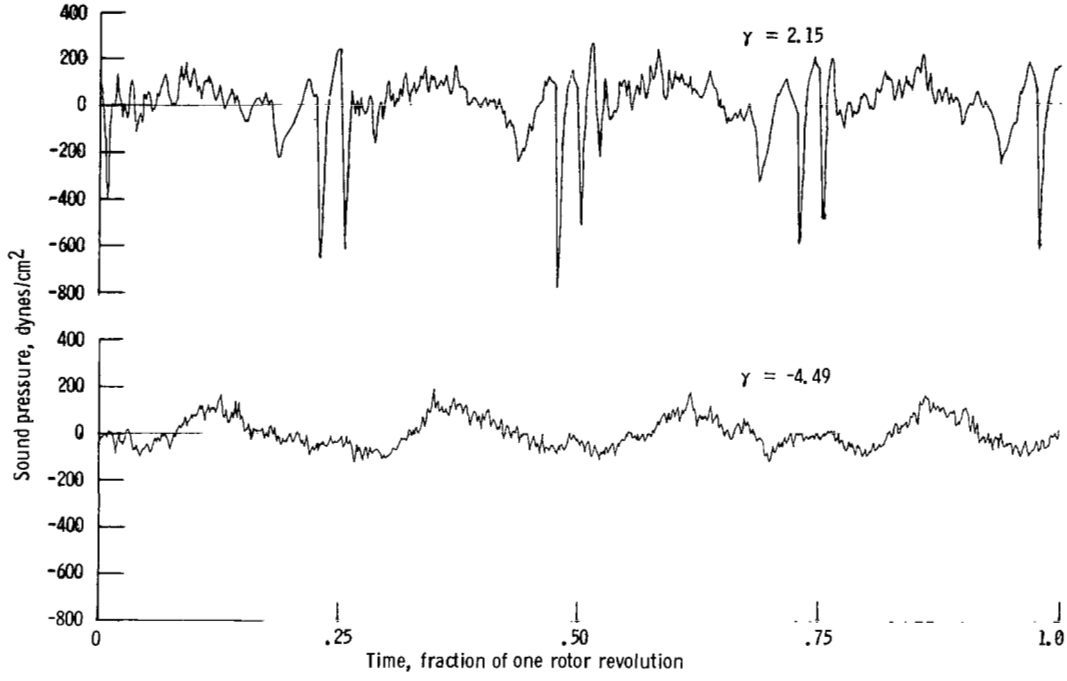

(b) Pressure time histories.

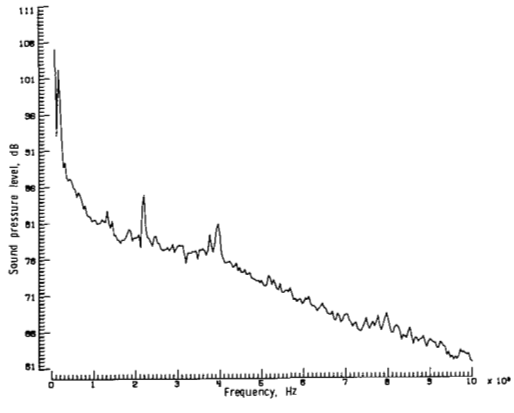

(c) Narrow-band analysis for $\gamma = -4.49^{\circ}$.

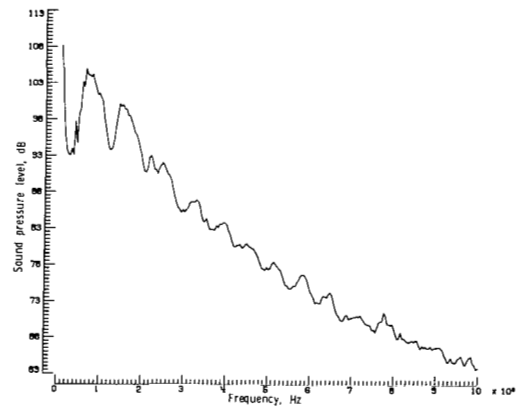

(d) Narrow-band analysis for $\gamma = 2.15^{\circ}$.

Figure 7.- Concluded.

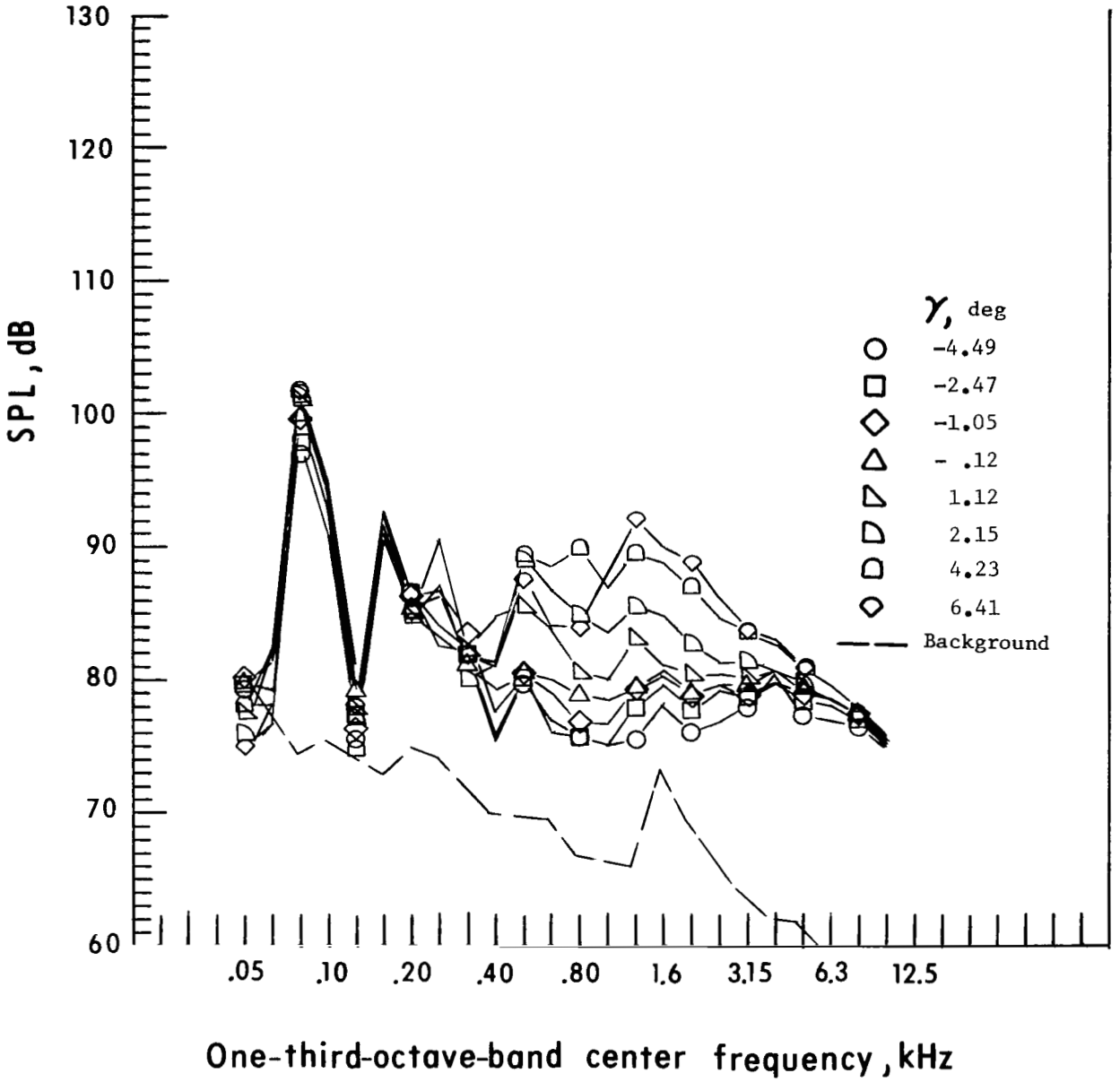

(a) One-third-octave-band spectra.

Figure 8.- Effect of descent-angle variation on noise generated by helicopter model as measured by microphone 4. V_∞ = 51.4 knots; square tips.

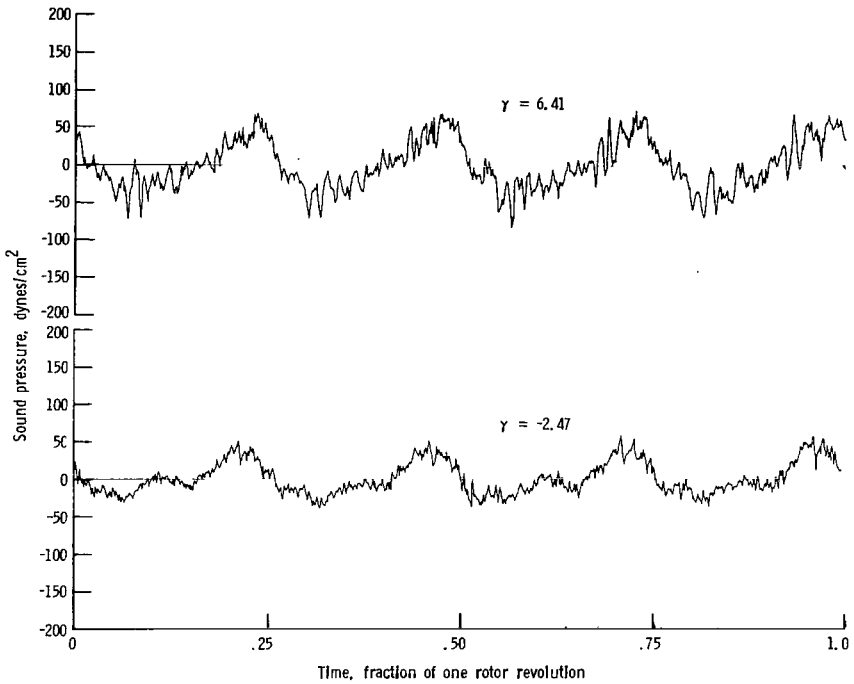

(b) Pressure time histories.

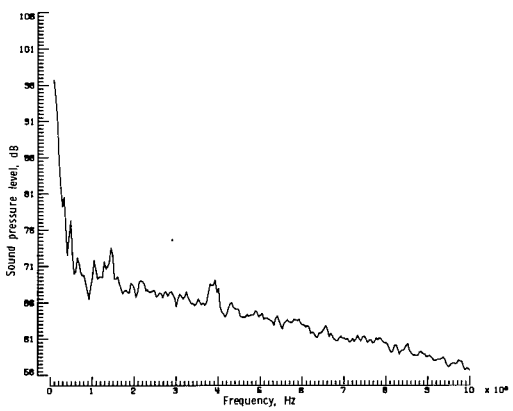

(c) Narrow-band analysis for $\gamma = -2.47^{\circ}$.

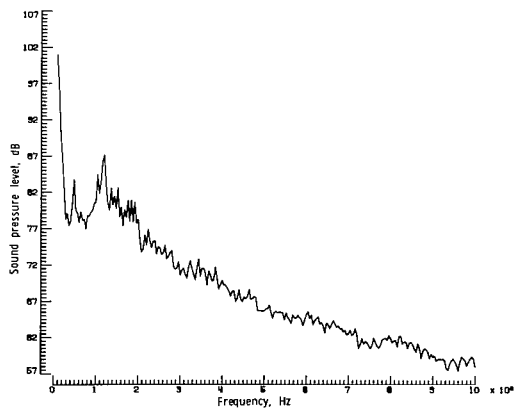

(d) Narrow-band analysis for $\gamma = 6.41^{\circ}$.

Figure 8.- Concluded.

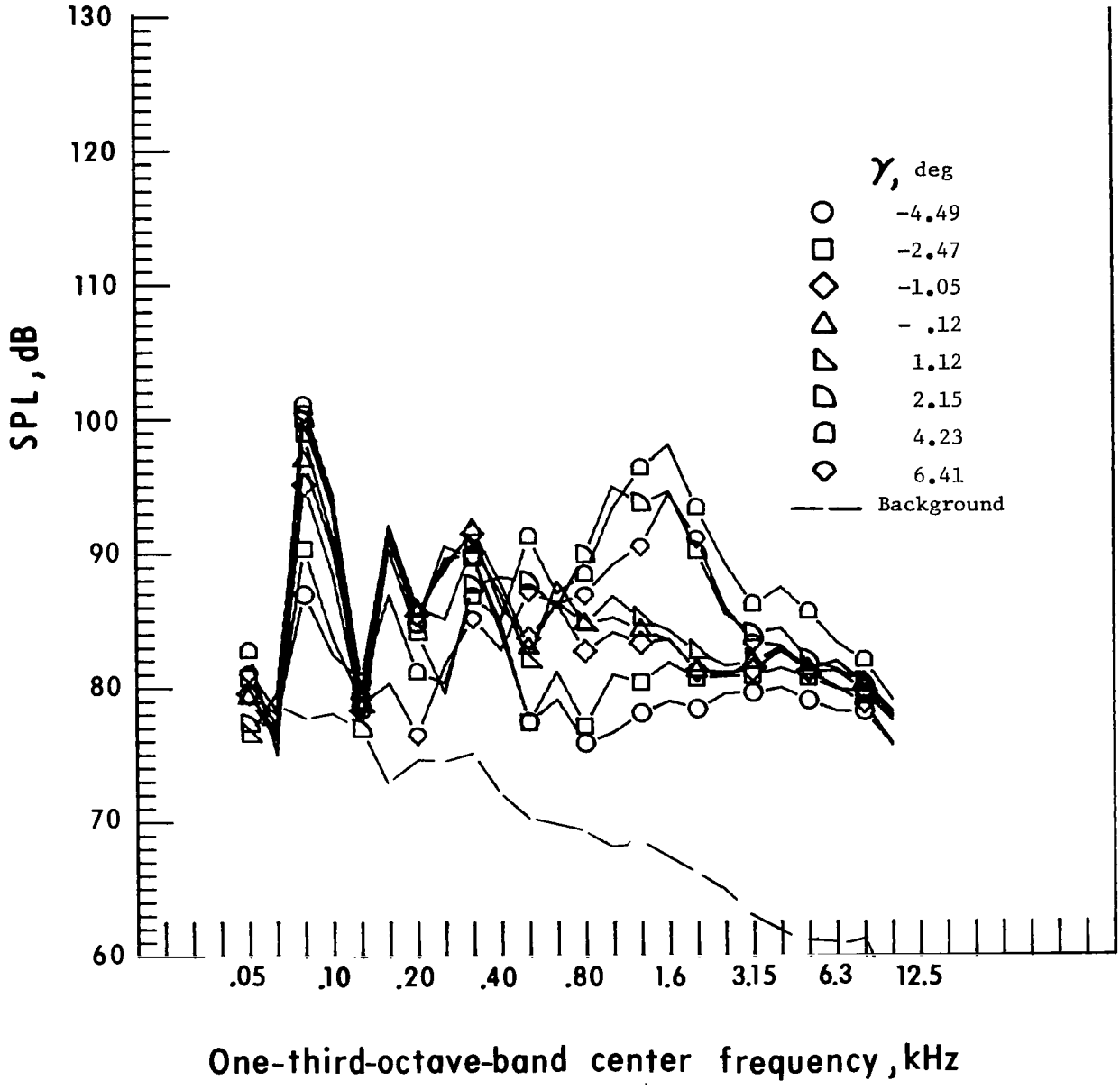

(a) One-third-octave-band spectra.

Figure 9.- Effect of descent-angle variation on noise generated by helicopter model as measured by microphone 5. V_∞ = 51.4 knots; square tips.

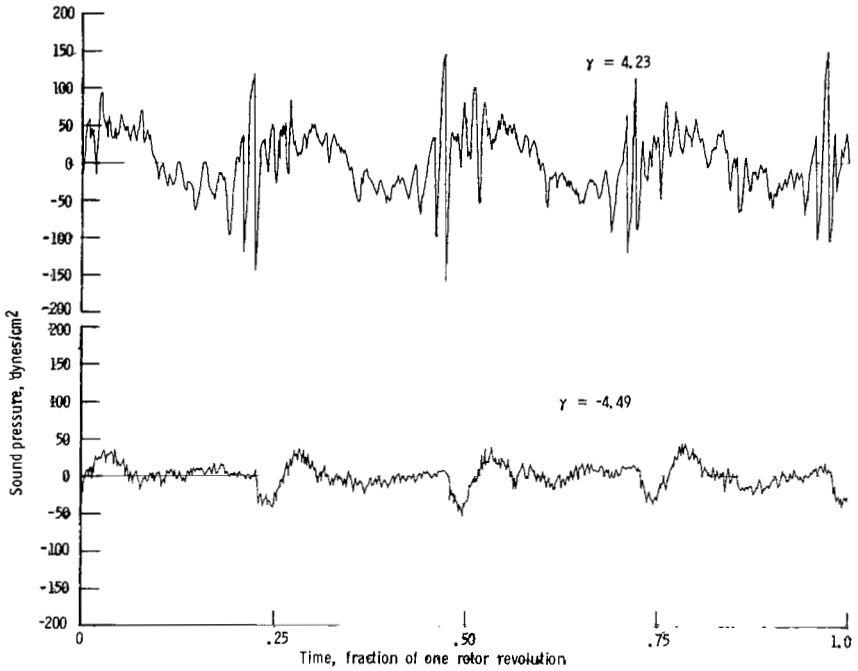

(b) Pressure time histories.

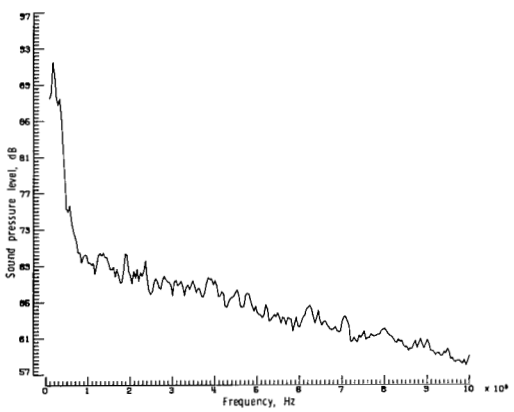

(c) Narrow-band analysis for $\gamma = -4.49^{\circ}$.

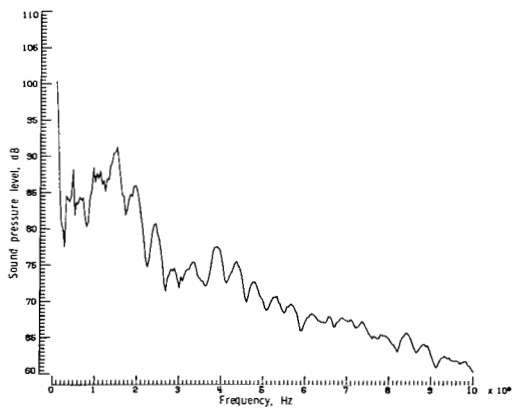

(d) Narrow-band analysis for $\gamma = 4.23^{\circ}$.

Figure 9.- Concluded.

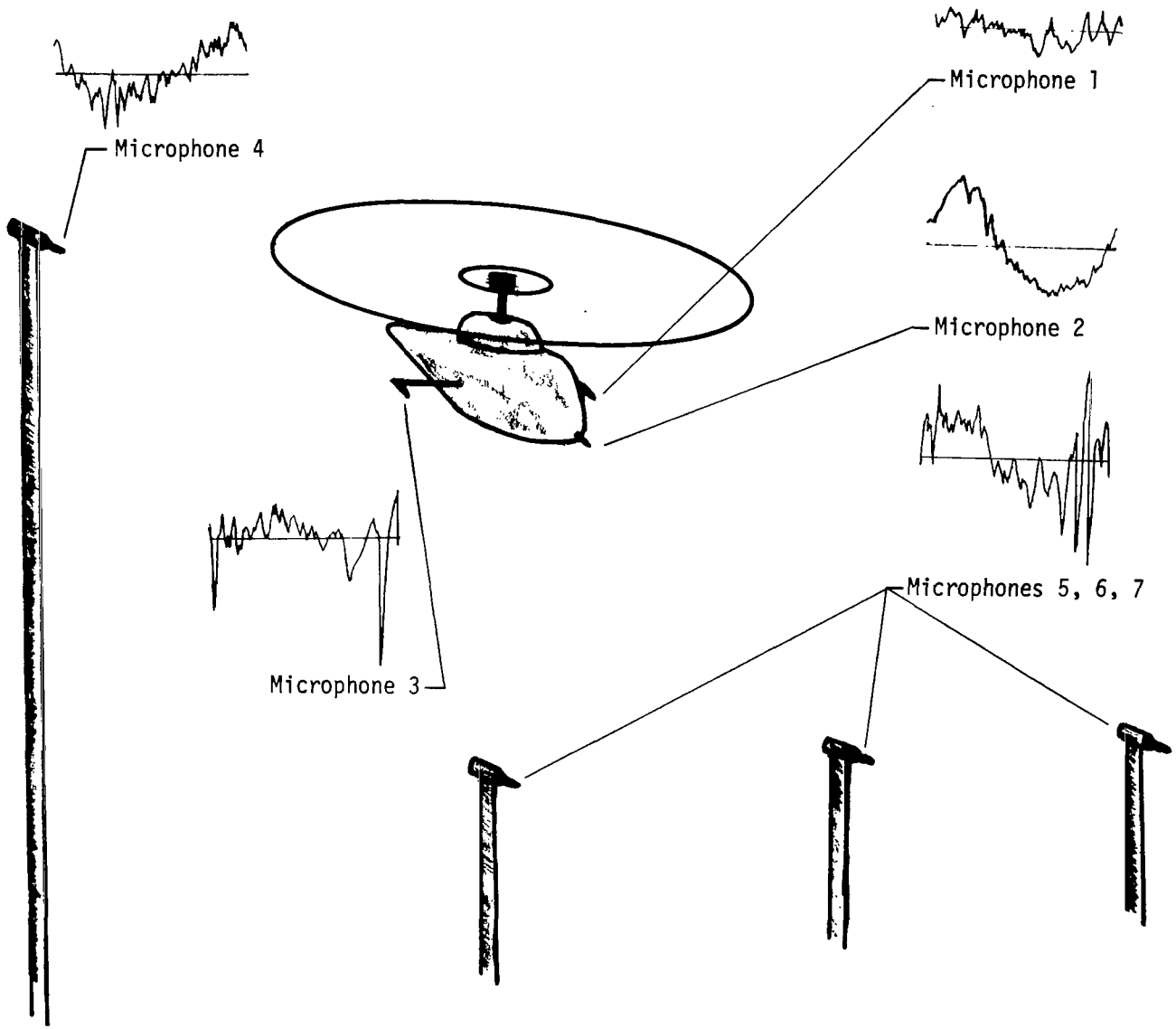

Figure 10.- Typical acoustic wave forms obtained at each microphone with blade slap generated. One blade passage shown.

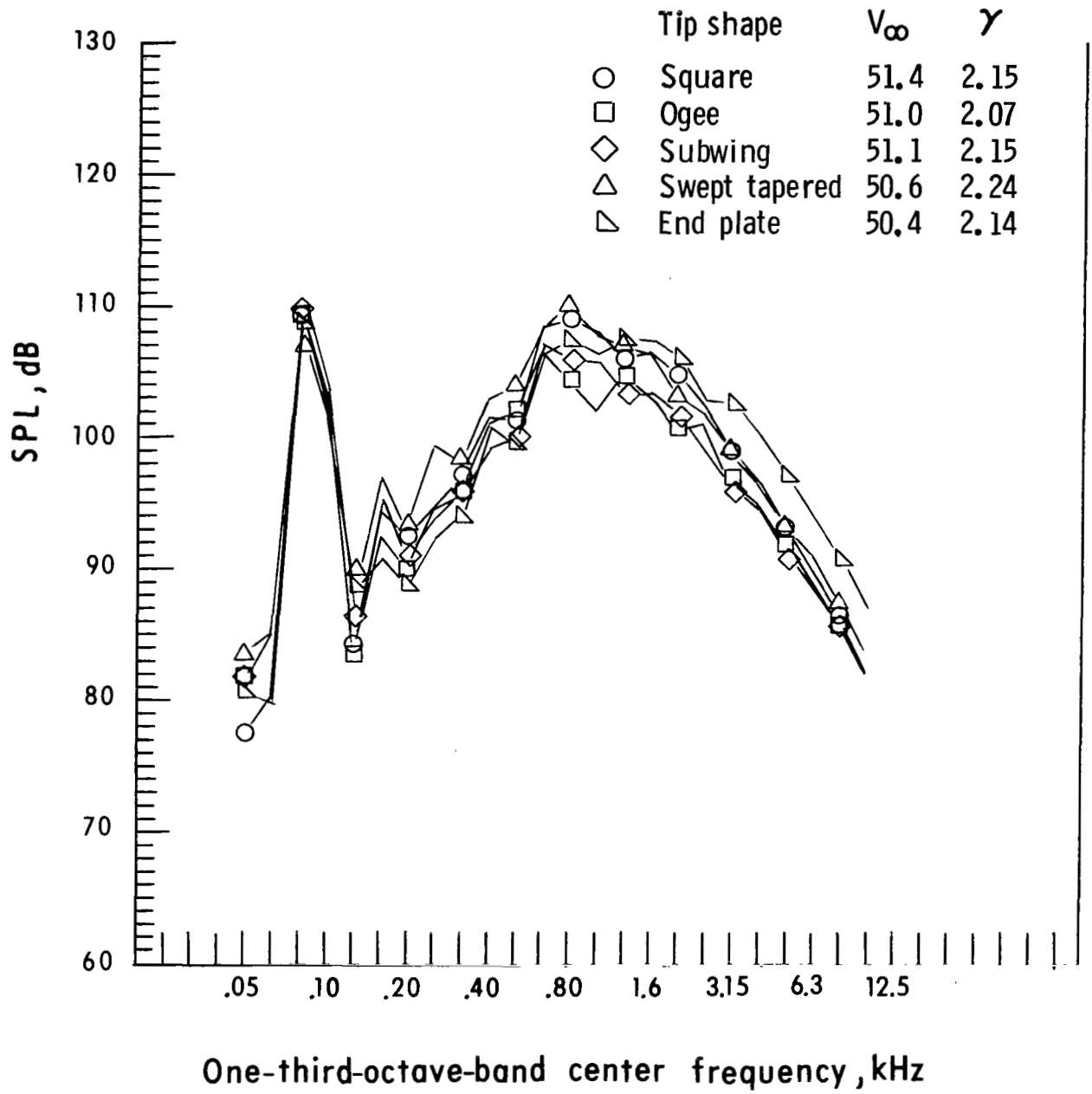

(a) Microphone 3; $\gamma \approx 2.1^{\circ}$.

Figure 11.- Effect of tip shape on noise generated by helicopter model at similar operating conditions.

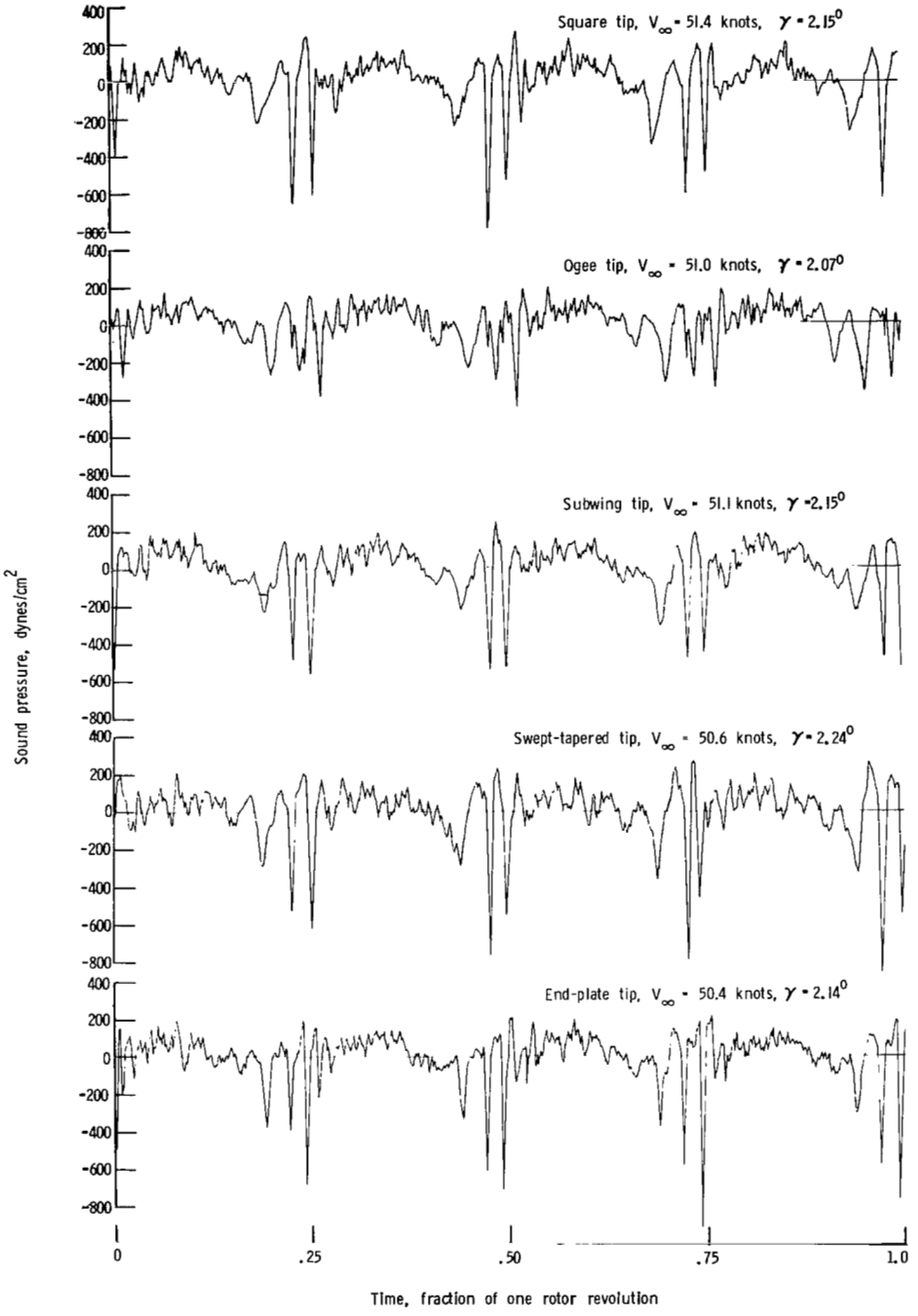

(b) Pressure time histories for microphone 3 at $\gamma \approx 2.1^{\circ}$.

Figure 11.- Continued.

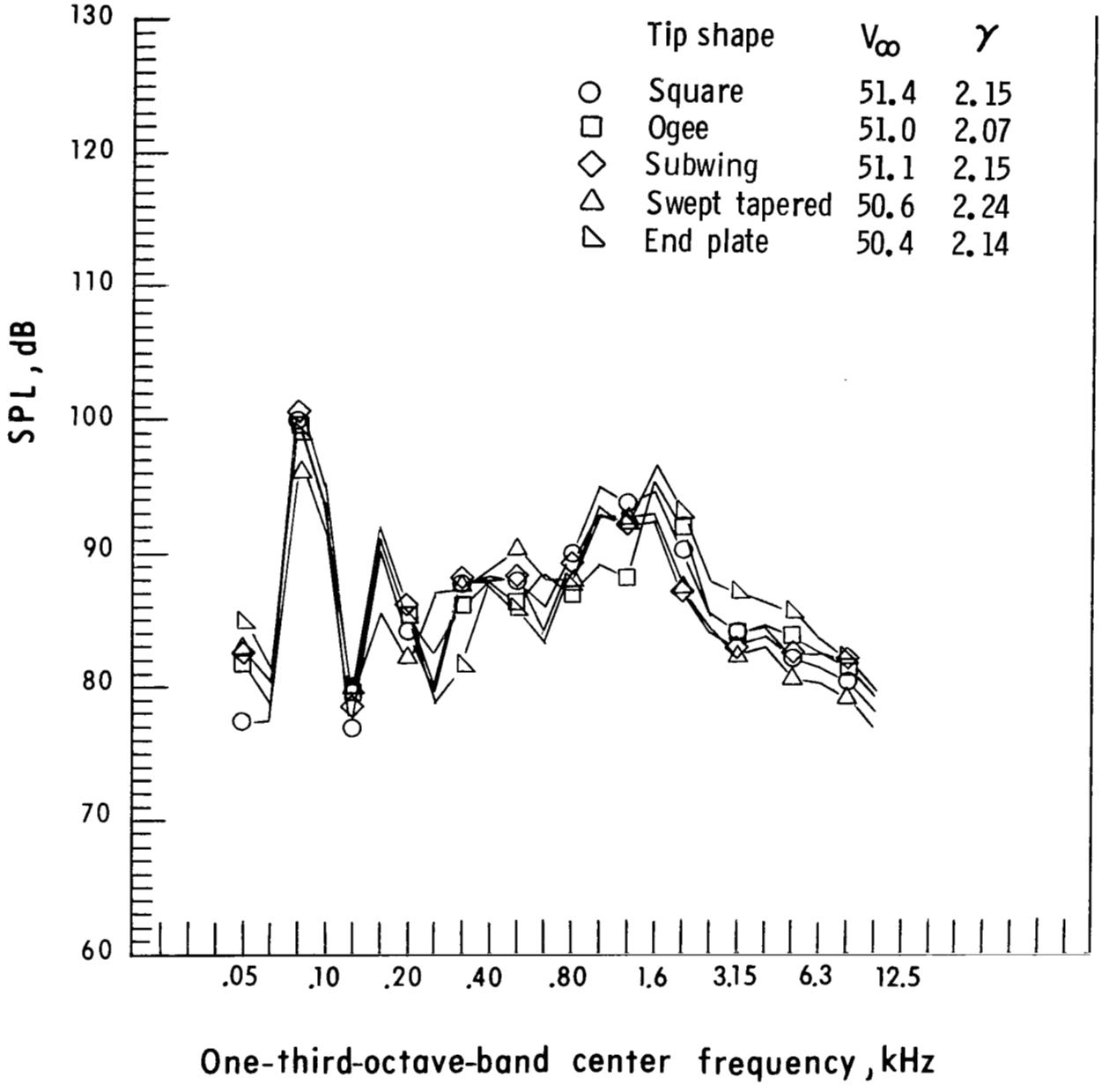

(c) Microphone 5; $\gamma \approx 2.1^{\circ}$.

Figure 11.- Continued.

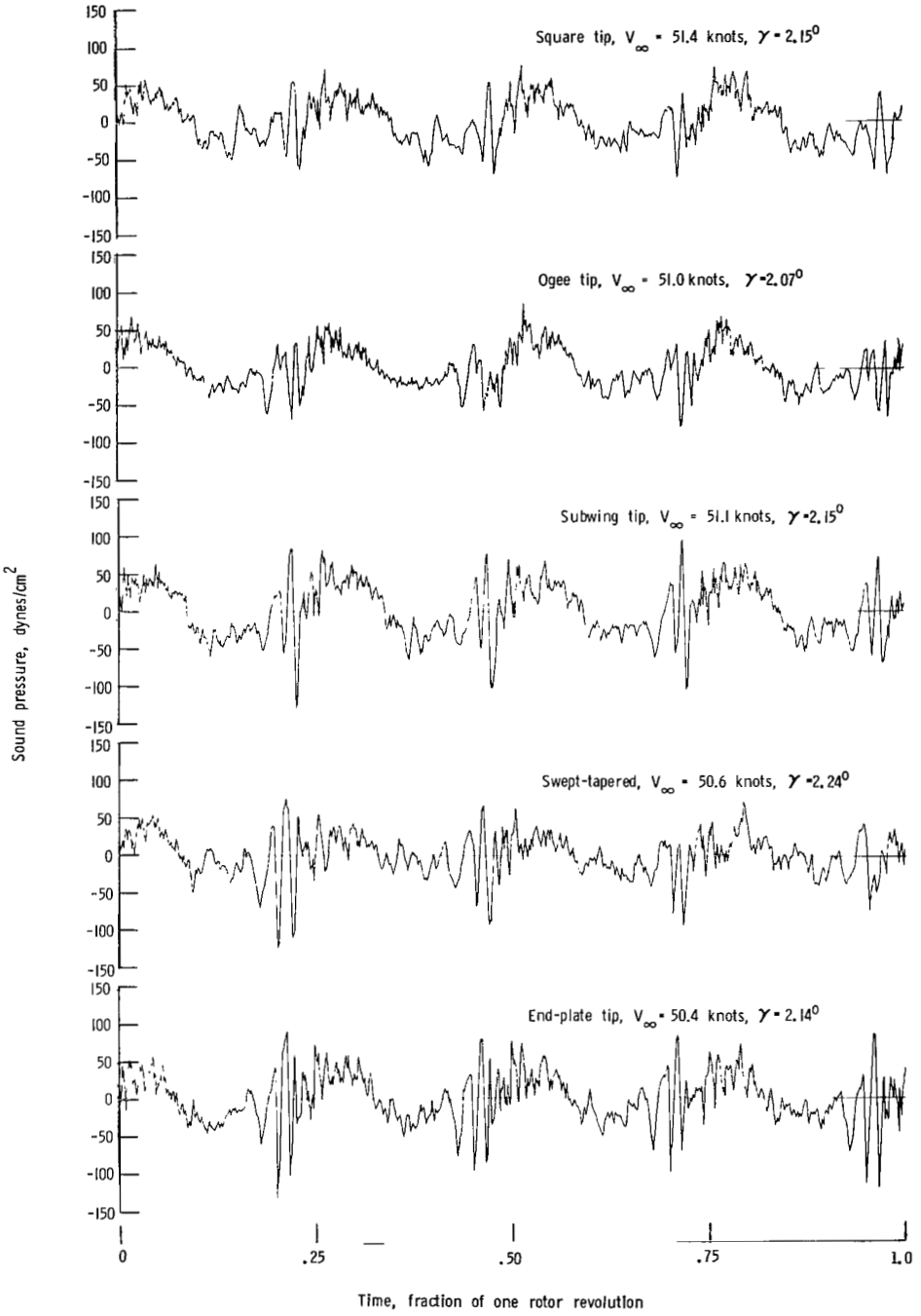

(d) Pressure time histories for microphone 5 at $\gamma \approx 2.1^\circ$.

Figure 11.- Continued.

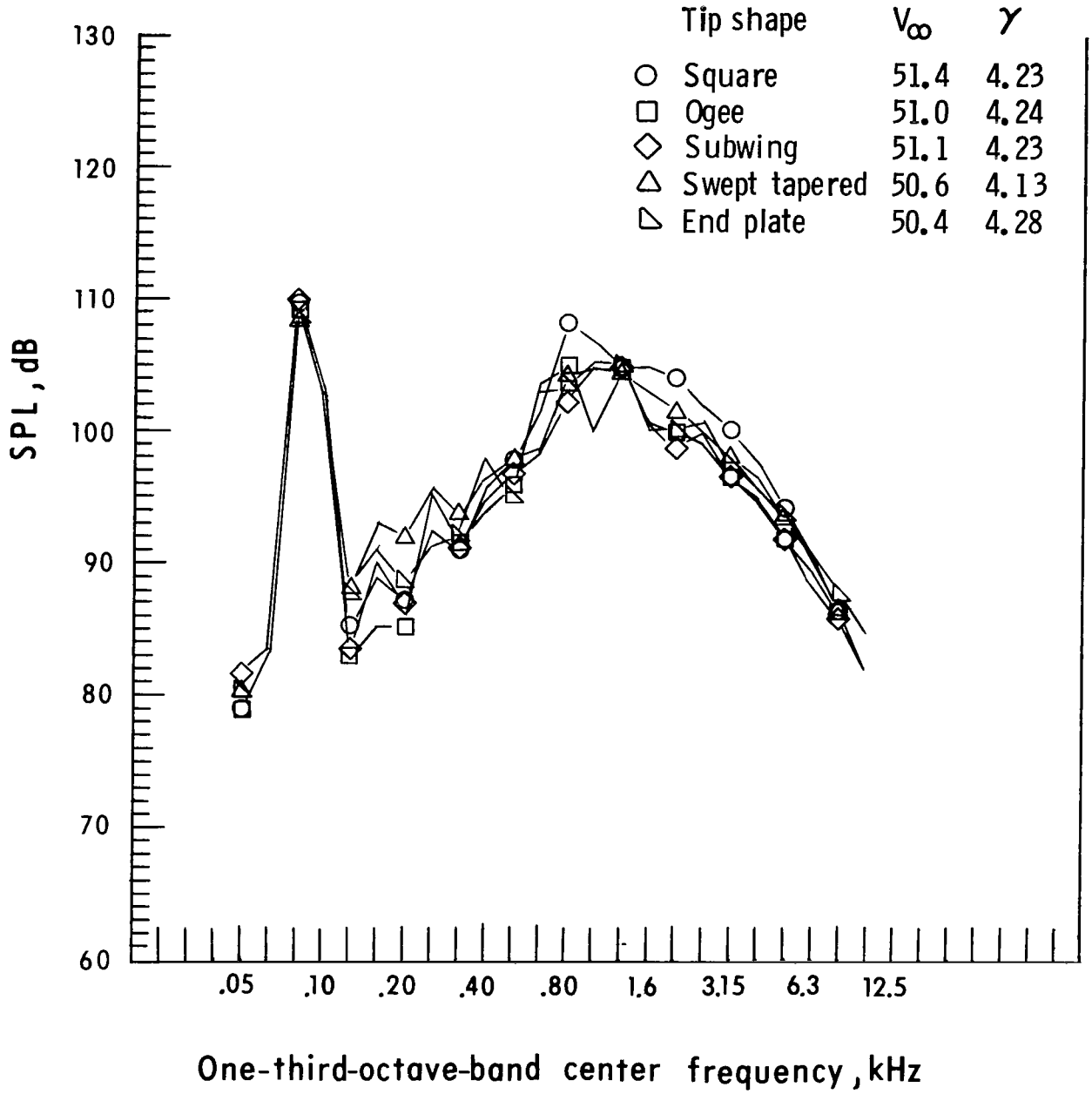

(e) Microphone 3; $\gamma \approx 4.2^{\circ}$.

Figure 11.- Continued.

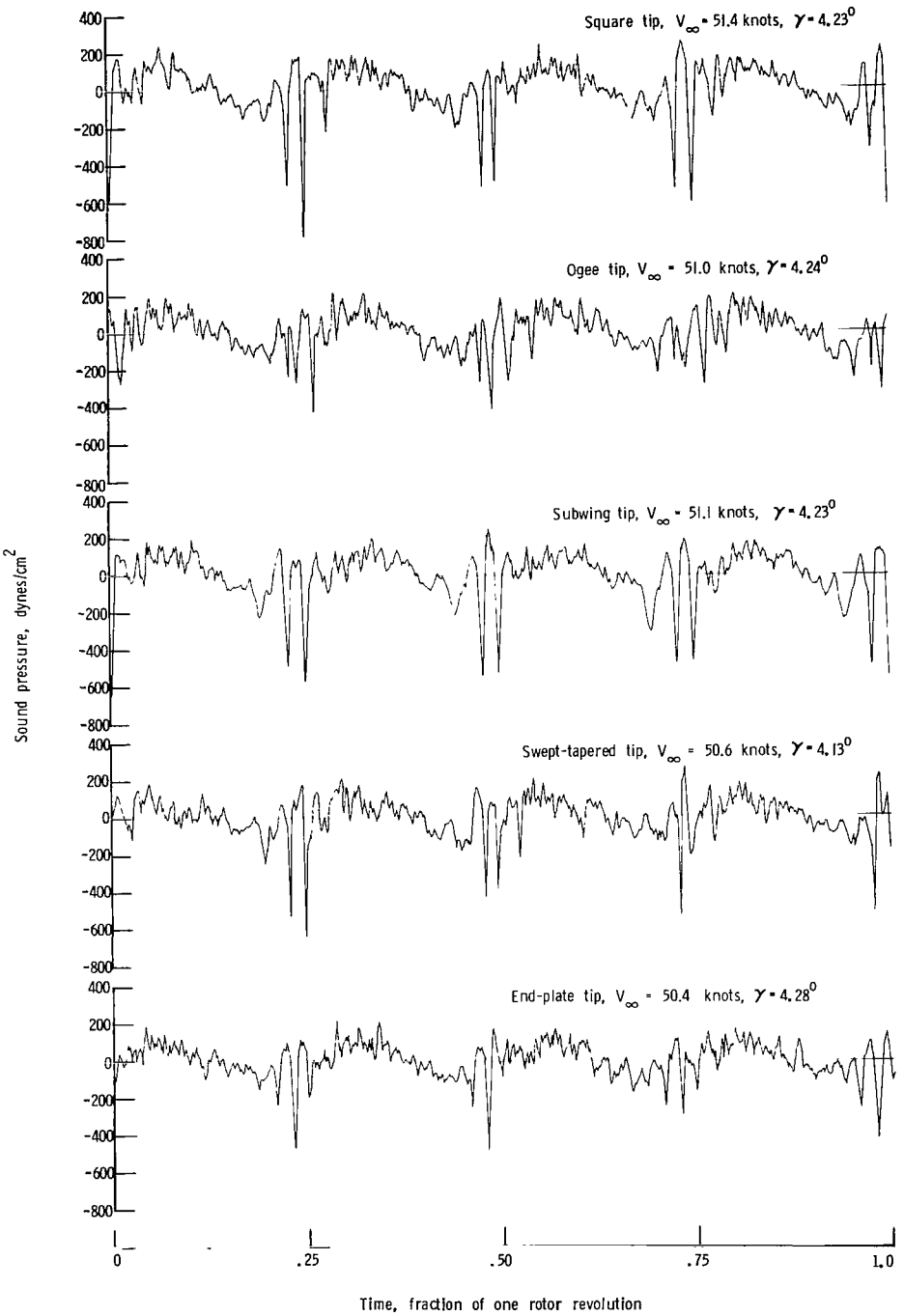

(f) Pressure time histories for microphone 3 at $\gamma \approx 4.2^{\circ}$.

Figure 11.- Continued.

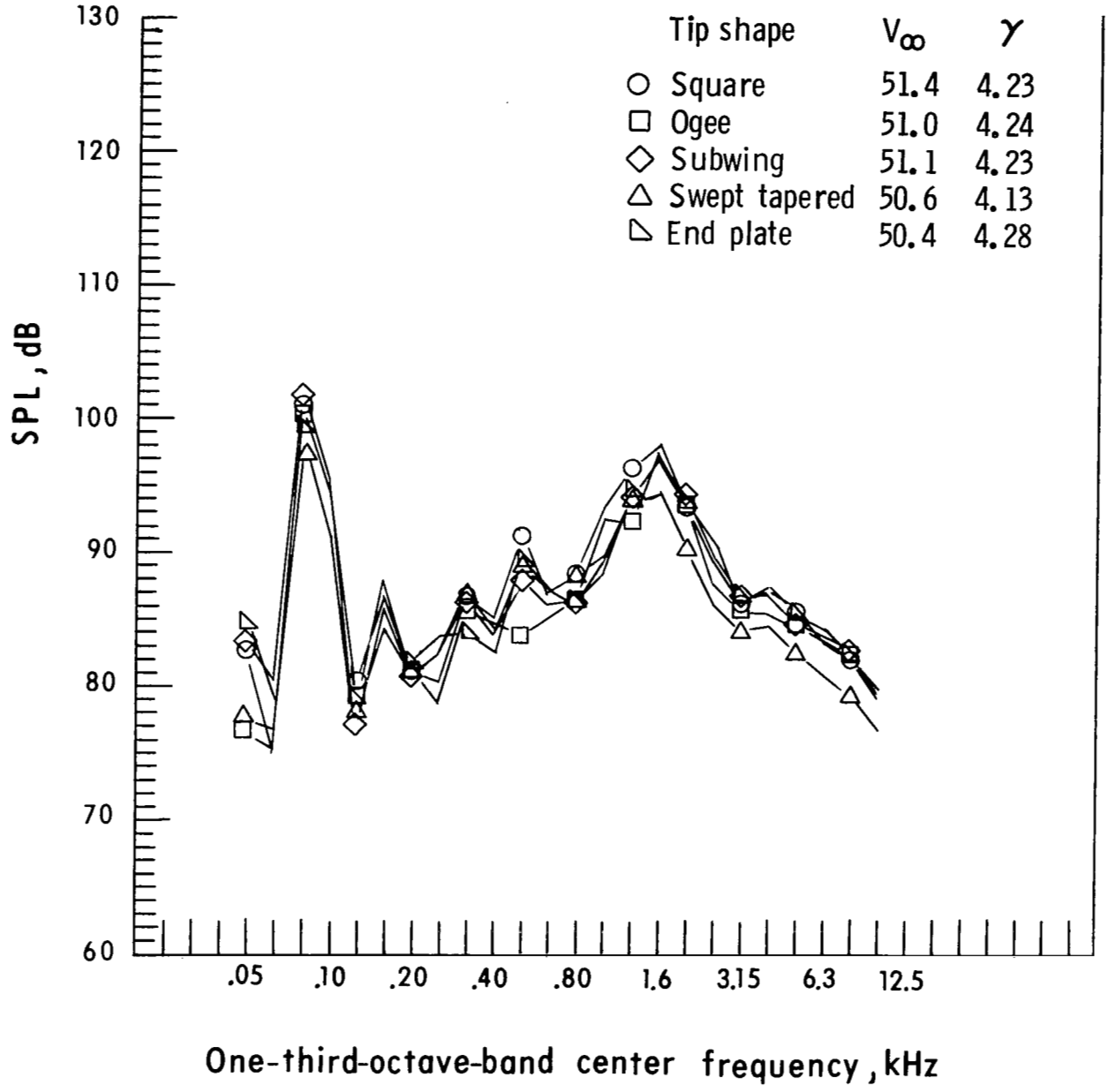

(g) Microphone 5; $\gamma \approx 4.2^{\circ}$.

Figure 11.- Continued.

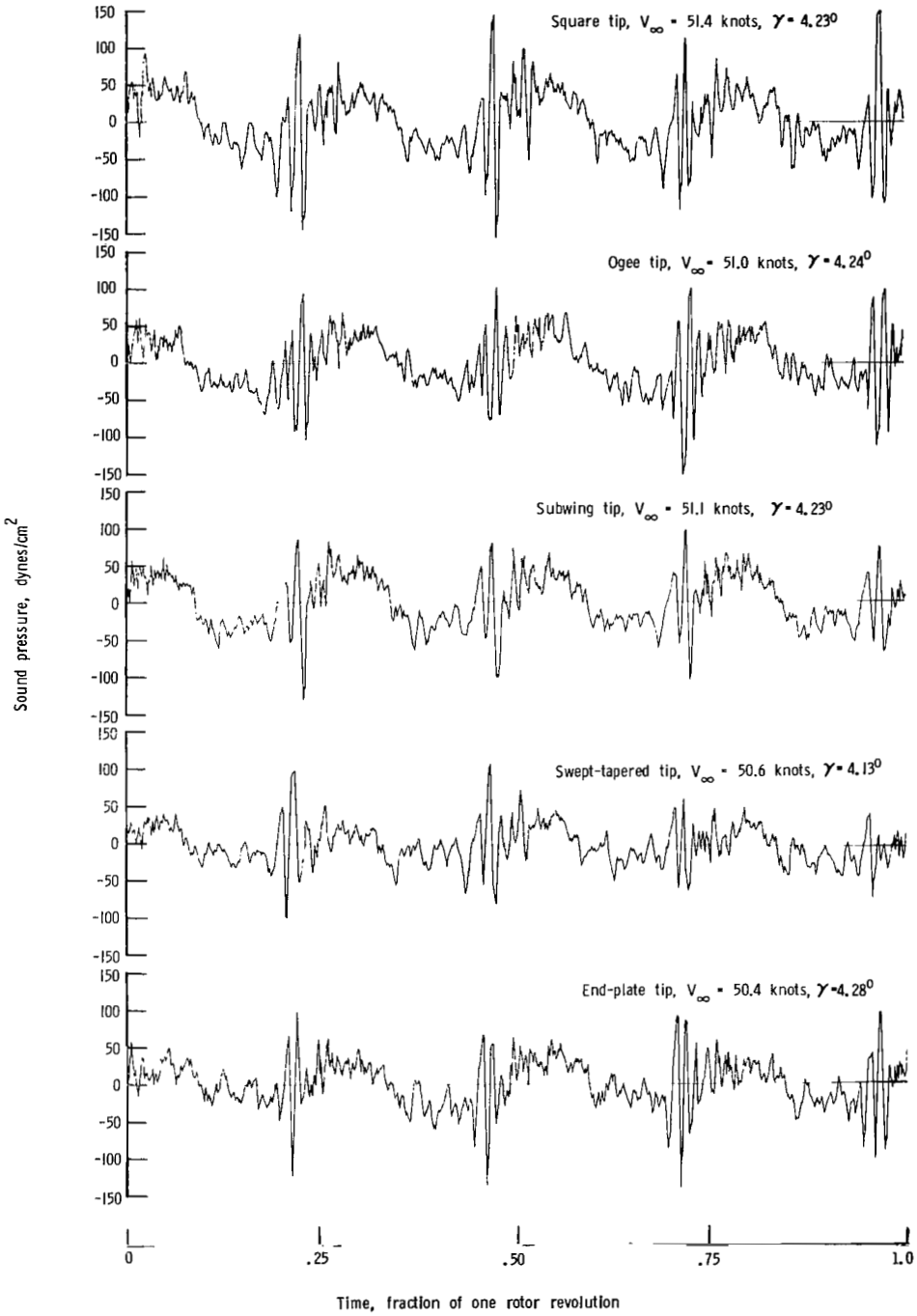

(h) Pressure histories for microphone 5 at $\gamma \approx 4.2^{\circ}$.

Figure 11.- Concluded.

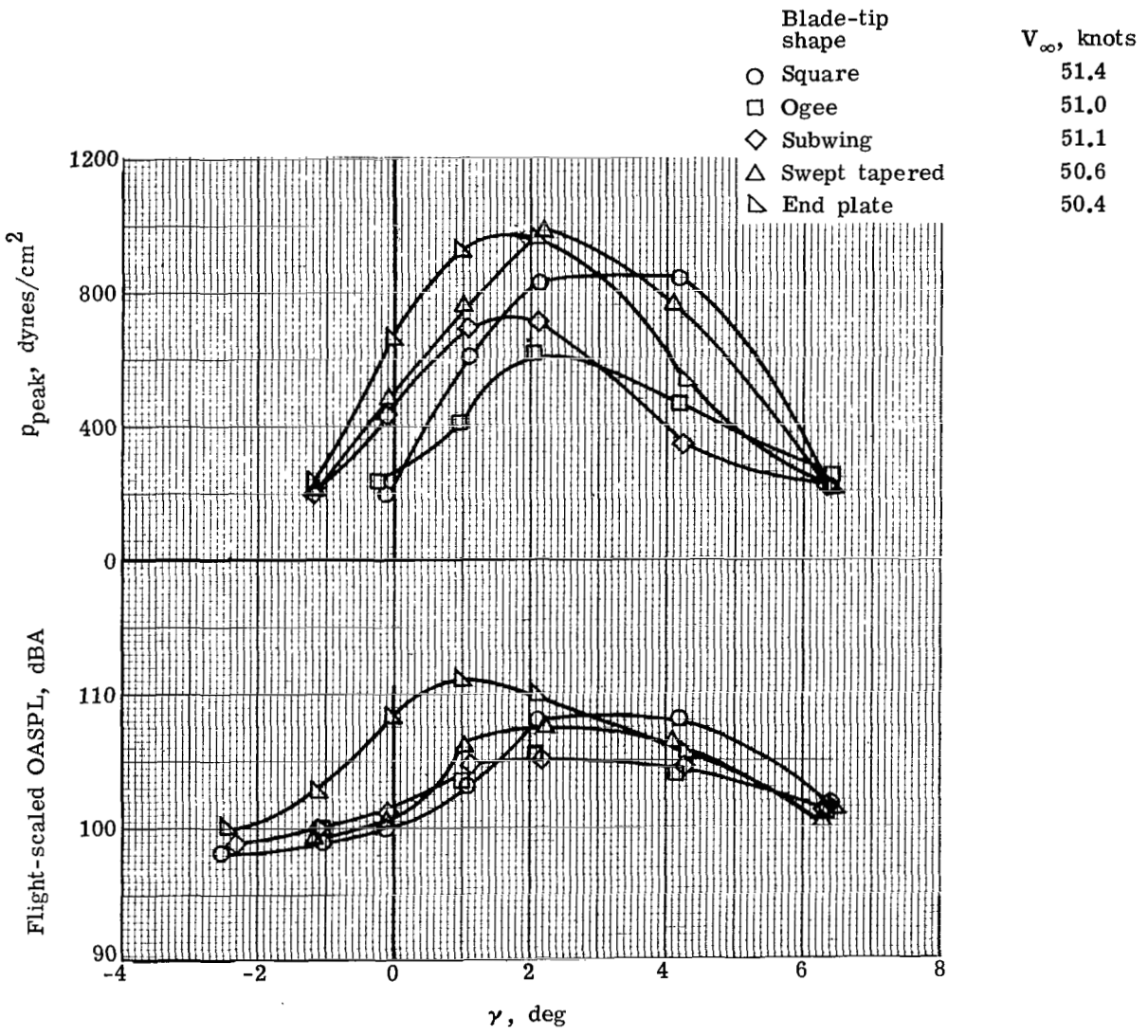

(a) Microphone 3.

Figure 12.- Effect of tip shape on blade-slap intensity variation with descent angle at $V_\infty \approx 51$ knots.

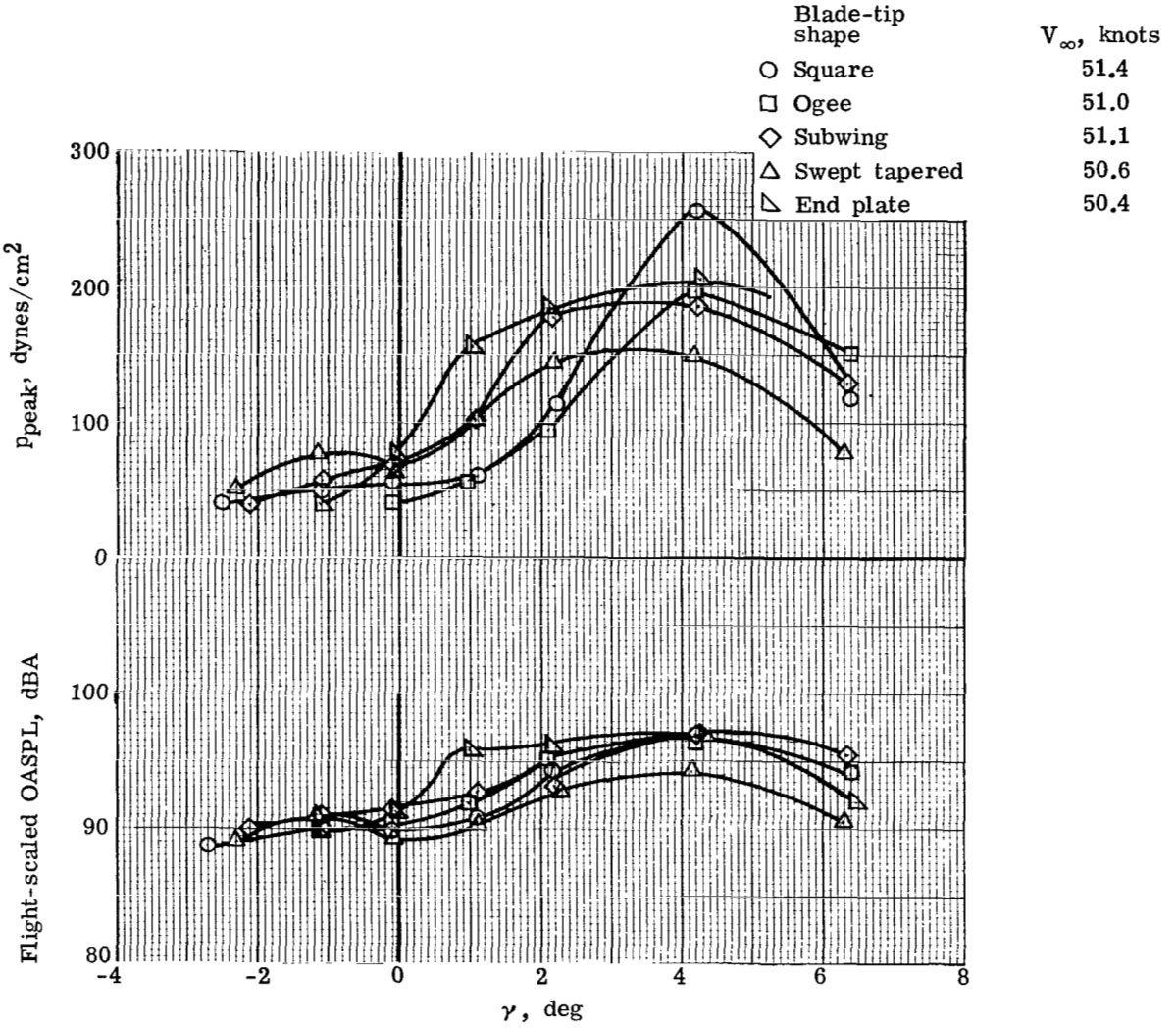

(b) Microphone 5.

Figure 12.- Continued.

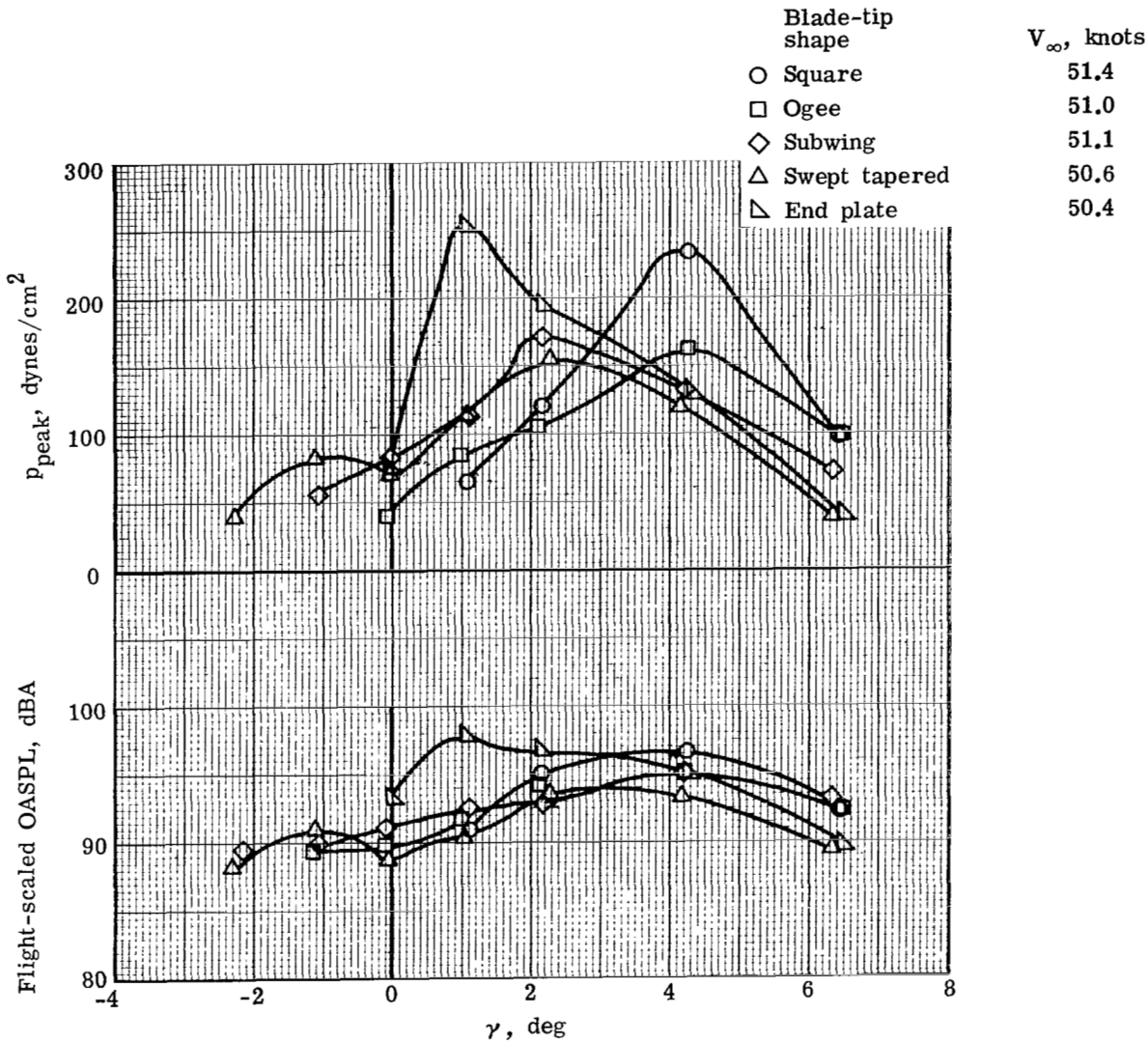

(c) Microphone 6.

Figure 12.- Continued.

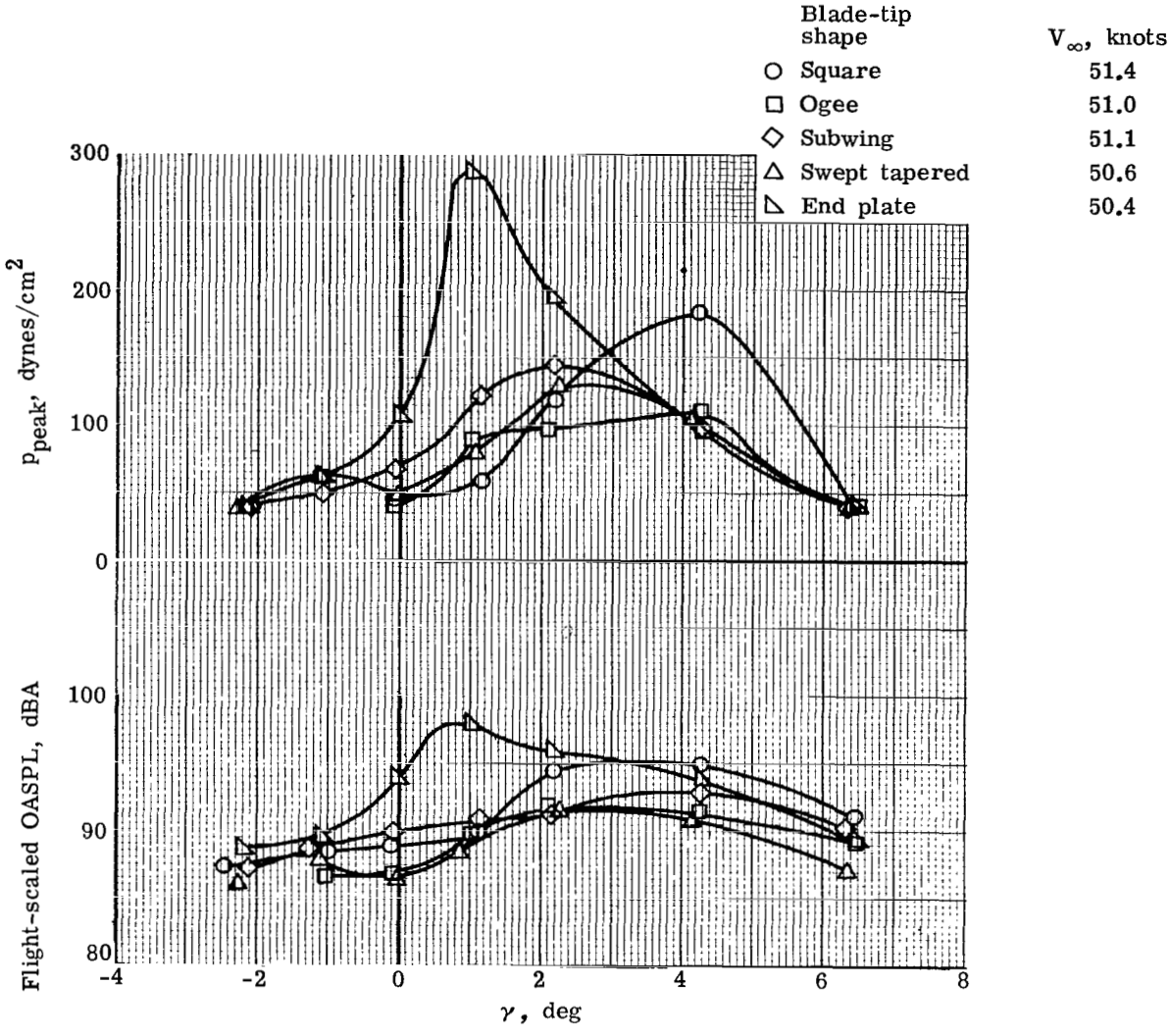

(d) Microphone 7.

Figure 12.- Concluded.

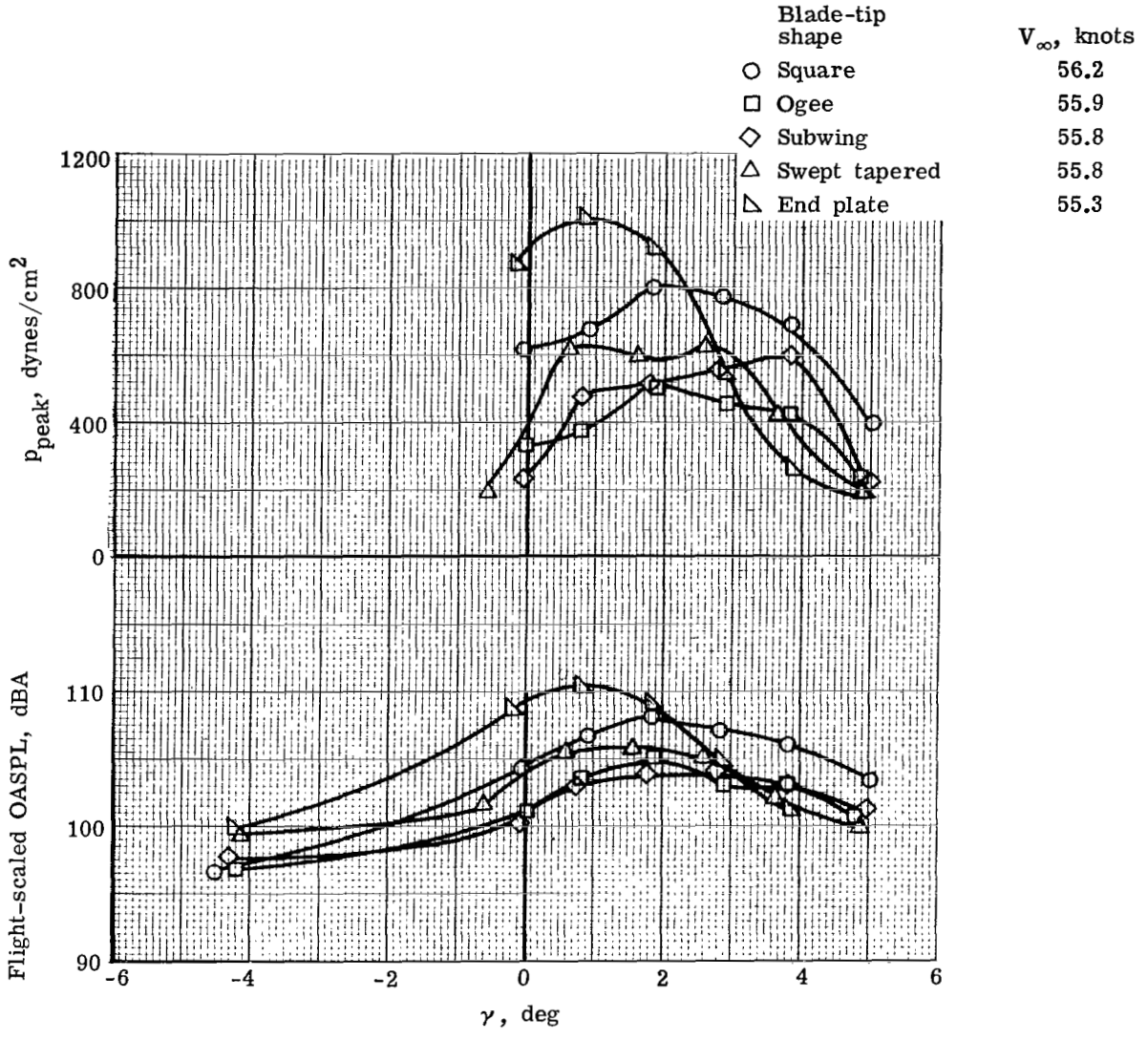

(a) Microphone 3.

Figure 13.- Effect of tip shape on blade-slap intensity variation with descent angle at $V_\infty \approx 56$ knots.

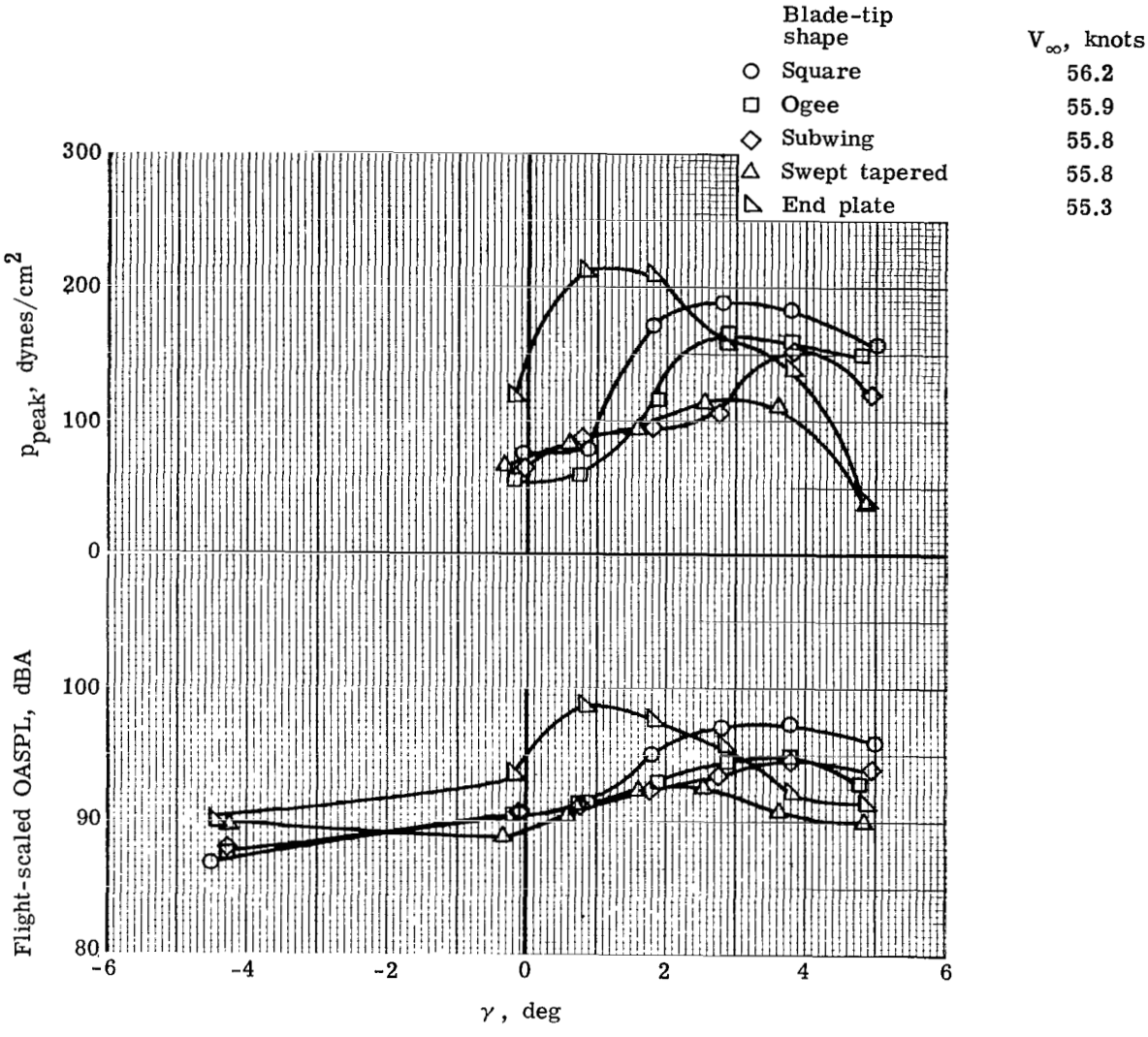

(b) Microphone 5.

Figure 13.- Continued.

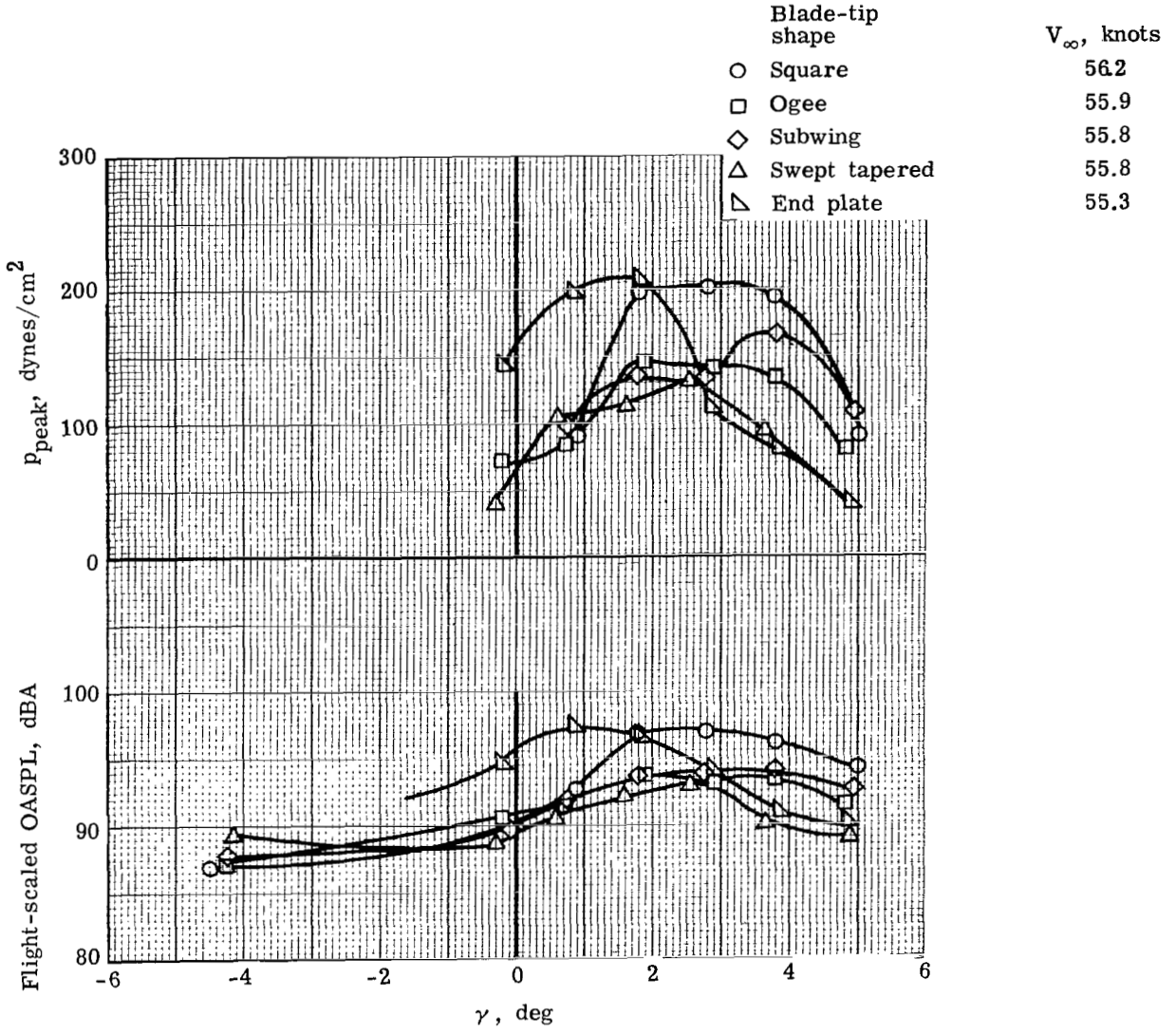

(c) Microphone 6.

Figure 13.- Continued.

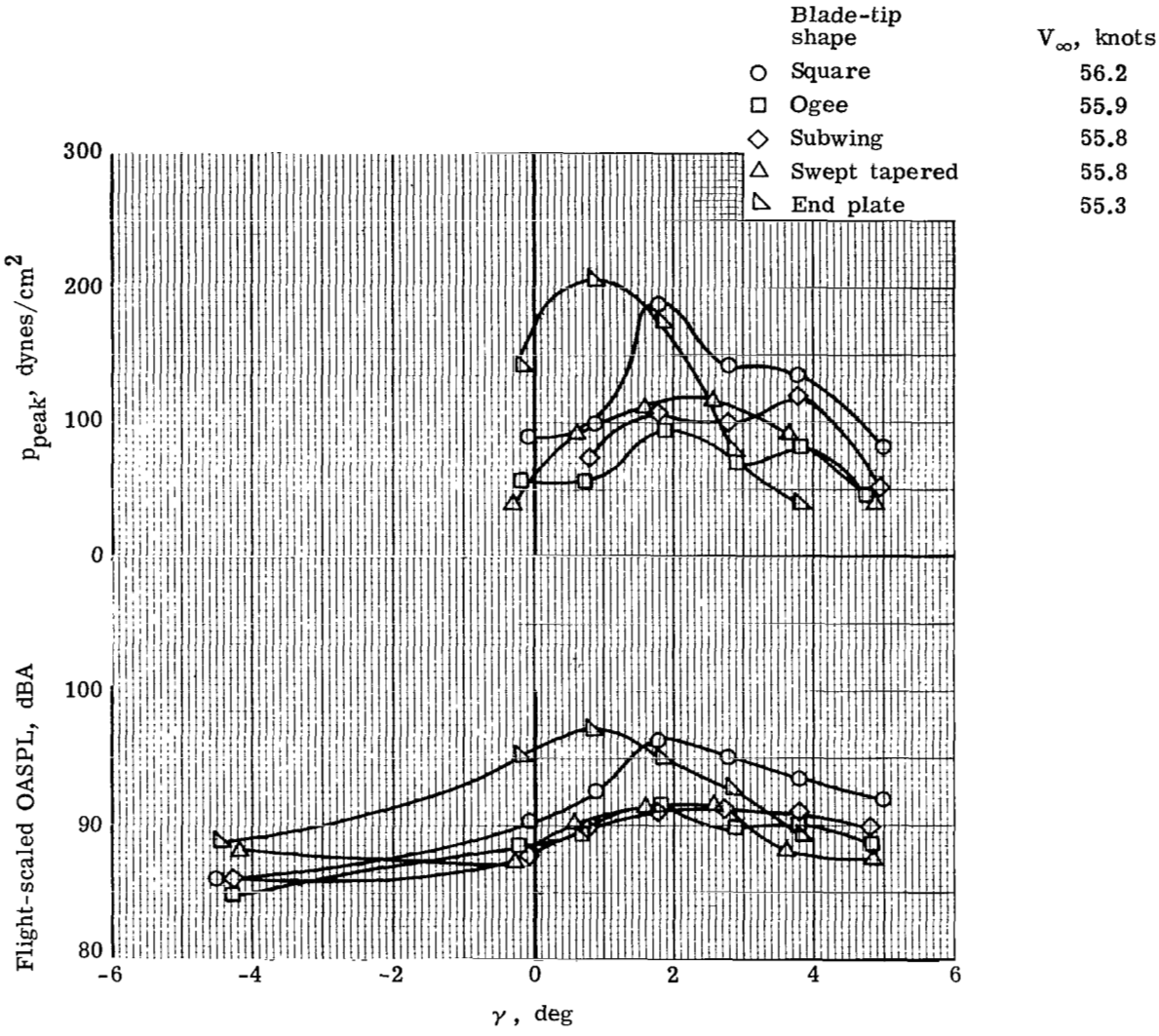

(d) Microphone 7.

Figure 13.- Concluded.

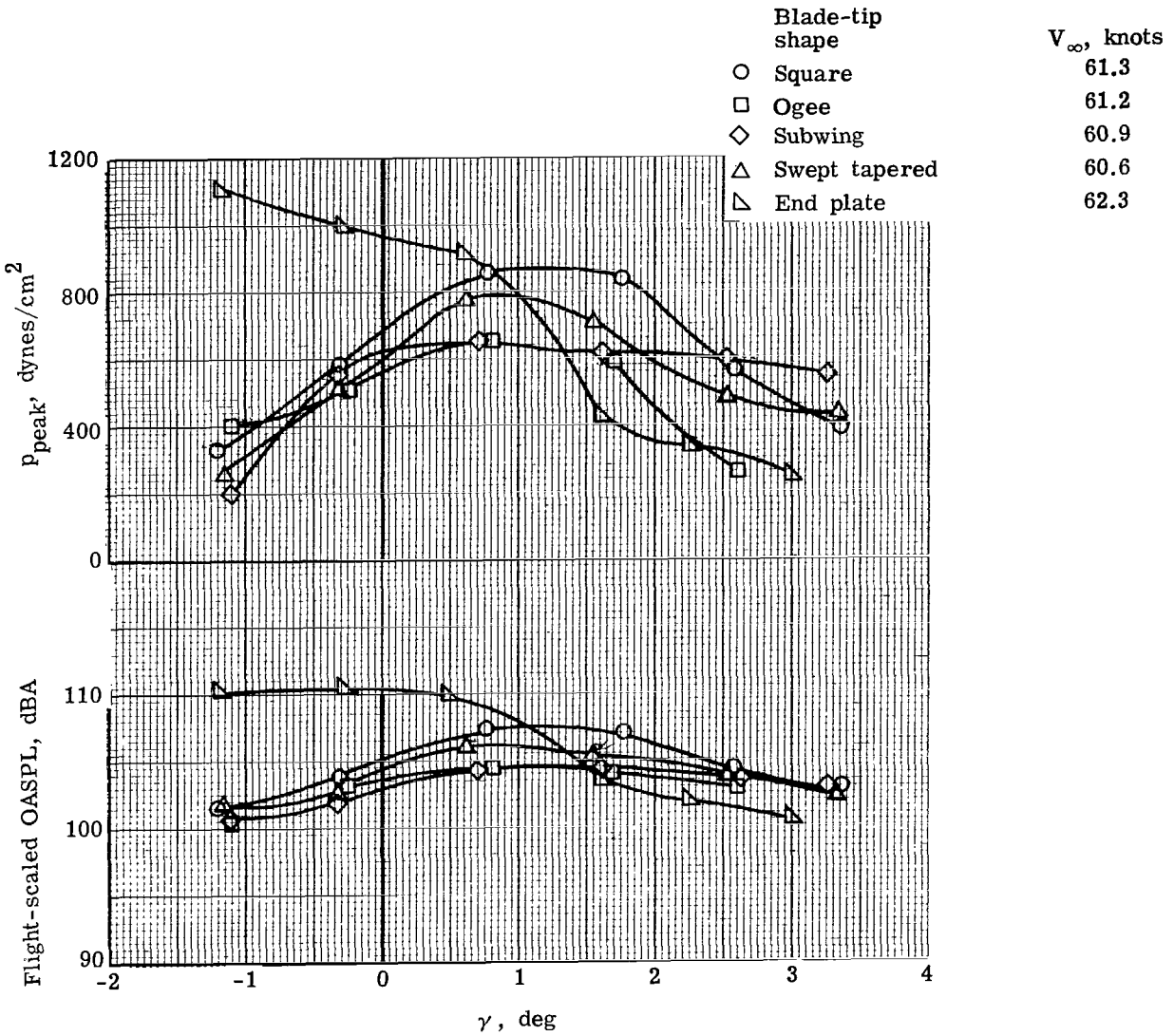

(a) Microphone 3.

Figure 14.- Effect of tip shape on blade-slap intensity variation with descent angle at $V_\infty \approx 61$ knots.

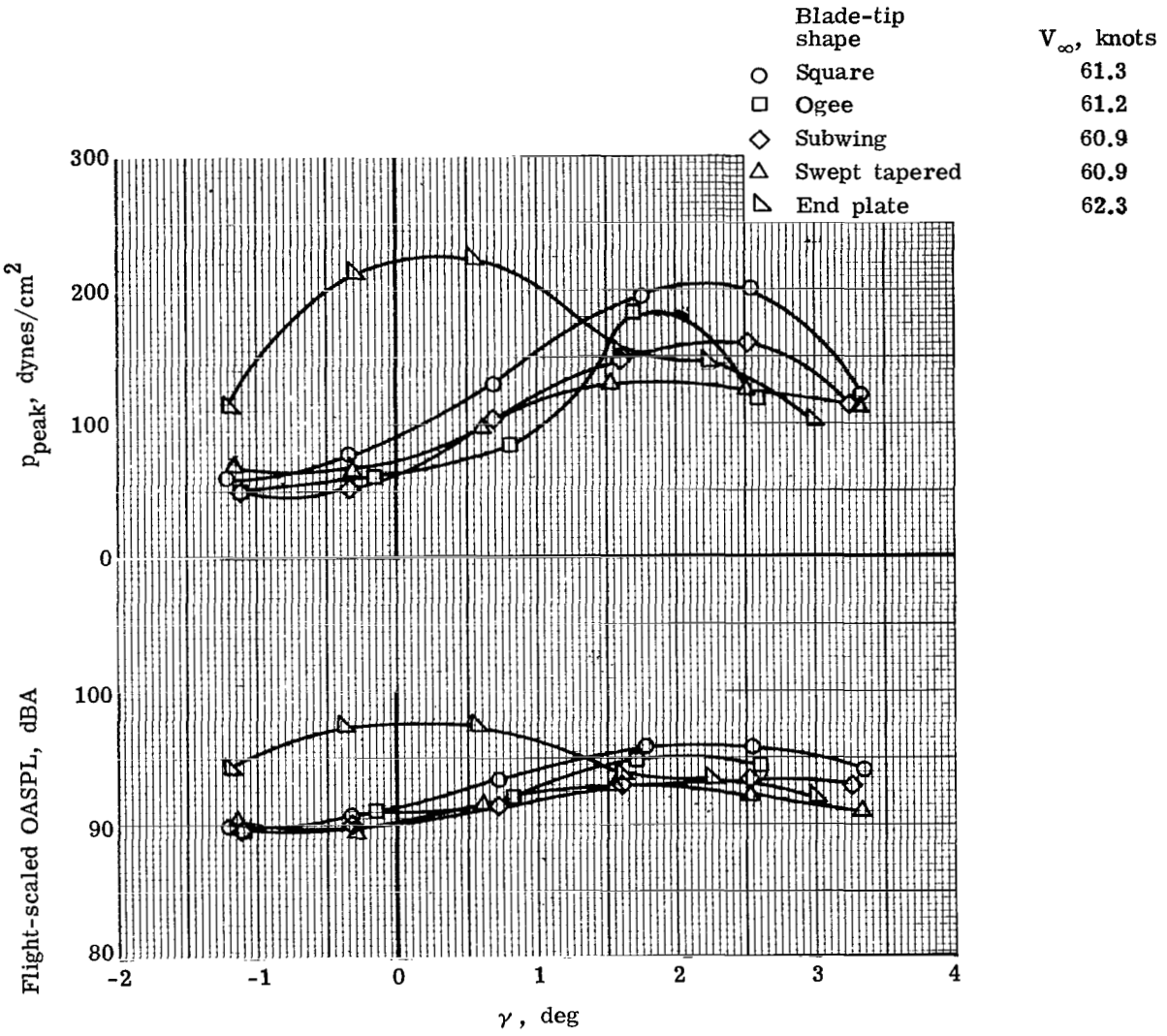

(b) Microphone 5.

Figure 14.- Continued.

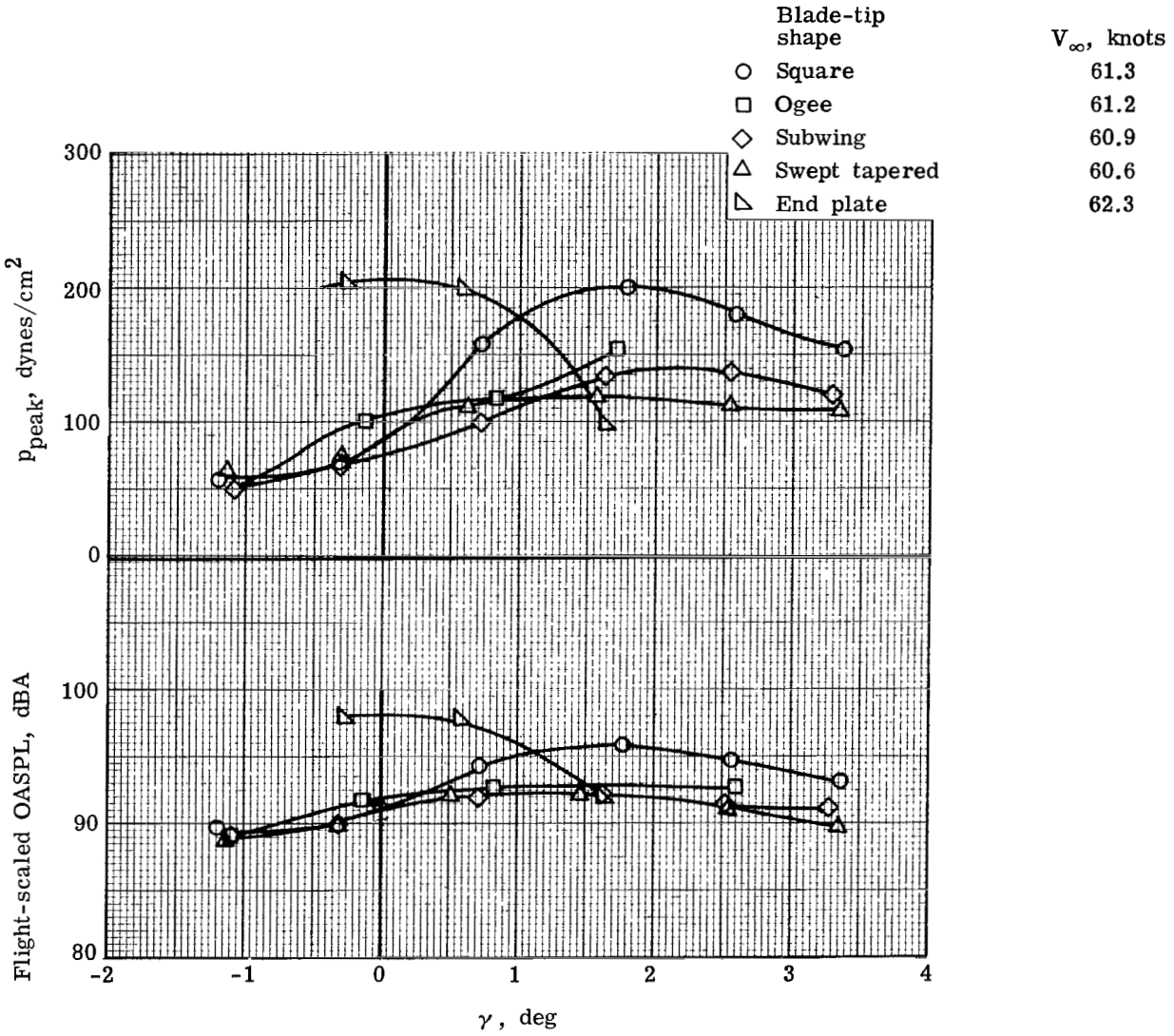

(c) Microphone 6.

Figure 14.- Continued.

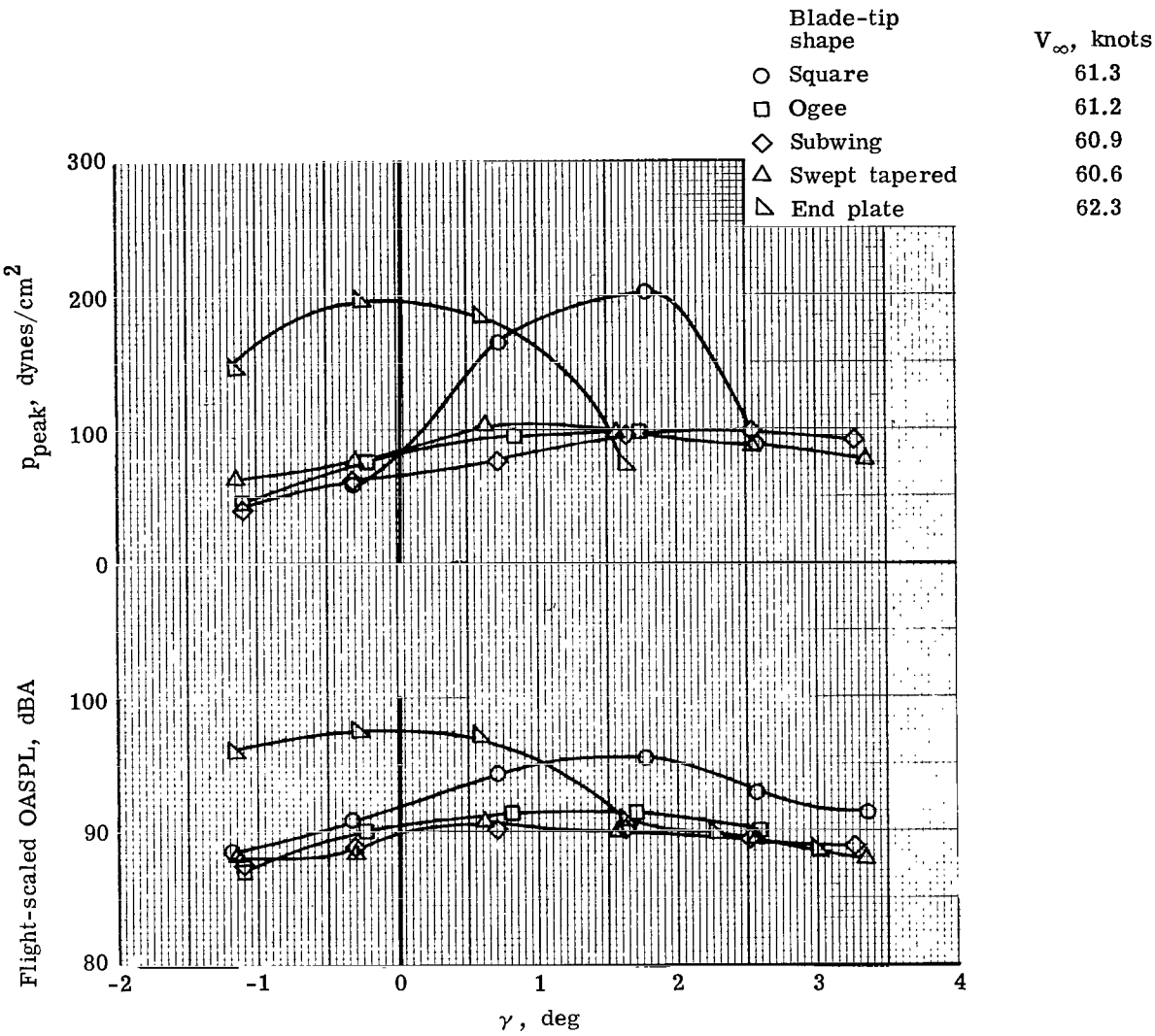

(d) Microphone 7.

Figure 14.- Concluded.

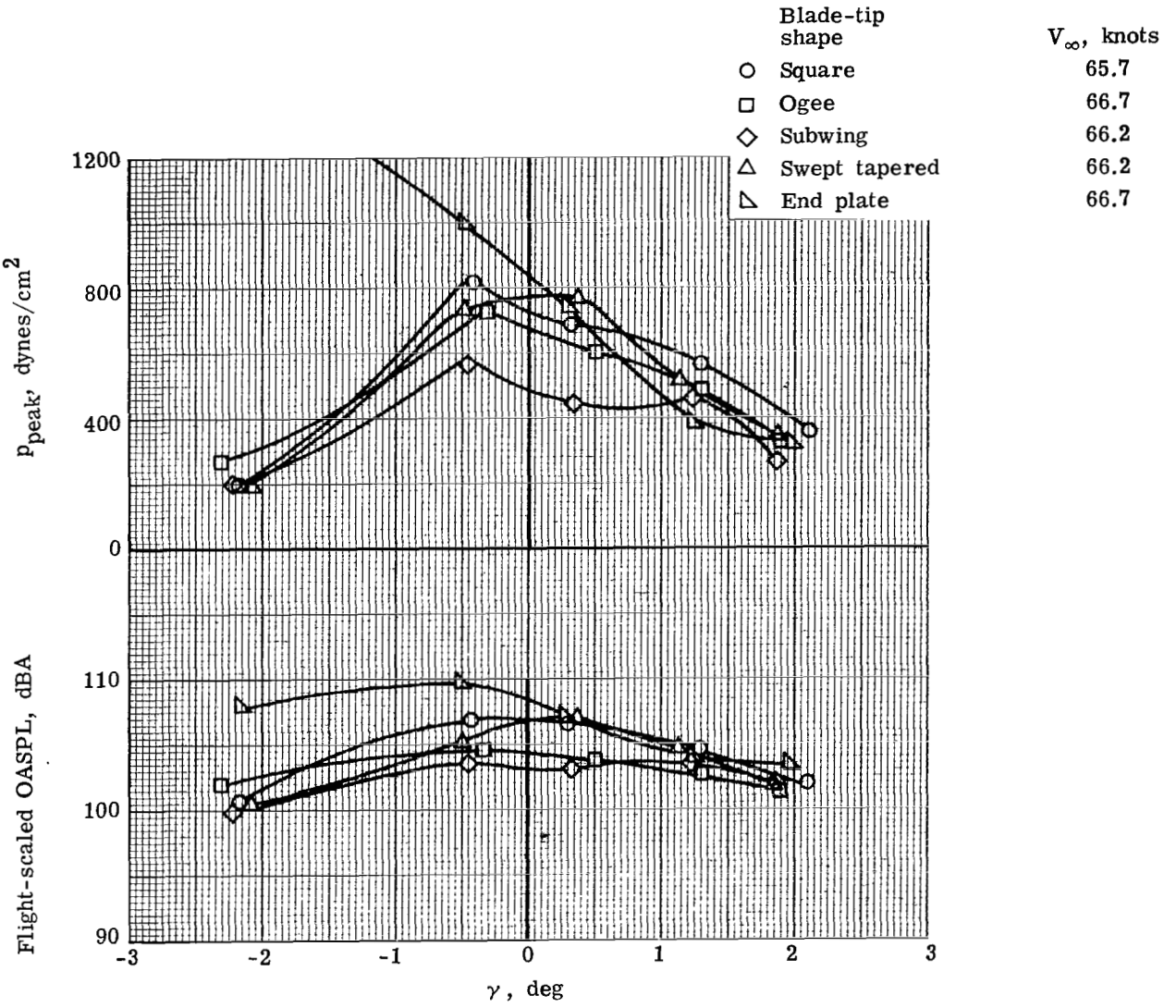

(a) Microphone 3.

Figure 15.- Effect of tip shape on blade-slap intensity variation with descent angle at $V_\infty \approx 66$ knots.

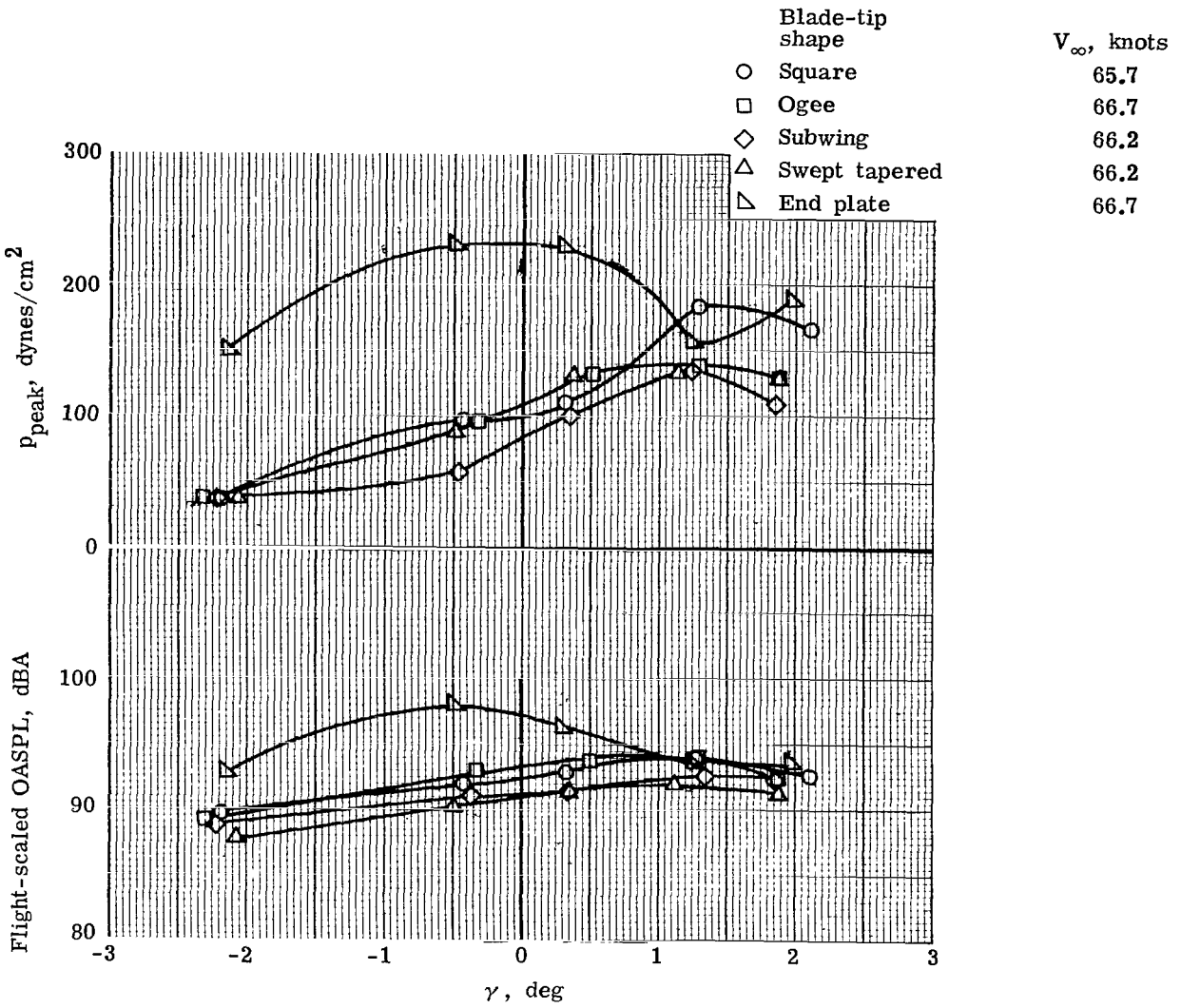

(b) Microphone 5.

Figure 15.- Continued.

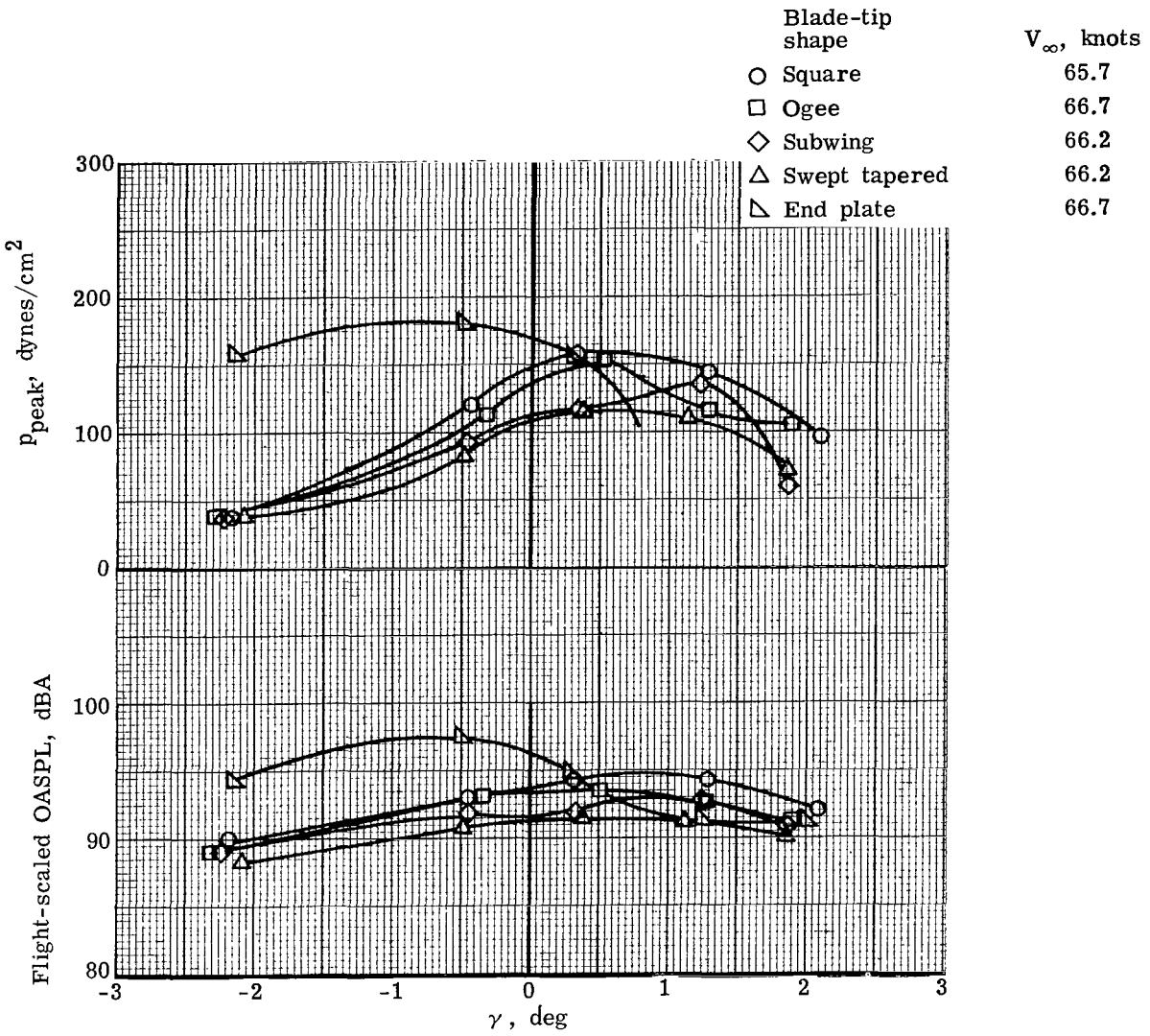

(c) Microphone 6.

Figure 15.- Continued.

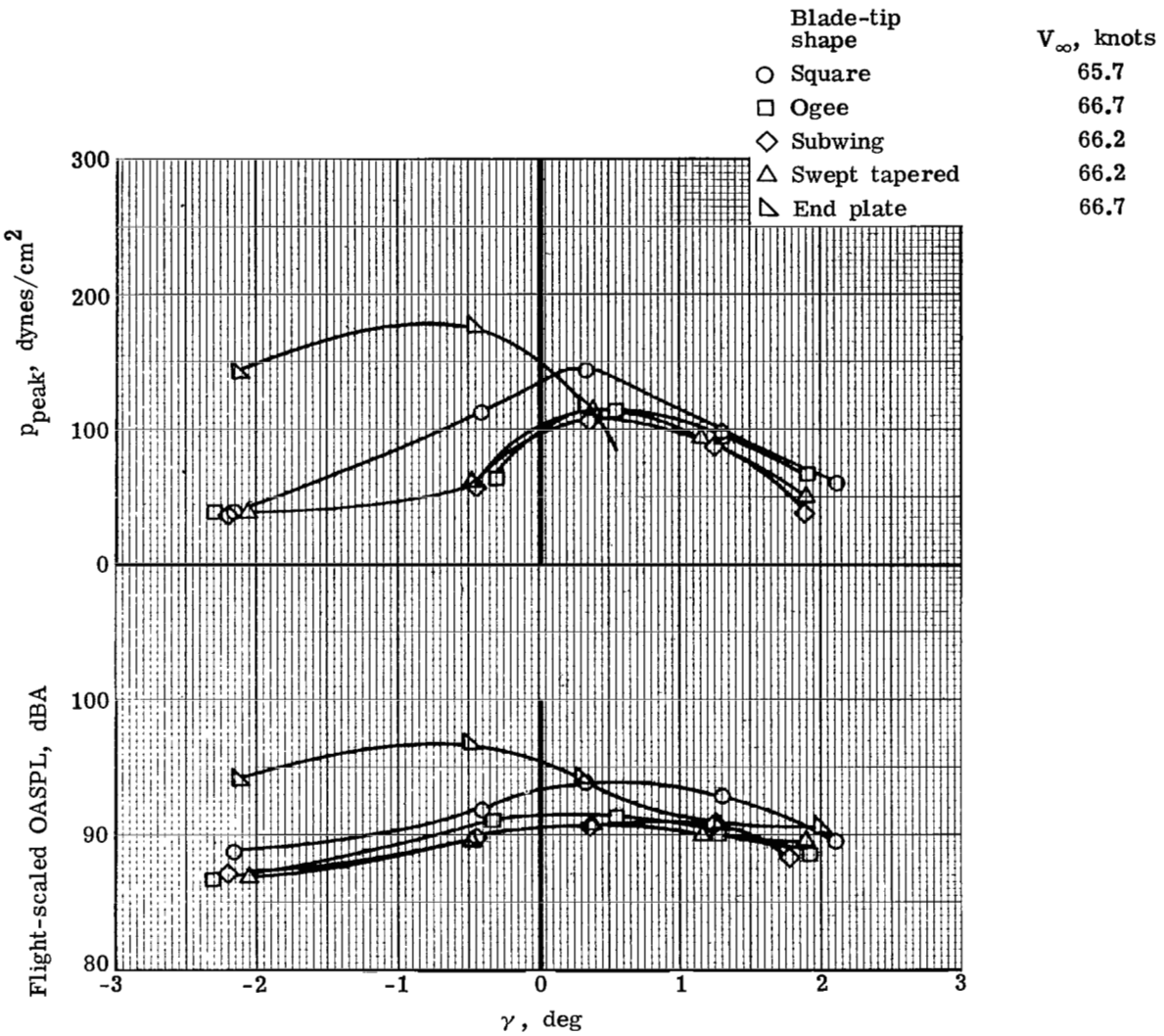

(d) Microphone 7.

Figure 15.- Concluded.

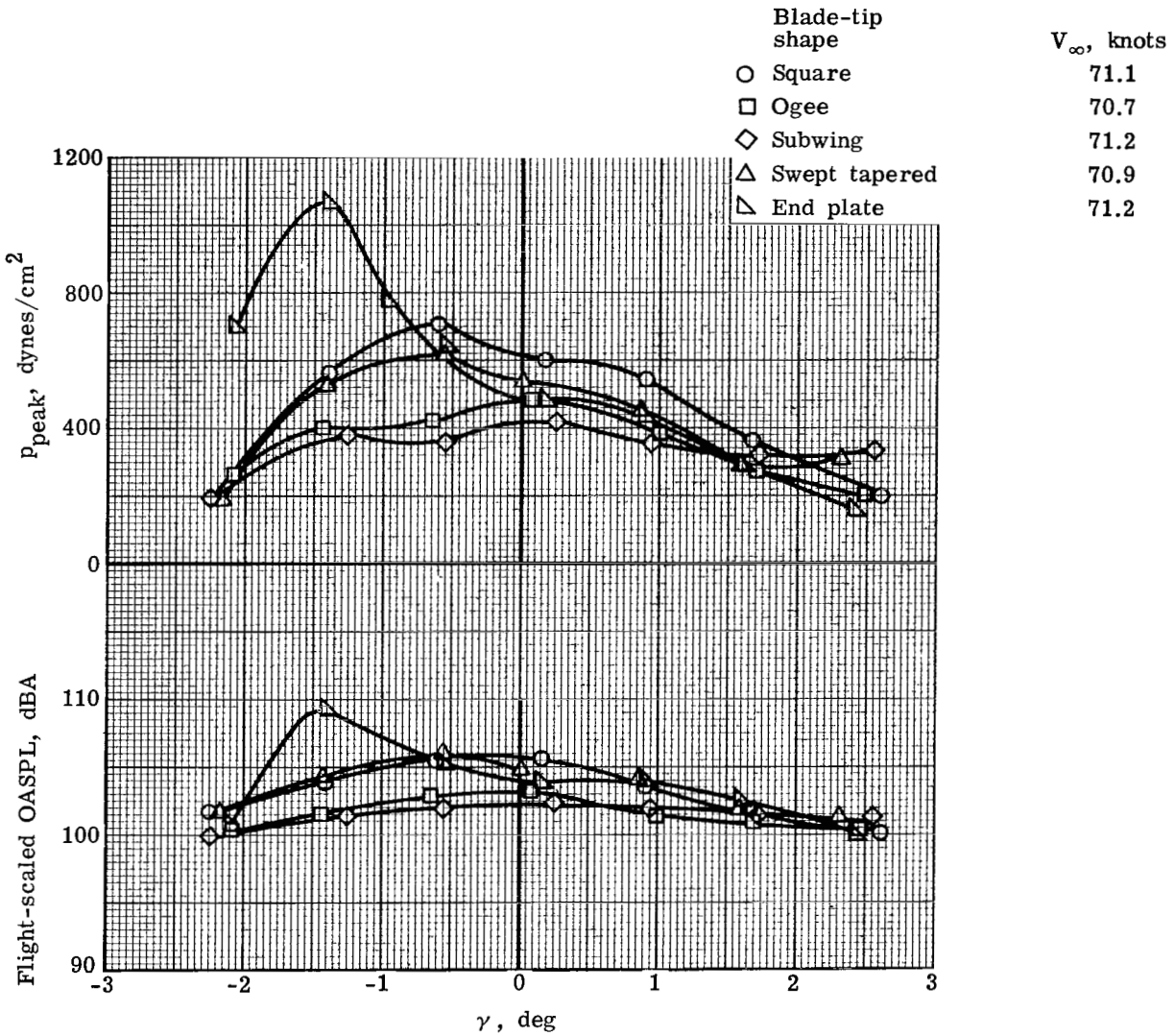

(a) Microphone 3.

Figure 16.- Effect of tip shape on blade-slap intensity variation with descent angle at $V_\infty \approx 71$ knots.

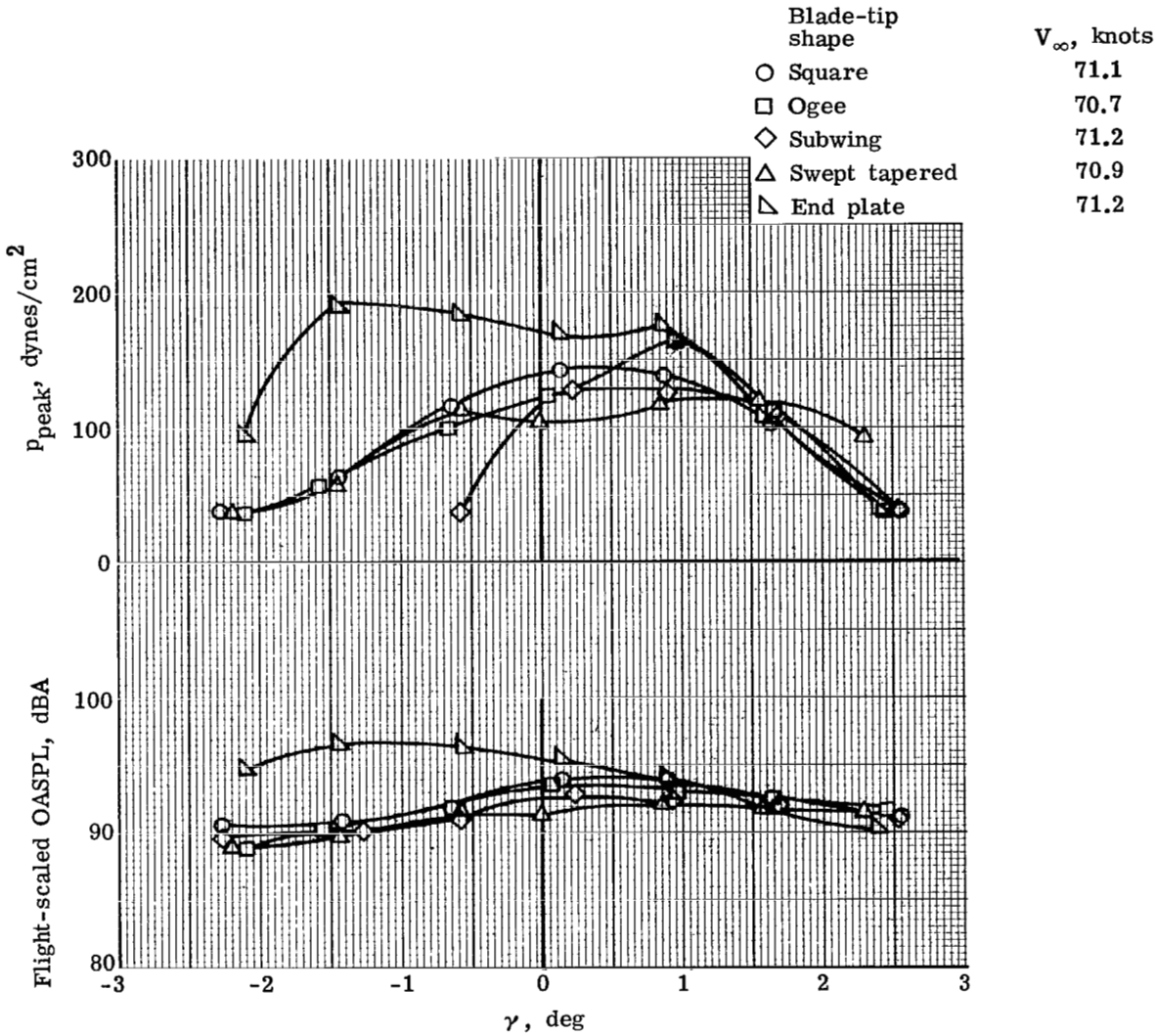

(b) Microphone 5.

Figure 16.- Continued.

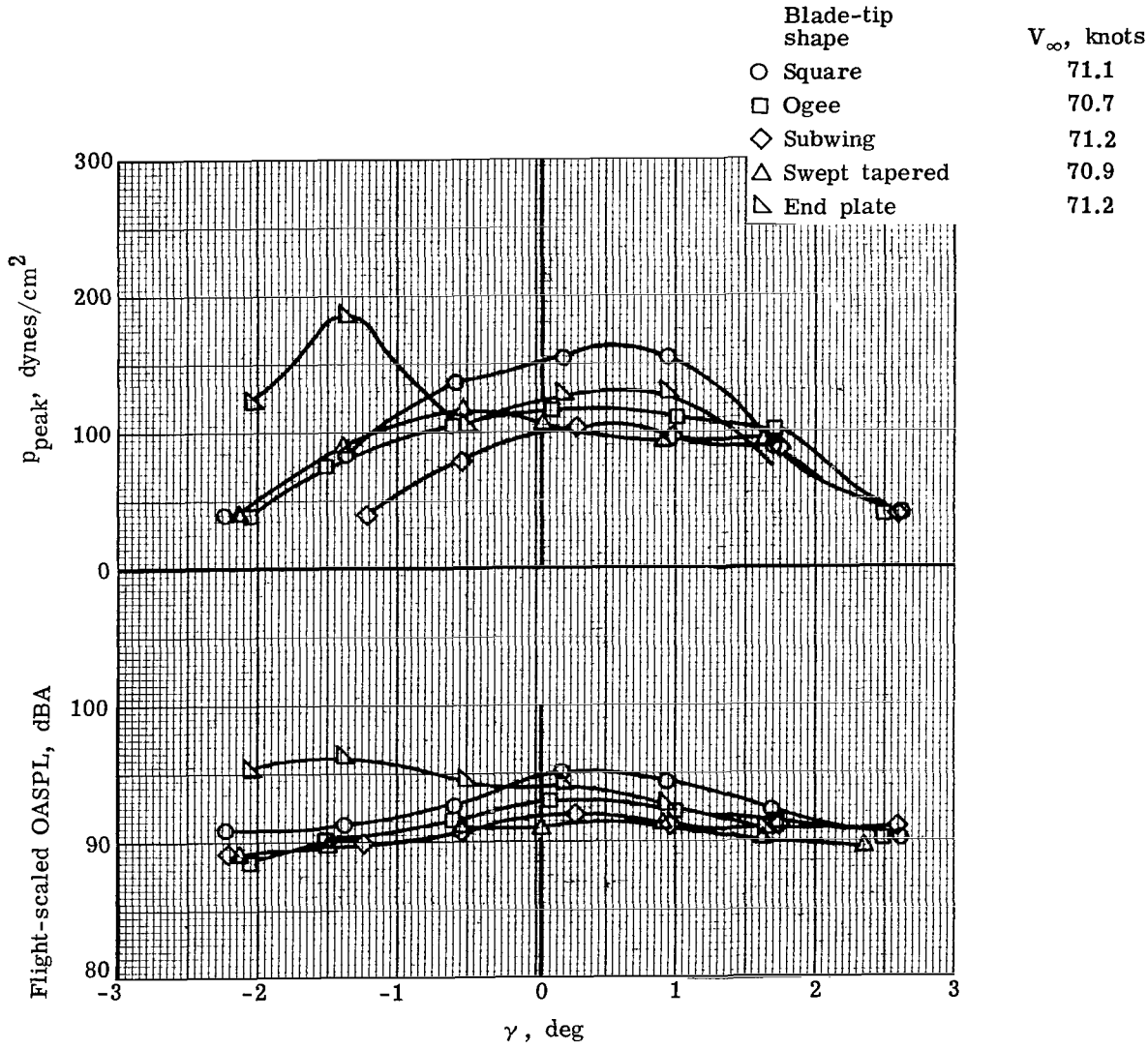

(c) Microphone 6.

Figure 16.- Continued.

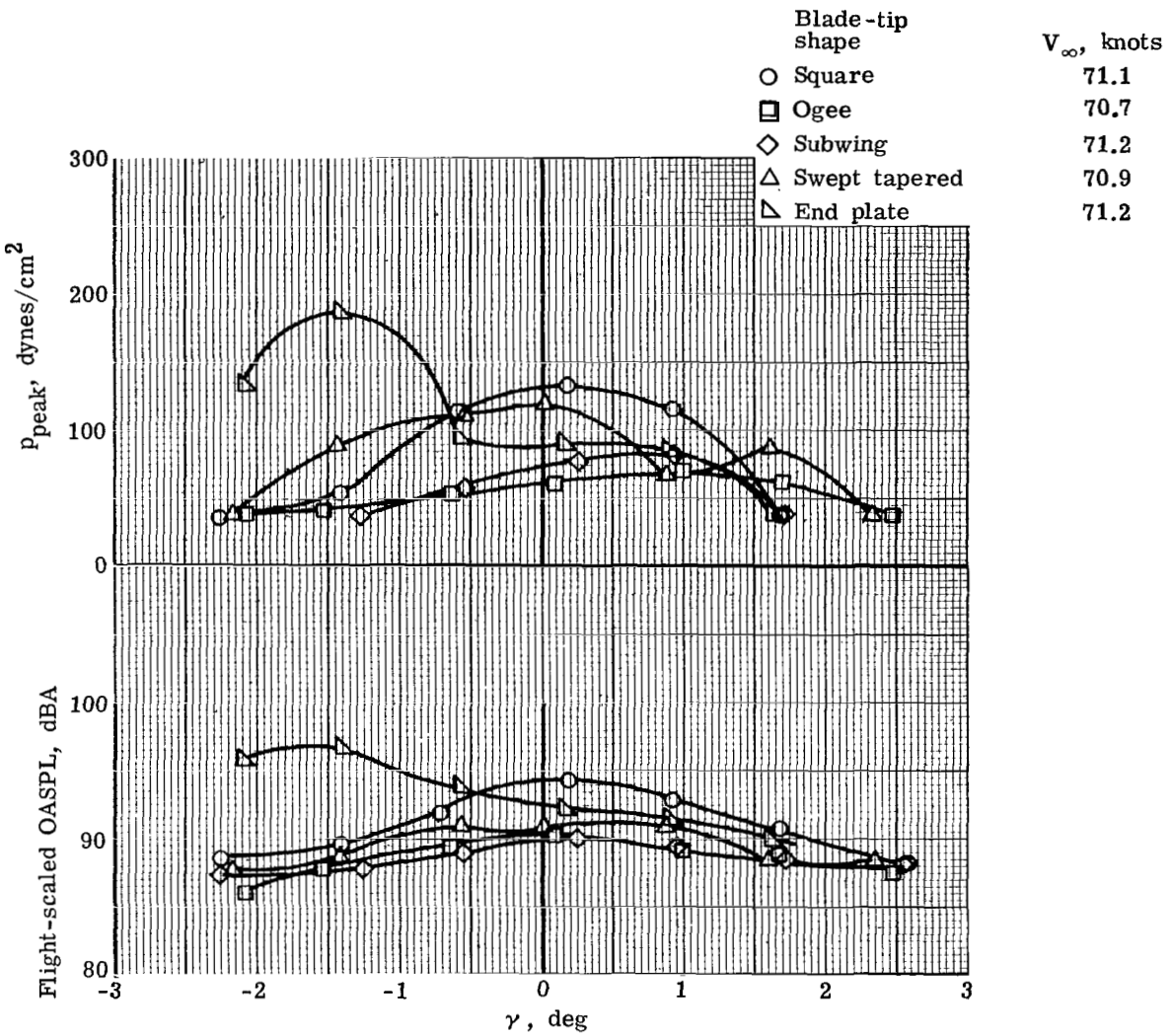

(d) Microphone 7.

Figure 16.- Concluded.

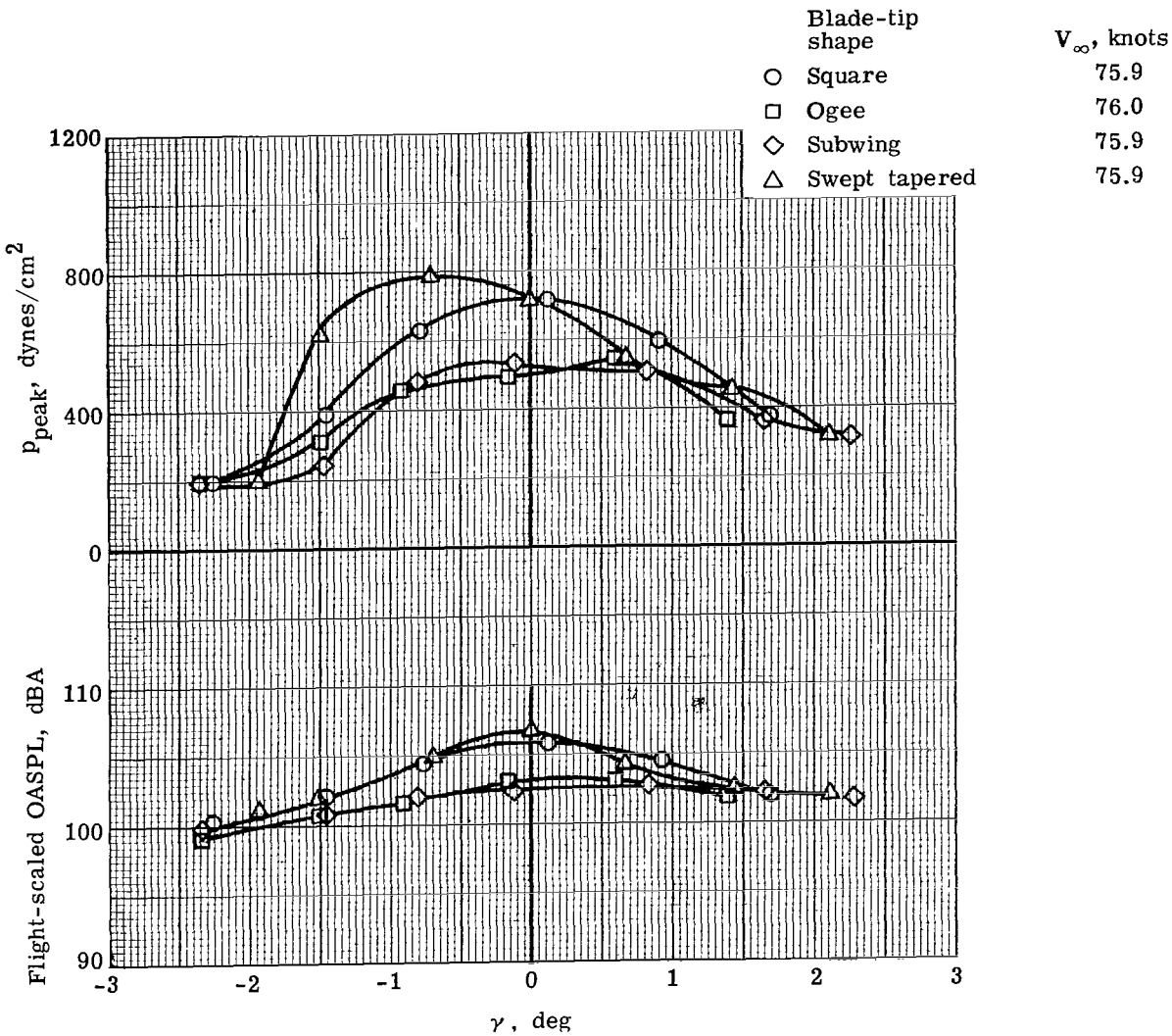

(a) Microphone 3.

Figure 17.- Effect of tip shape on blade-slap intensity variation with descent angle at $V_\infty \approx 76$ knots.

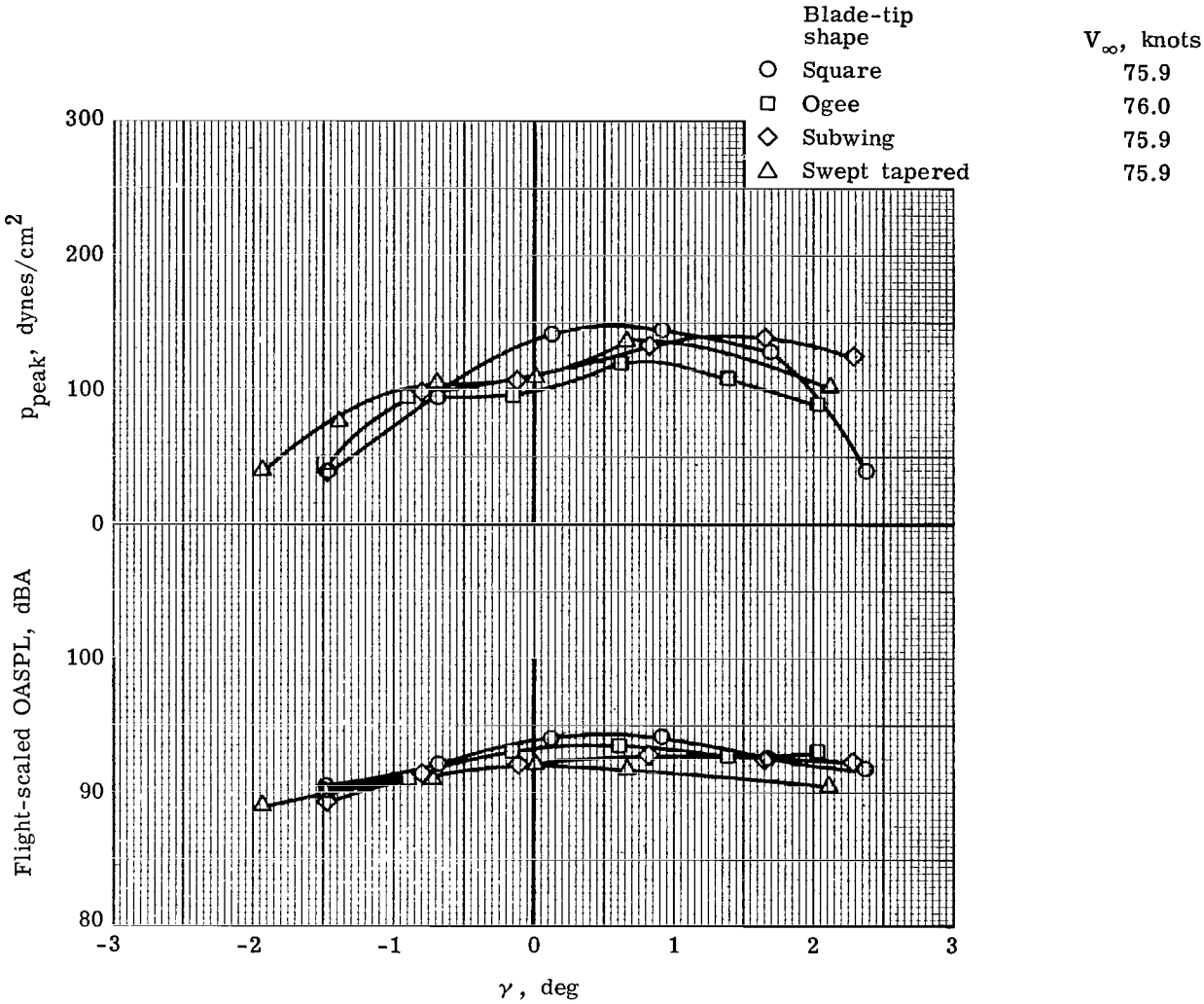

(b) Microphone 5.

Figure 17.- Continued.

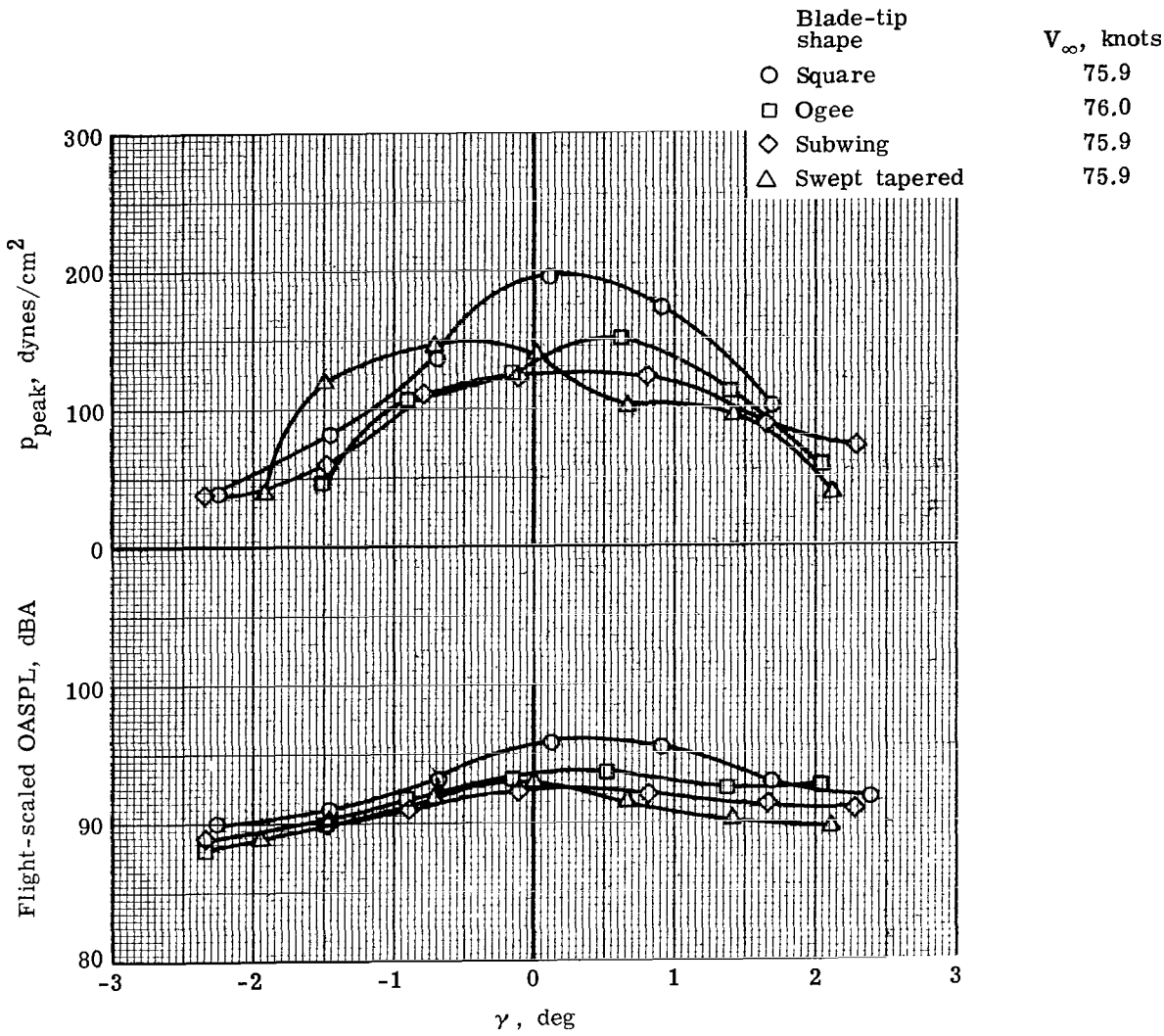

(c) Microphone 6.

Figure 17.- Continued.

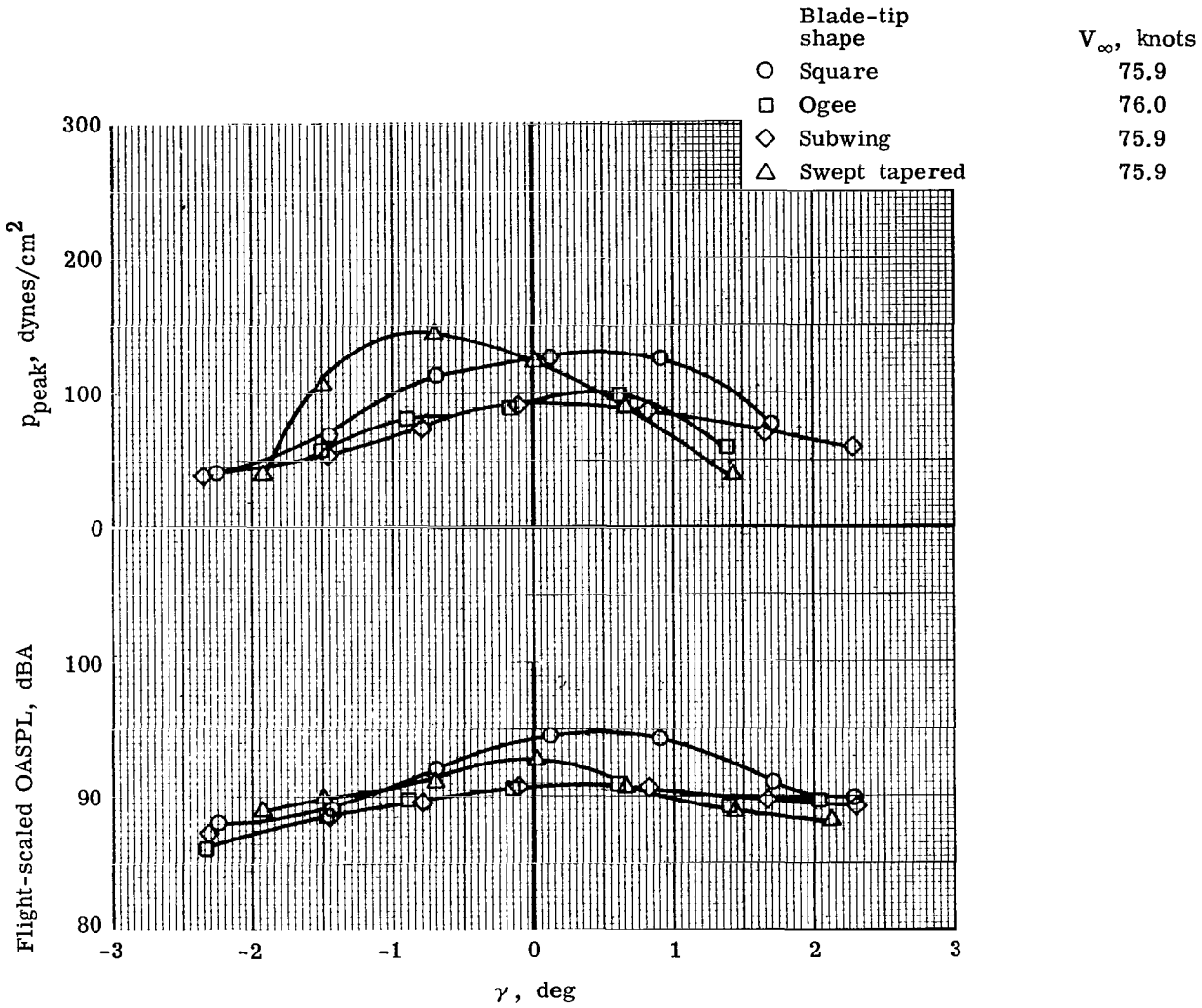

(d) Microphone 7.

Figure 17.- Concluded.

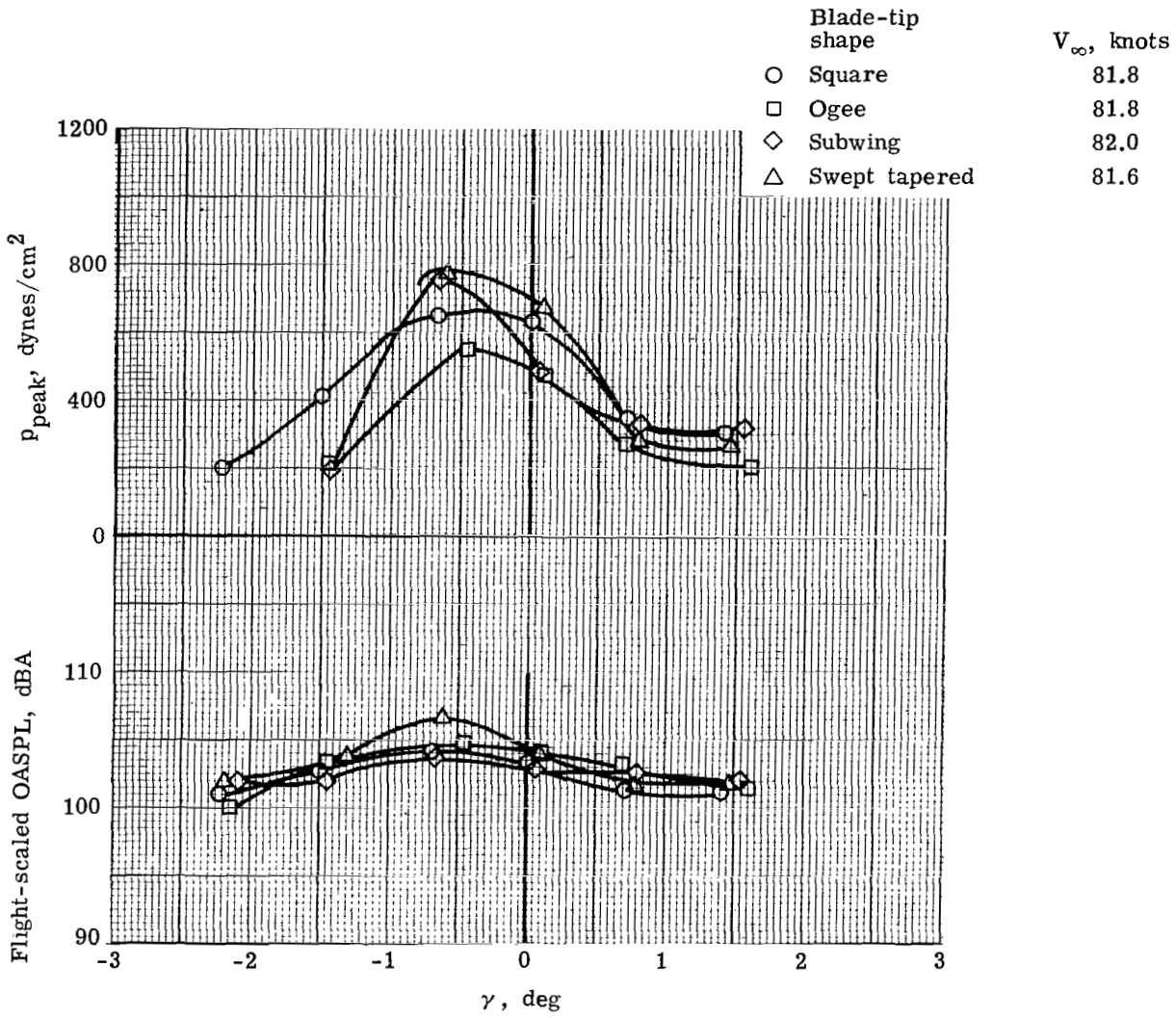

Figure 18.- Effect of tip shape on blade-slap intensity variation with descent angle for microphone 3 at $V_\infty \approx 82$ knots.

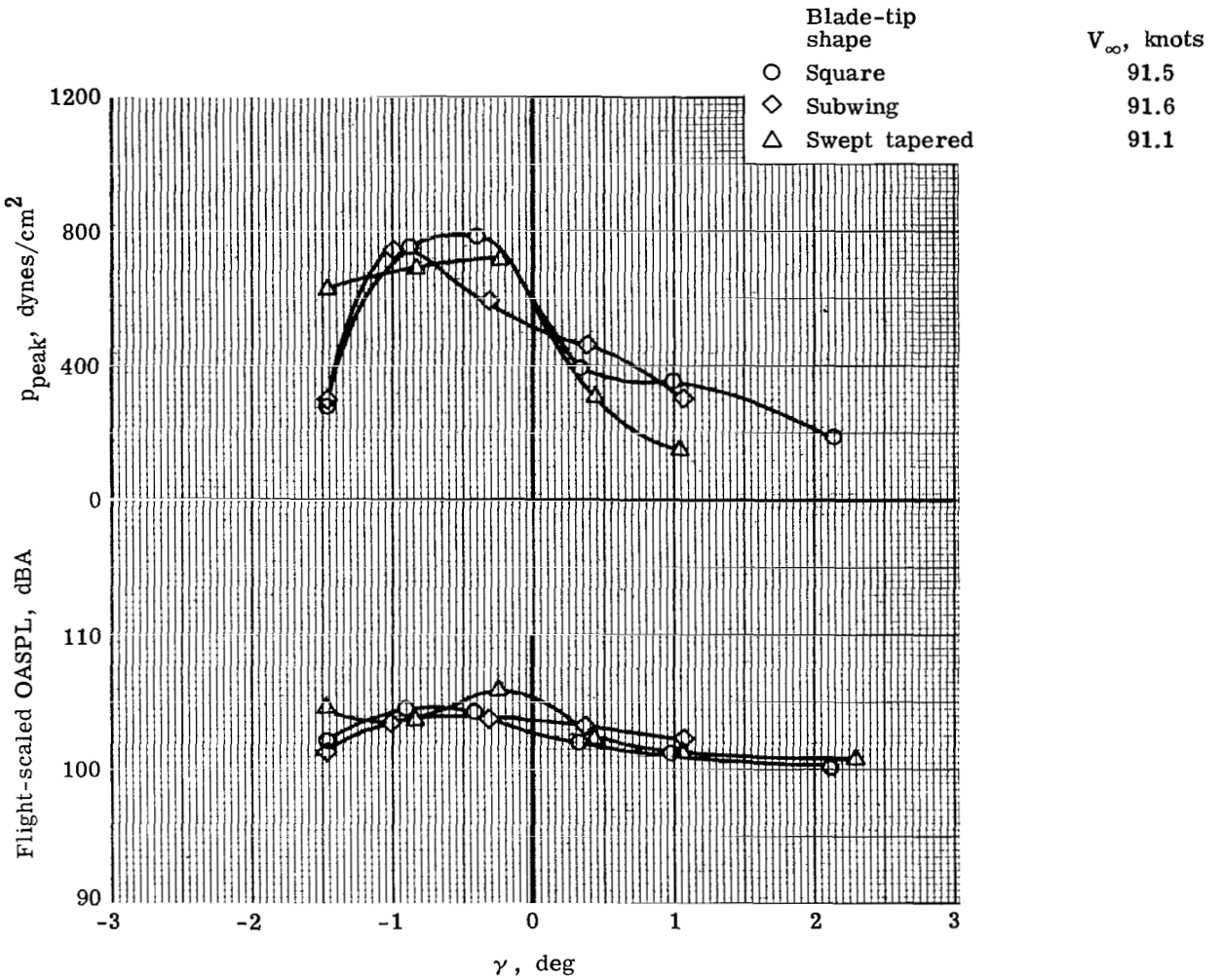

Figure 19.- Effect of tip shape on blade-slap intensity variation with descent angle for microphone 3 at $V_\infty \approx 91$ knots.

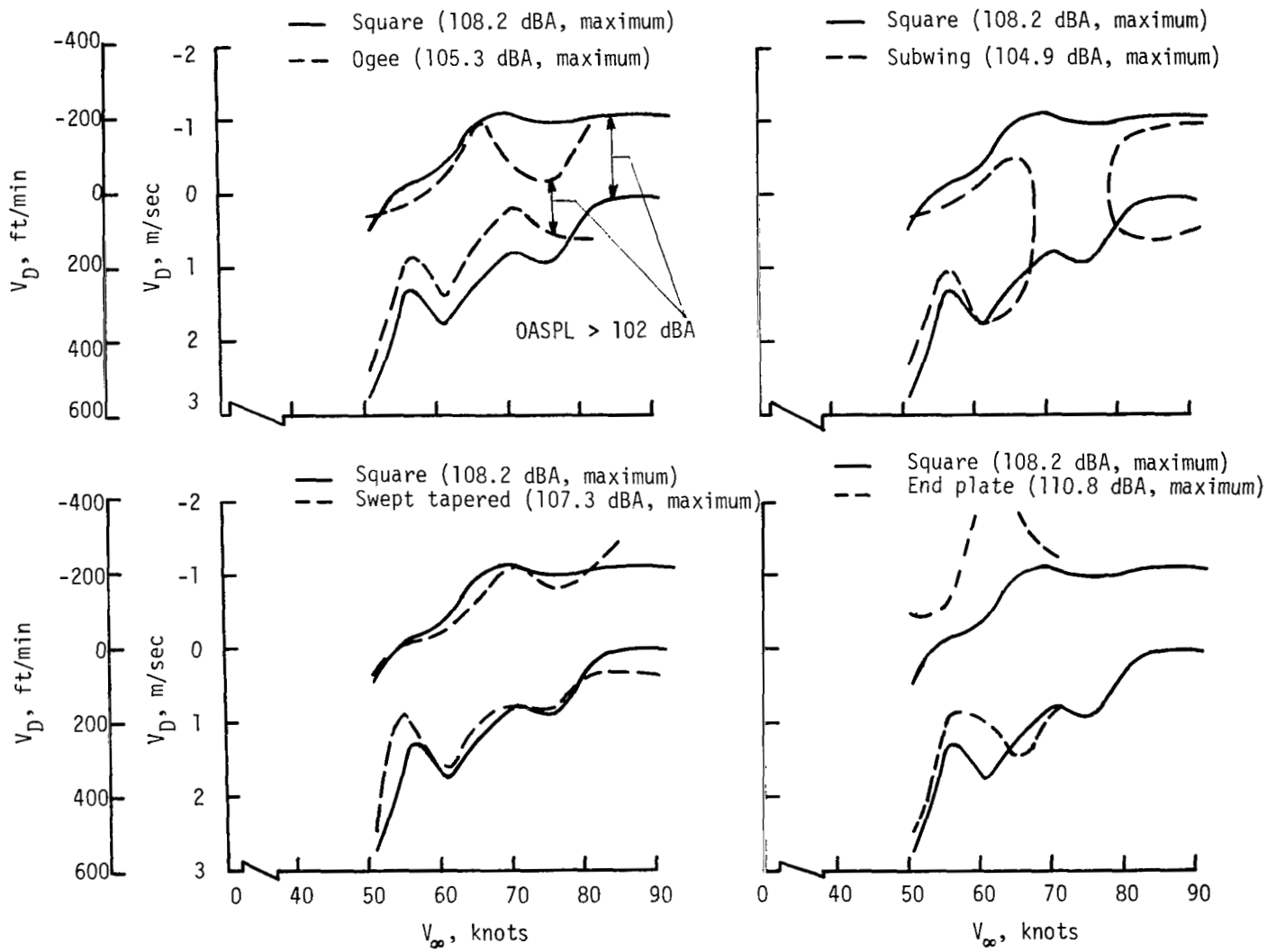

(a) Microphone 3; 103 dBA.

Figure 20.- Flight envelope of constant flight-scaled, A-weighted OASPL with various tips installed.

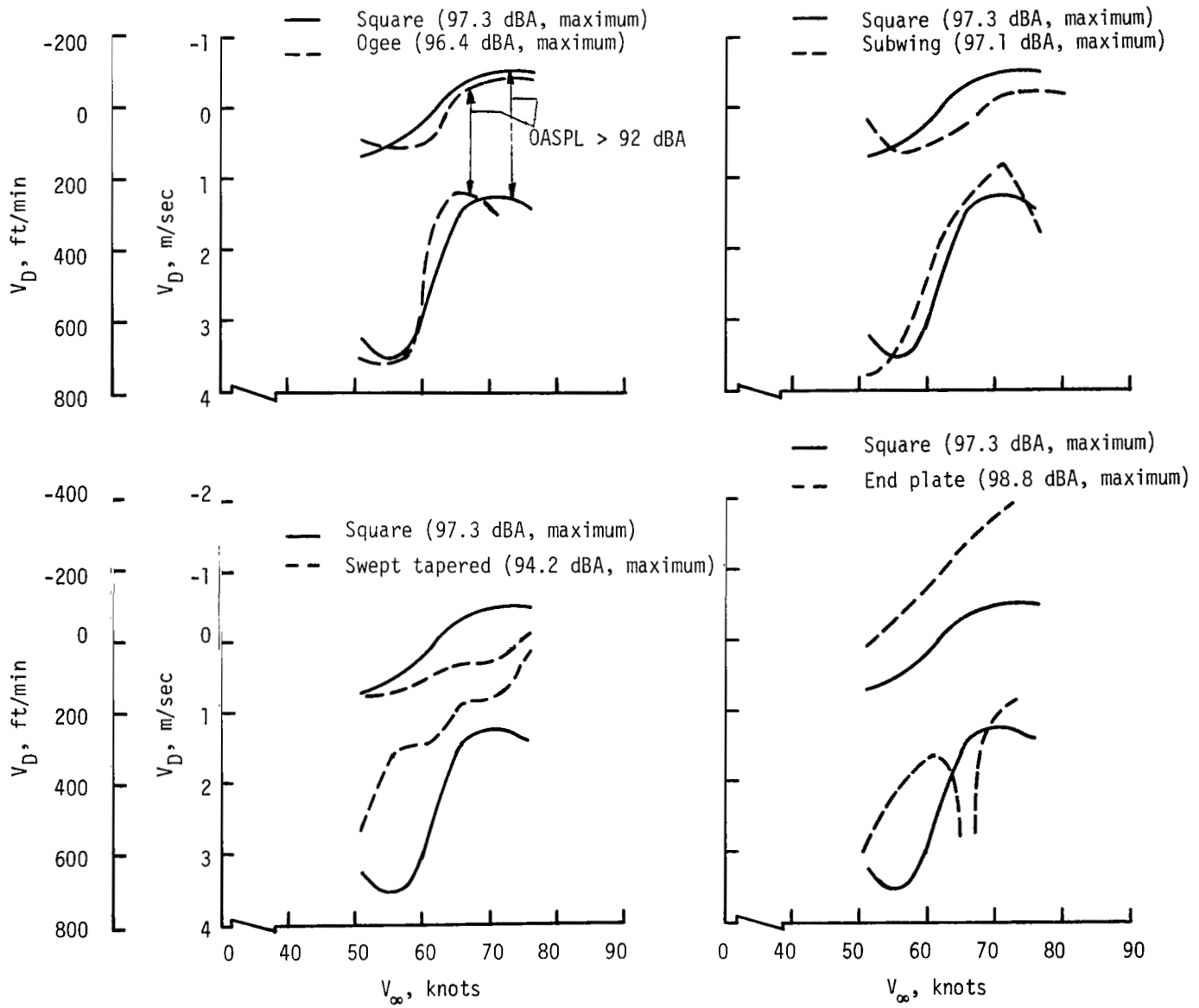

(b) Microphone 5; 92 dBA.

Figure 20.- Concluded.

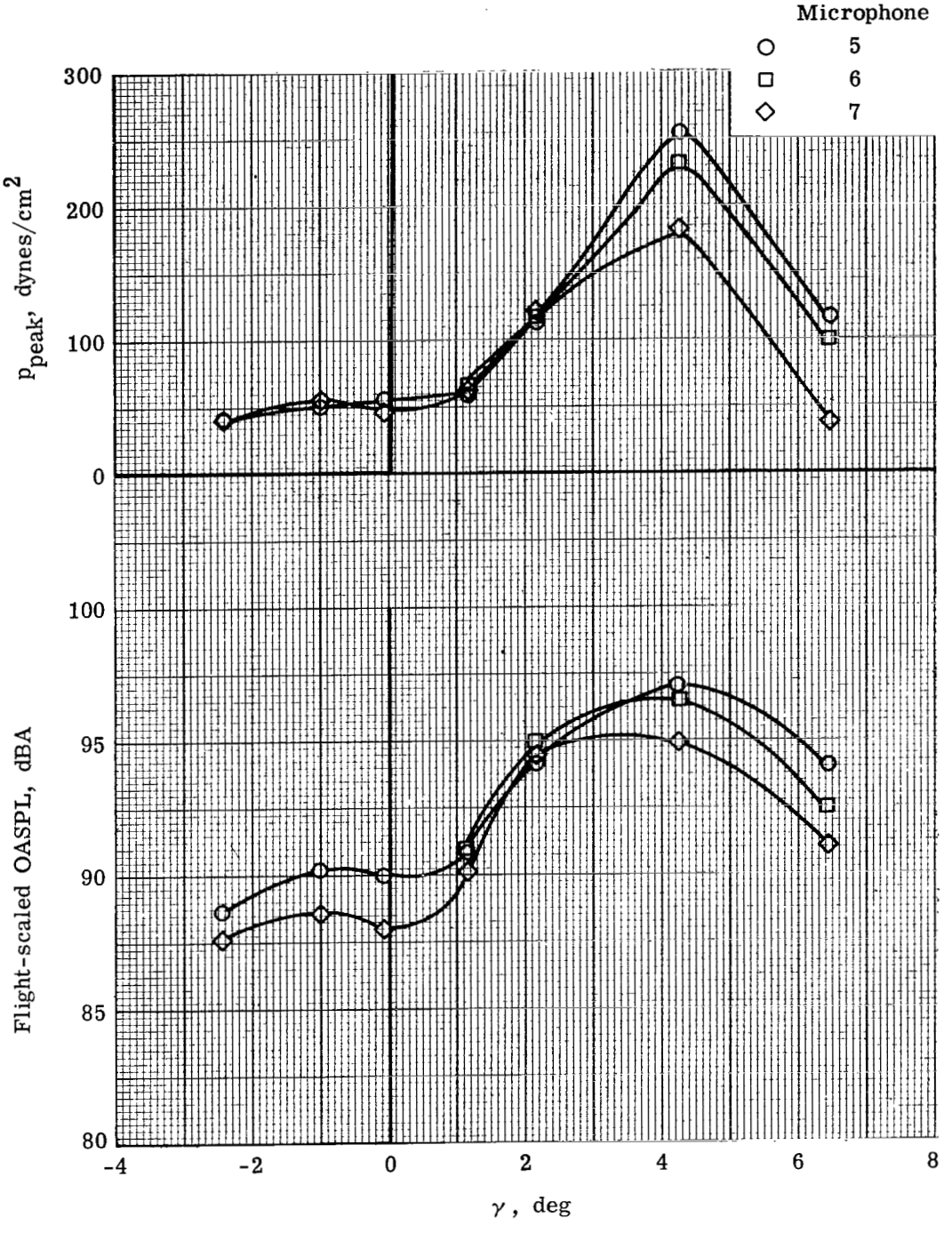

(a) V_∞ = 51.4 knots.

Figure 21.- Lateral-directivity characteristics of blade-slap intensity for square tip.

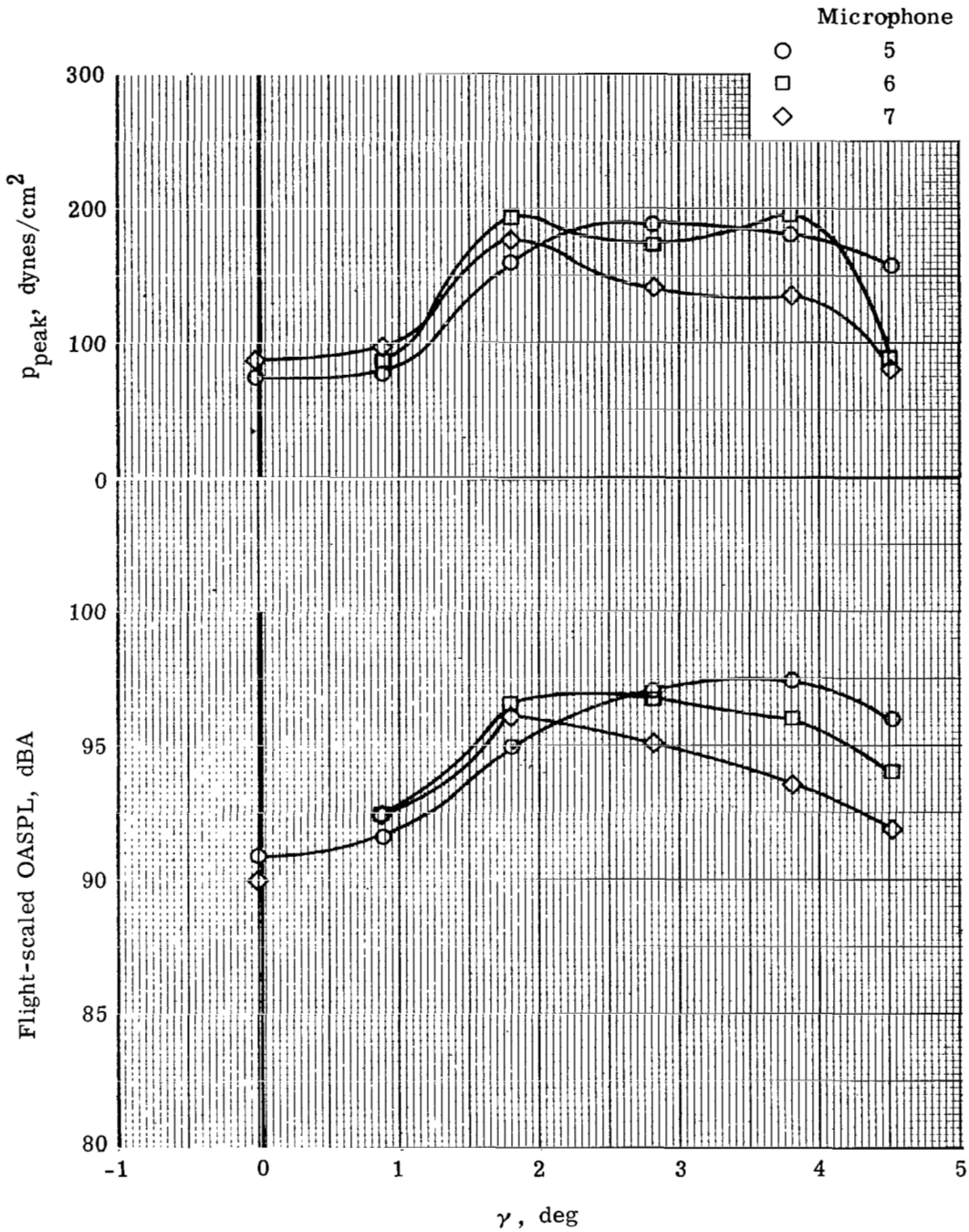

(b) V_∞ = 56.2 knots.

Figure 21.- Continued.

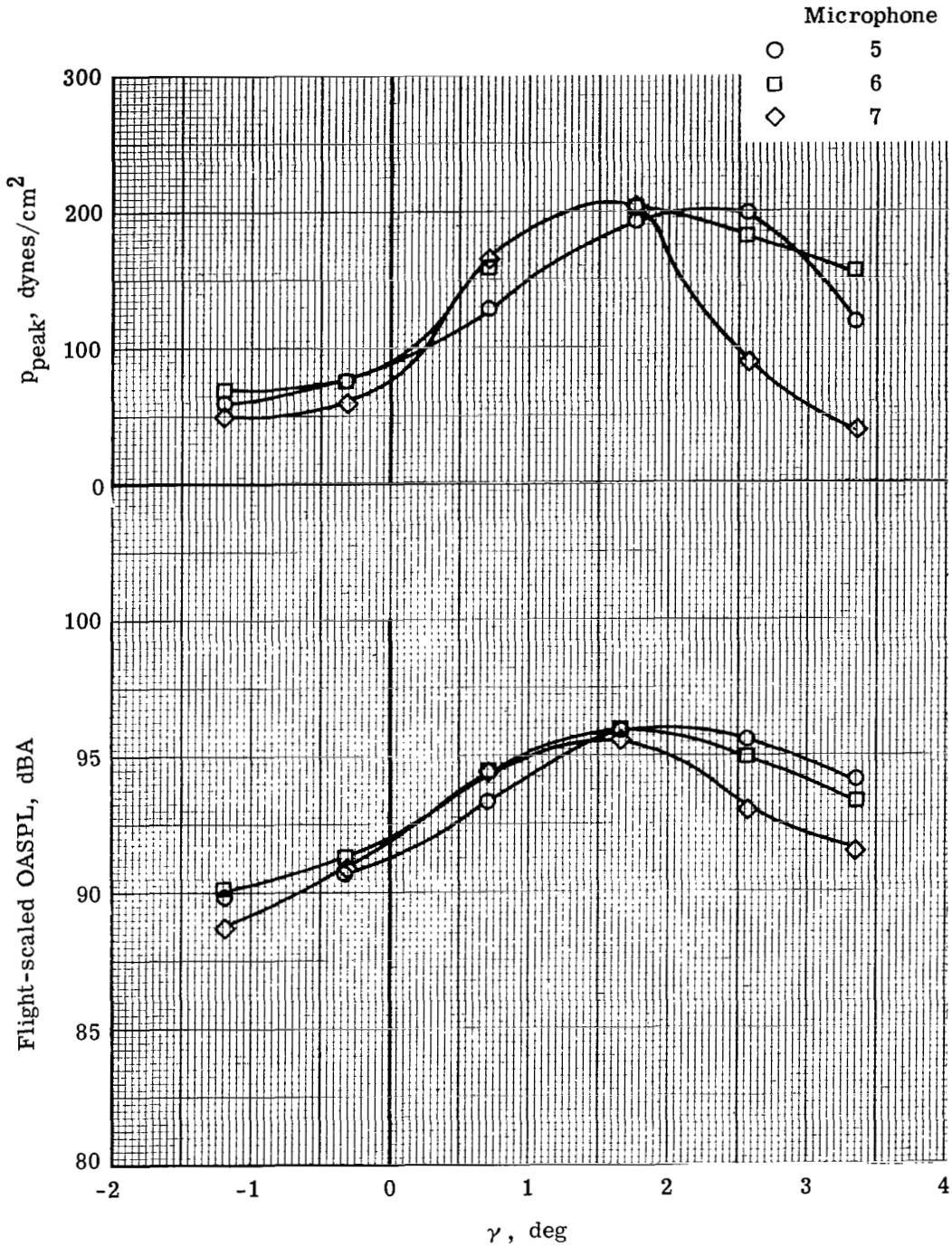

(c) V_∞ = 61.3 knots.

Figure 21.- Continued.

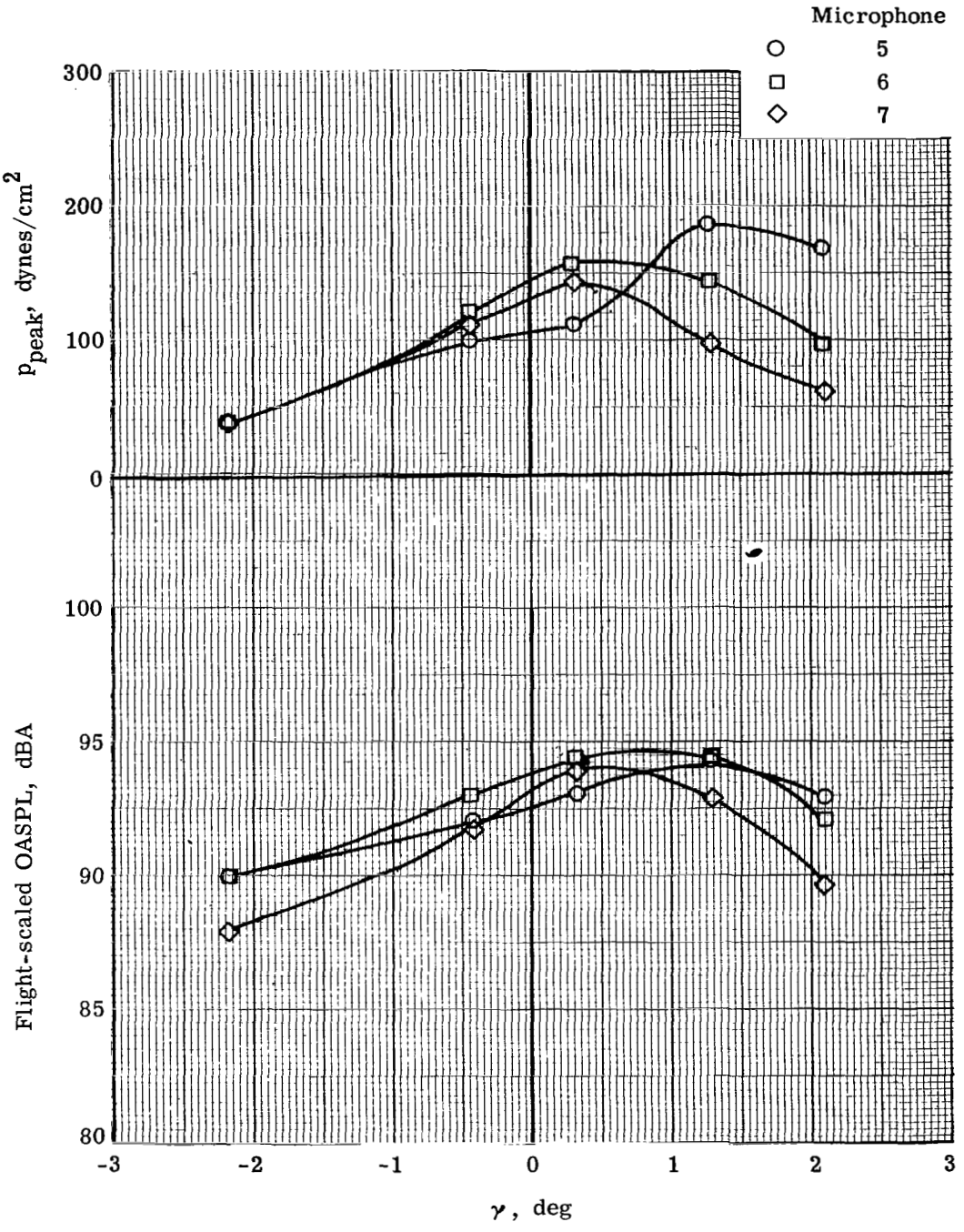

(d) V_∞ = 65.7 knots.

Figure 21.- Continued.

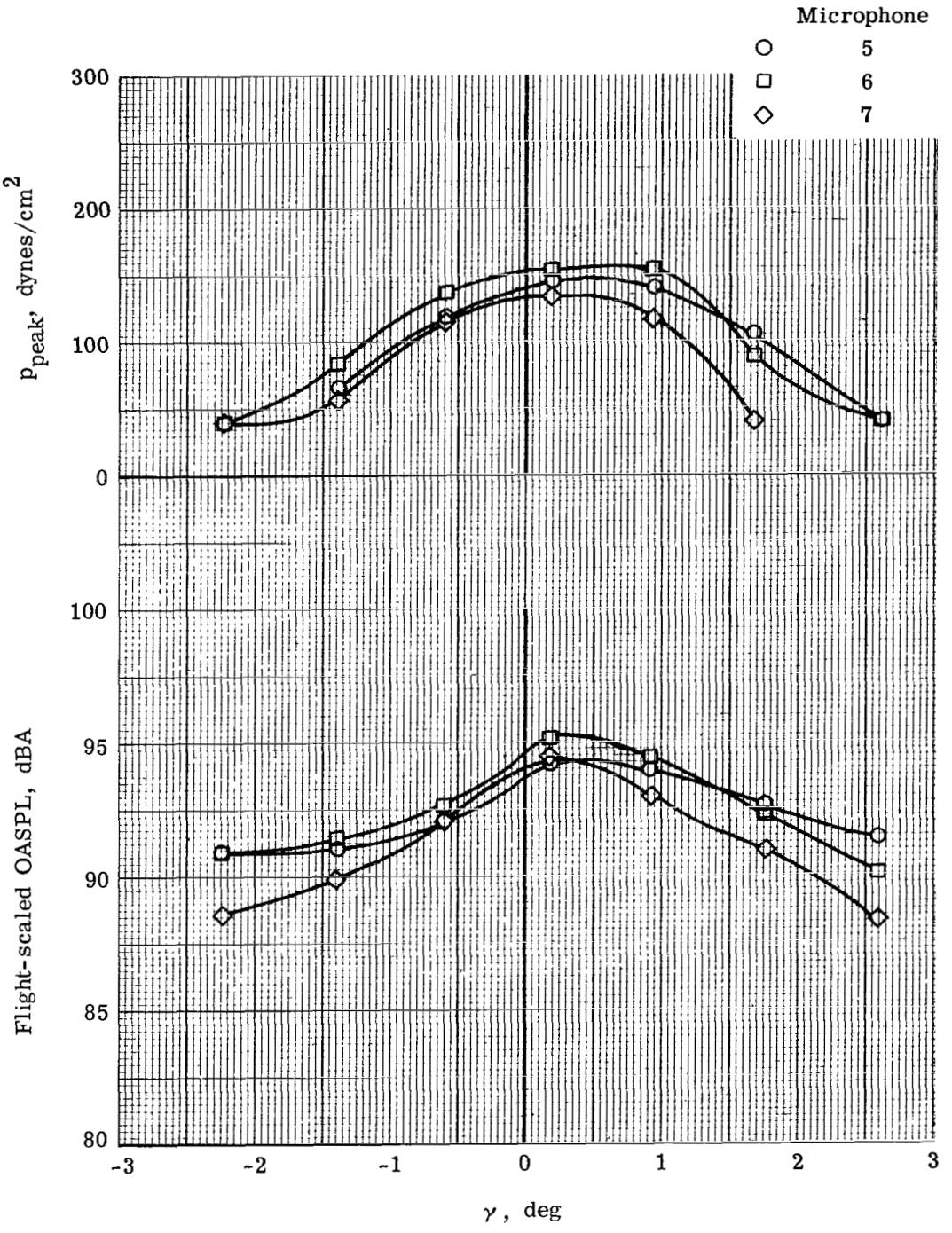

(e) V_∞ = 71.1 knots.

Figure 21.- Continued.

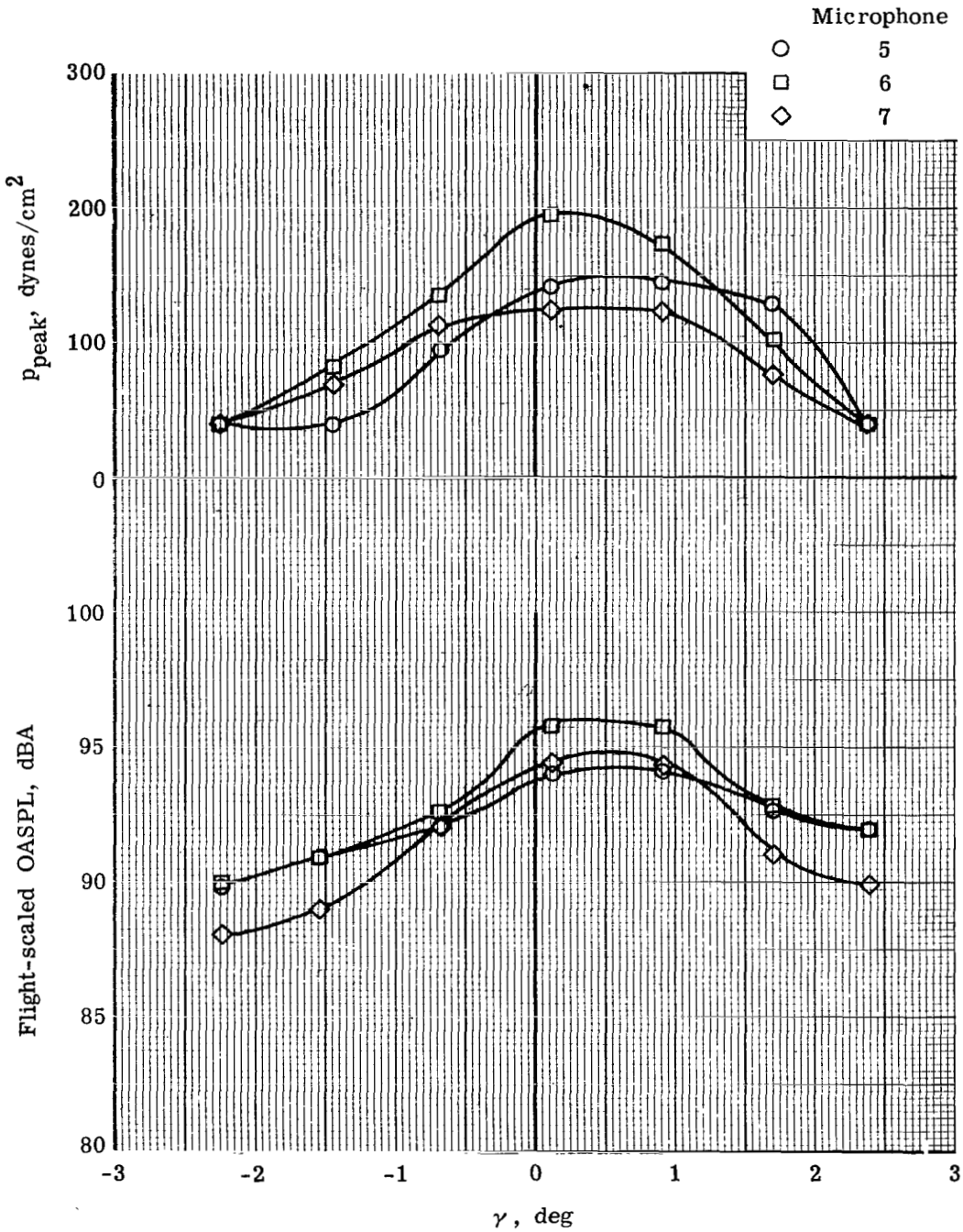

(f) V_∞ = 75.9 knots.

Figure 21.- Concluded.

1. Report No.	2. Government Accession No.	3. Recipient's Catalog No.
NASA TP-1608 AVRADCOM TR-80-B1		

4. Title and Subtitle	5. Report Date
EVALUATION OF HELICOPTER NOISE DUE TO BLADE-VORTEX INTERACTION FOR FIVE TIP CONFIGURATIONS	December 1979
	6. Performing Organization Code
7. Author(s)	8. Performing Organization Report No.
Danny R. Hoad	L-13207
9. Performing Organization Name and Address	10. Work Unit No.
NASA Langley Research Center and Structures Laboratory AVRADCOM Research and Technology Laboratories Hampton, VA 23665	505-10-23-05
	11. Contract or Grant No.
12. Sponsoring Agency Name and Address	13. Type of Report and Period Covered
National Aeronautics and Space Administration Washington, DC 20546 and U.S. Army Aviation Research and Development Command St. Louis, MO 63166	Technical Paper
	14. Army Project No.
	1L262209AH76

15. Supplementary Notes

Danny R. Hoad: Structures Laboratory, AVRADCOM, Research and Technology Laboratories.

16. Abstract

An experimental investigation of the effect of tip-shape modification on blade-vortex interaction induced helicopter blade-slap noise has been conducted. The general rotor model system (GRMS) with a 3.148-m (10.33-ft) diameter, four-bladed, fully articulated rotor was installed in the Langley Research Center V/STOL tunnel. Tests were conducted over a range of simulated flight and descent velocities which have been shown to produce blade slap. Aerodynamic performance parameters of the rotor system were monitored to ensure properly matched flight conditions among the tip shapes. The tunnel was operated in the open-throat configuration with treatment to improve the acoustic characteristics of the test chamber. Four promising tips (based on previous investigations) were used (ogee, subwing, 60° swept tapered, and end plate), along with a standard square tip as a baseline configuration. This investigation provided a detailed acoustic evaluation on the same rotor system of the relative applicability of the various tip configurations for blade-slap noise reduction. (This report applies to the evaluation changes in tip shape on the rotor performance and acoustic signature.)

17. Key Words (Suggested by Author(s))	18. Distribution Statement
Helicopter noise Blade slap Blade-vortex interaction	Unclassified - Unlimited Subject Category 71

19. Security Classif. (of this report)	20. Security Classif. (of this page)	21. No. of Pages	22. Price*
Unclassified	Unclassified	77	$6.00

*For sale by the National Technical Information Service, Springfield, Virginia 22161

NASA-Langley, 1979

National Aeronautics and
Space Administration

Washington, D.C.
20546

Official Business
Penalty for Private Use, $300

THIRD-CLASS BULK RATE

Postage and Fees Paid
National Aeronautics and
Space Administration
NASA-451

U.S.MAIL

14 1 1U,H, 121779 S00903DS
DEPT OF THE AIR FORCE
AF WEAPONS LABORATORY
ATTN: TECHNICAL LIBRARY (SUL)
KIRTLAND AFB NM 87117

NASA

S

ASTER: If Undeliverable (Section 158
Postal Manual) Do Not Return